IN TWO SECTIONS—SECTION ONE

Transactions

of the

A.S.M.E.

JANUARY, 1946

VOL. 68, NO. 1

Transactions

of The American Society of Mechanical Engineers

Published on the tenth of every month, except March, June, September, and December

Published monthly by The American Society of Mechanical Engineers. Publication office at 20th and Northampton Streets, Easton, Pa. The editorial department is located at the headquarters of the Society, 29 West Thirty-Ninth Street, New York 18, N. Y. Cable address, "Dynamic," New York. Price $1.50 a copy, $12.00 a year; to members and affiliates, $1.00 a copy, $7.50 a year. Changes of address must be received at Society headquarters two weeks before they are to be effective on the mailing list. Please send old as well as new address. . . . By-Law: The Society shall not be responsible for statements or opinions advanced in papers or . . . printed in its publications (B13, Par. 4). . . . Entered as second-class matter March 2, 1928, at the Post Office at Easton, Pa., under the act of August 24, 1912. . . .

Rate of Temperature Change in Short-Length Round Timbers

By J. D. MacLEAN,[1] MADISON, WIS.

This paper discusses factors affecting the rate of temperature change in wood and includes time-temperature curves for use in determining the temperature obtained at different points in short-length log sections when heated in steam or hot water. One group of curves shows the temperature distribution from the ends to the mid-length and at different points between the circumference and axis, of logs 12, 24, 36, 48, and 60 in. in diameter. Other charts show the time-temperature distribution at various points between the circumference and axis at the mid-length of log sections of any diameter between 12 and 60 in. Examples are given illustrating the procedure for using the charts in finding the temperature at a parcular point, under different heating conditions.

Introduction

GREEN logs of various species are often heated in steam or in hot water to condition them for veneer-cutting. These logs are relatively short, and the ratio of diameter to length is large in comparison with round timbers in the form of posts, poles, and piling. In timbers in which the ratio of diameter to length is small, the effect of longitudinal heating can extend only a limited distance, while the portion between the end regions is raised to any desired temperature. Because of the comparatively short length of veneer logs, however, it is necessary to consider the effect of heat transfer in the longitudinal as well as in the transverse direction. The relative amount of heating that takes place in these two directions depends upon a number of variables, such as cross-sectional dimensions, length, heating period, and temperature of the heating medium.

The purpose of this paper is to discuss methods of finding the rate of temperature change in timbers of this kind. No attempt is made to discuss the temperatures needed for satisfactory results in veneer-cutting, for some woods apparently require less heating than others. When the optimum temperature is known, however, the data presented provide a guide for selecting the required heating period for logs of different species and of different dimensions. The data also furnish a useful aid in studying the effect of different heating conditions on veneer-cutting operations.

A large amount of experimental work has been done at the Forest Products Laboratory to study the rate of temperature change in wood when heated in different mediums and to investigate the effect of variables, such as species, moisture content, density, or specific gravity, and variation in the rate of heating in the radial, tangential, and longitudinal directions. A number of papers have been published which discuss the results of these experiments (1 through 10).[2]

[1] Engineer, Forest Products Laboratory, Forest Service, U. S. Department of Agriculture. (The Forest Products Laboratory is maintained in co-operation with the University of Wisconsin.)

Contributed by the Wood Industries Division of The American Society of Mechanical Engineers.

Effect of Variables on Rate of Temperature Change

Heating Medium. Experiments with different heating mediums show that for the same heating period and the same temperature conditions, steam heats wood faster than water, and water heats faster than such liquids as preservative oils (6). In general, water heated wood about 5 to 10 per cent more slowly than steam. All of the liquids, however, heated the wood somewhat faster than hot plates (6, 8). The slowest rate of heating was obtained in air at a low humidity, but the rate was increased as the humidity of the air was increased (10).

Variation in the rate at which wood heats in different mediums is apparently caused by such variables as type of surface contact, rate of circulation when liquids and gases are used, specific heat of the heating substance, and heat of vaporization as in the case of steam.

Differences in Moisture Content. Wood seasoned well below 30 per cent moisture content, which is about the fiber saturation point, was found to heat more slowly than green wood. Results obtained in heating green wood nevertheless indicate that differences in moisture content above the fiber saturation point have no significant effect on the rate of heating in the range of temperatures commonly employed (4). For practical purposes, therefore, it may be assumed that green timbers of any given species will heat at about the same rate at any moisture content above the fiber saturation point.

Direction of Grain. Studies made of the relative rate of heating in the radial and tangential directions (at right angles and parallel to the rings, respectively) showed there was no important difference in the rate of temperature change for these two directions, but the rate of heating in the longitudinal direction or along the fibers was found to be from $2^1/_4$ to $2^3/_4$ times faster than in the transverse direction (2, 6, 7). For practical purposes it should be sufficiently accurate to assume that on the average the rate of temperature change longitudinally is about $2^1/_2$ times faster than it is across the grain or in a plane at right angles to the axis of the tree. This ratio has been used in the calculation of temperature data that will be discussed later.

Density or Specific Gravity and Species. Experiments on specimens of the same species and on those of different species having different specific gravities showed that with any given heating medium, the rate of heating varied inversely with the specific gravity (6). The rate of temperature change is apparently influenced by the density of the wood rather than by the species, which affects the results merely to the extent that different species may vary in density.

The specific gravity of wood is usually based upon the volume at current moisture content and weight when oven-dry.

Table 1 shows the average specific-gravity values for various species of hardwoods and softwoods. These values are based upon volume when green and weight when oven-dry and are convenient to use when employing the time-temperature curves

[2] Numbers in parentheses refer to the Bibliography at the end of the paper.

TABLE 1 AVERAGE SPECIFIC GRAVITY OF VARIOUS SPECIES OF SOFTWOODS AND HARDWOODS[a]

Species	Average specific gravity (based on volume when green, and weight when oven-dry)
Hardwoods:	
Ash, white (Fraxinus americana)	0.55
Aspen, bigtooth (Populus grandidentata)	0.35
Basswood, American (Tilia americana)	0.32
Beech, American (Fagus grandifolia)	0.56
Birch, yellow (Betula lutea)	0.55
Chestnut, American (Castanea dentata)	0.40
Elm, American (Ulmus americana)	0.46
Elm, rock (Ulmus thomasii)	0.57
Hackberry (Celtis occidentalis)	0.49
Hickory, mockernut (Hicoria alba)	0.64
Maple, silver (Acer saccharinum)	0.44
Maple, sugar (Acer saccharum)	0.56
Oak, red (commercial) (Quercus sp.)	0.56
Oak, white (commercial) (Quercus sp.)	0.59
Pecan (Hicoria pecan)	0.60
Sweetgum (Liquidambar styraciflua)	0.44
Sycamore, American (Platanus occidentalis)	0.46
Tupelo, black (Nyssa sylvatica)	0.46
Tupelo, water (Nyssa aquatica)	0.46
Walnut, black (Juglans nigra)	0.51
Yellow poplar (Liriodendron tulipifera)	0.38
Softwoods:	
Baldcypress (Taxodium distichum)	0.42
Douglas fir, coast (Pseudotsuga taxifolia)	0.45
Douglas fir, Rocky Mountain (Pseudotsuga taxifolia)	0.40
Fir, white (Abies sp.)	0.37
Hemlock, Eastern (Tsuga canadensis)	0.38
Hemlock, Western (Tsuga heterophylla)	0.38
Larch, Western (Larix occidentalis)	0.48
Pine, Eastern white (Pinus strobus)	0.34
Pine, jack (Pinus banksiana)	0.39
Pine, loblolly (Pinus taeda)	0.47
Pine, longleaf (Pinus palustris)	0.54
Pine, ponderosa (Pinus ponderosa)	0.38
Pine, red (Pinus resinosa)	0.44
Pine, shore (Pinus contorta)	0.38
Pine, shortleaf (Pinus echinata)	0.46
Pine, slash (Pinus caribaea)	0.56
Pine, sugar (Pinus lambertiana)	0.35
Pine, Western white (Pinus monticola)	0.36
Red cedar, Eastern (Juniperus virginiana)	0.44
Red cedar, Western (Thuja plicata)	0.31
Redwood (Sequoia sempervirens)	0.38
Spruce, Engelmann (Picea engelmanni)	0.31
Spruce, Sitka (Picea sitchensis)	0.37
Spruce, white (Picea glauca)	0.37
Tamarack (Larix laricina)	0.49
White-cedar, Northern (Thuja occidentalis)	0.29

[a] Data for other species can be found in "Strength and Related Properties of Woods Grown in the United States," U. S. Dept. of Agriculture, technical Bulletin 479.

shown in the figures. The method of using the data on density, or specific gravity, is discussed in the following section.

Computation of Temperature

The rate of temperature change in any solid depends upon the diffusivity which, like conductivity, may be considered a constant for normal ranges of temperature. This factor is a measure of the rate of temperature change and may be defined as the change in temperature produced in a unit volume of the substance by the quantity of heat that passes in unit time through unit area of a layer of unit thickness and having unit difference of temperature between the faces. If the diffusivity is represented by the symbol h^2, the specific heat by c, the density by ρ, and the conductivity by K, the relation of these variables is shown by the algebraic expression, $h^2 = \frac{K}{c\rho}$. Thus the diffusivity varies inversely as the product of specific heat and density, and directly as the conductivity.

Fig. 1 shows the relation of diffusivity and the specific gravity of wood determined from tests made on green material heated in steam. As previously mentioned, water was found to heat a little more slowly than steam, and for the purpose of calculation it should be satisfactory to assume that the rate of heating in water is about 90 per cent as fast as in steam. On this basis the dotted line in Fig. 1 represents the relation of diffusivity and specific gravity for green wood heated in water. If, for example, green wood having a specific gravity of about 0.5 were heated in steam, the diffusivity would be determined from Fig. 1 as about

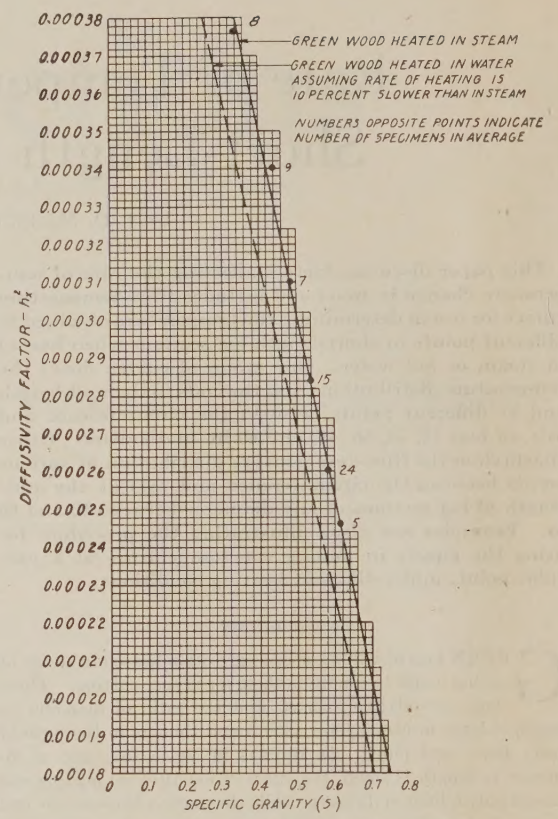

Fig. 1 Relation of Diffusivity and Specific Gravity

0.000302, while the corresponding diffusivity for heating in water would be about 0.000272. These diffusivity factors are in inch-second units.

Since the rate of temperature change depends to a certain extent upon the method of heating, the diffusivity values determined from experimental tests may be considered as values which apply for the heating medium used.

Wood is a substance that is naturally more or less variable in structure; hence temperature calculations cannot be made with the same precision that would be possible if it were a homogeneous material or a substance having the same physical properties in all directions. Nevertheless, the calculated temperature values, which are based upon average results from experimental tests, are sufficiently accurate for practical purposes, and whatever differences there may be between the computed temperatures and those actually obtained in a given timber will be small provided care is taken to maintain the heating conditions assumed.

In the early part of the heating period a variable amount of time is usually needed to bring the heating medium to the desired maximum temperature. A gradual change in the surface temperature is therefore obtained during this period, while the temperature calculations are necessarily based upon the assumption that the surfaces of the timbers are maintained at a constant temperature from the time the heating period is started.

If the temperature rise is fairly uniform, a convenient way to make an adjustment for the lower average temperature to which the wood is exposed during the early period of heating is to assume that the full temperature is applied for one half of this period. For example, if 2 hr were taken to bring the heating medium to the maximum temperature, the 2-hr period would be

counted as 1 hr at the maximum temperature. While this is an approximate method of adjusting for the period of variable temperature, it is generally satisfactory for moderate periods of changing surface temperature when the rate of temperature rise of the heating medium is reasonably uniform. A consideration of this lower average temperature at the beginning of the heating period naturally becomes of less importance as the total time of heating is increased. When the heating conditions are not controlled so that they are approximately uniform over most of the heating period, individual judgment must be exercised in determining the total time the timbers should be heated to compensate for the variable conditions.

Factors Involved in Temperature Calculations

Equation [4] in the Appendix was derived for computing the temperature data shown in Figs. 4 to 16, inclusive. Definitions of the symbols used and a brief outline of the development of this equation are also given in the Appendix.

An examination shows that the following factors are included in the fundamental equation:

1 Initial wood temperature = U_0
2 Temperature of heating medium = U_1
3 Diffusivity factor for radial heating = h^2
4 Diffusivity factor for longitudinal heating = q^2
5 Heating period = T (sec)
6 Radius of timber = a (in.)
7 Length of timber = L (in.)
8 Distance from nearest end surface, of point at which temperature is to be computed = Z (in.)
9 Distance from axis, of point at which temperature is to be computed = r (in.)
10 Temperature at the point (r, Z) under consideration = U

Fig. 2 shows the distance from the end surface and the distance from the circumference at which temperatures were computed for plotting the time-temperature curves. Fig. 3 is a chart for finding the corresponding wood temperatures when the heating conditions are different from those assumed in computing the temperature data plotted.

In the preparation of the time-temperature curves shown in Figs. 4 to 16, inclusive, the initial wood temperature U_0 was taken as 70 F, the heating-medium temperature U_1 as 212 F, the diffusivity factor for radial heating h^2 as 0.000270 (in-sec), and the diffusivity factor q^2 for longitudinal heating as about 2.5 times h^2, in round figures 0.000680, making the ratio slightly over 2.5, or about 2.52. It may be noted in Fig. 1 that the diffusivity factor of 0.000270 corresponds to about that for green wood having a specific gravity of 0.5, when heated in water.

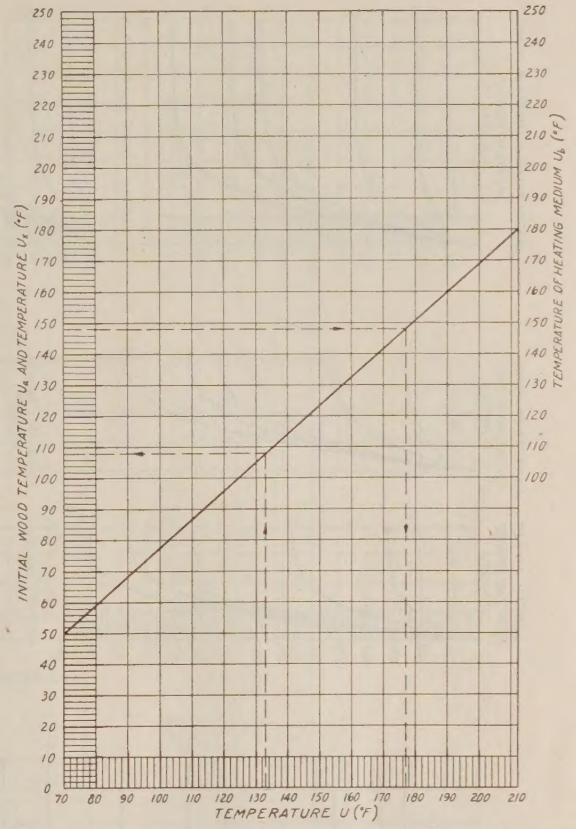

Fig. 3 Chart for Finding Corresponding Temperature U_x Within Timber When Initial Wood Temperature U_a, Heating-Medium Temperature U_b, or Both, Are Different From Those Assumed in Computing Plotted Temperatures

(Dotted lines illustrate examples.)

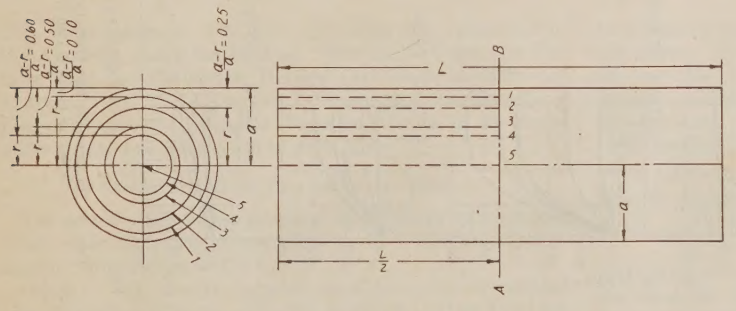

TEMPERATURE CURVES IN GROUP 1 ARE TEMPERATURES FROM END SURFACE TO MID-SECTION A-B AT DIFFERENT DISTANCES FROM THE CIRCUMFERENCE. NUMBERED 1, 2, 3, 4, AND 5
TEMPERATURE CURVES IN GROUP 2 SHOW TEMPERATURE DISTRIBUTION FROM CIRCUMFERENCE TO CENTER OF MID-SECTION A-B, AND TEMPERATURE CURVES IN GROUP 3 SHOW TEMPERATURES IN MID-SECTION AT DISTANCES OF 0.25a, 0.50a, 0.75a, AND a INCHES FROM THE CIRCUMFERENCE WHERE a=RADIUS IN INCHES

Fig. 2 Sketch Showing Distance From End Surface and Distance From Circumference at Which Temperatures Are Computed

Since the diffusivity for the longitudinal direction q^2 is taken as $2.52h^2$, the exponential function

$$e^{-T\left(h^2\lambda_n^2 + \frac{\pi^2 q^2 m^2}{L^2}\right)}$$

in the general Equation [3] can be written in the form

$$e^{-h^2T\left(\lambda_n^2 + \frac{2.52\pi^2 m^2}{L^2}\right)}$$

and a similar substitution can be made for q^2 in the terms of Equation [4] (Appendix). A change in the diffusivity factor for radial heating will therefore represent a proportional change in the longitudinal diffusivity factor q^2.

Although the temperature curves given in the various charts were computed by assuming the particular diffusivities and temperature conditions cited, these curves may be used for any predetermined conditions of temperature and for any species having diffusivities different

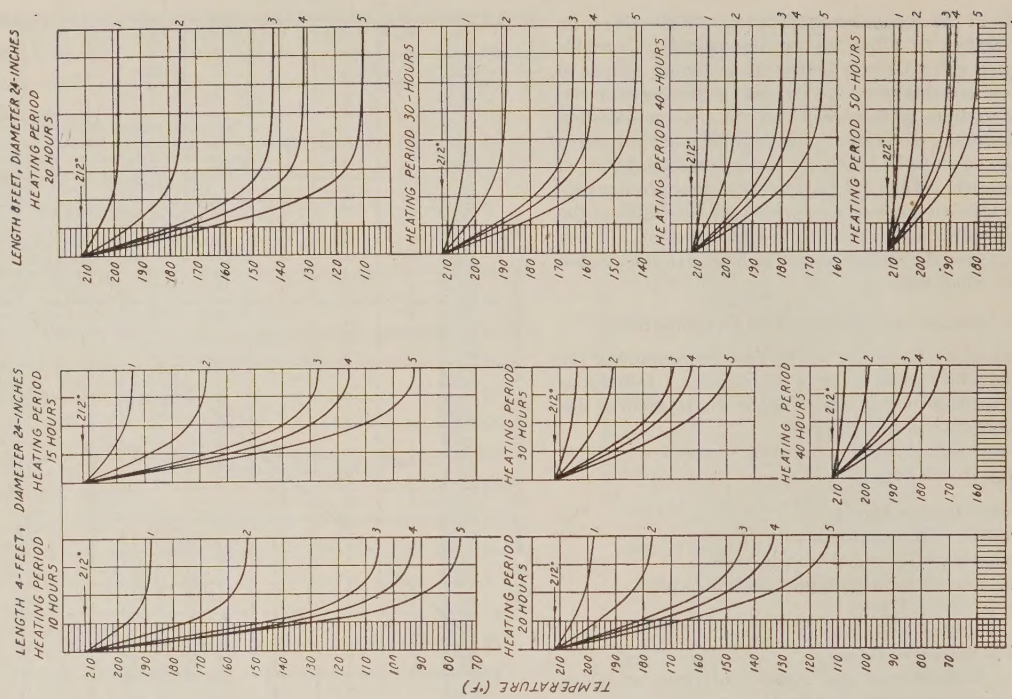

FIG. 5 TEMPERATURES OBTAINED AT DIFFERENT DISTANCES FROM END OF LOGS 4 AND 8 FT LONG AND 24 IN. DIAM

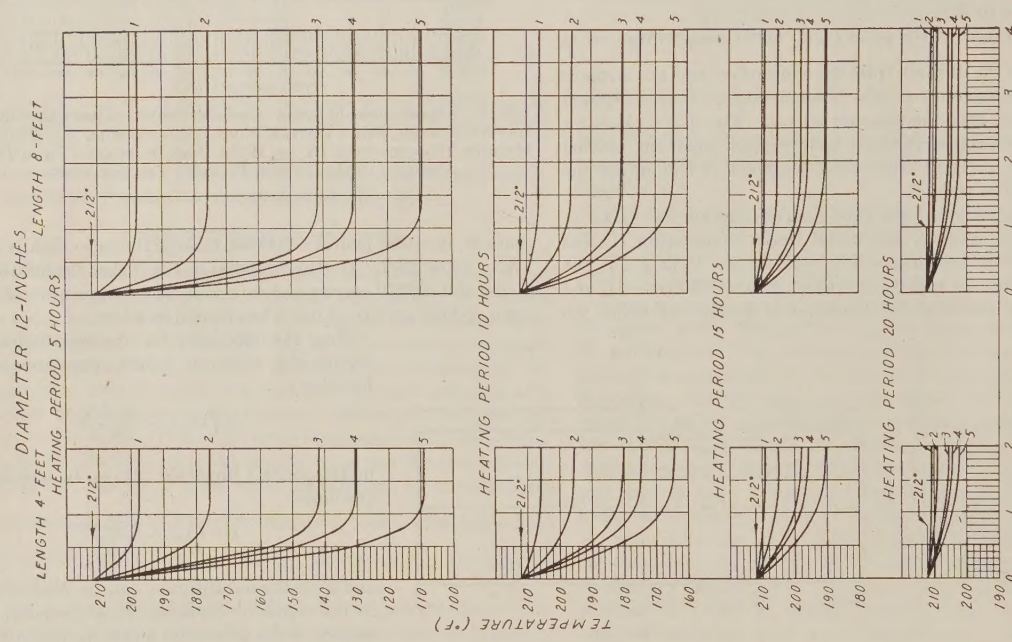

FIG. 4 TEMPERATURES OBTAINED AT DIFFERENT DISTANCES FROM END OF LOGS 4 AND 8 FT LONG AND 12 IN. DIAM

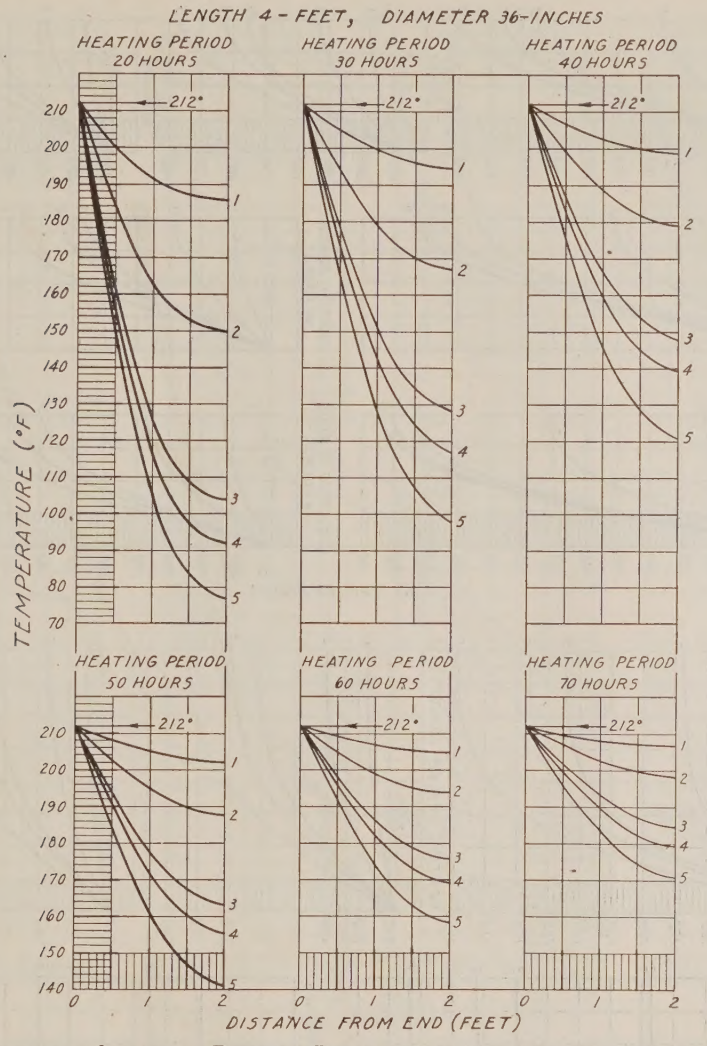

FIG. 6 TEMPERATURES OBTAINED AT DIFFERENT DISTANCES FROM END OF LOG 4 FT LONG AND 36 IN. DIAM

from those assumed. The method of doing this is explained in the Appendix under the heading, "Method of Using the Figures When the Diffusivity, Heating Conditions, or Both Are Different From Those Assumed in Computing the Time-Temperature Curves." Examples illustrating the use of the curves under different conditions will be given later.

DATA PLOTTED IN TEMPERATURE CURVES

The temperature curves comprise three groups in which the initial wood temperature was taken as 70 F and the heating-medium temperature as 212 F.

Group 1. Figs. 4 to 11, inclusive, show the computed temperature distribution from the end to the mid-length of logs 4 and 8 ft long and having diameters of 1, 2, 3, 4, and 5 ft. Each set of curves is for a different heating period, in most cases varying in intervals of 5 to 10 hr, depending upon the diameter.

Five temperature curves showing the temperature at the different distances from the circumference shown in Fig. 2 are given for each heating period. The top curve in Figs. 4 to 11, inclusive, shows the temperature in the zone or isothermal region at a distance from the circumference equal to $^1/_{10}$ (a) where a is the radius. The second, third, fourth, and fifth curves from the top show the corresponding temperatures in the zones that are at distances of $^1/_4$ (a), $^1/_2$ (a), $^3/_5$ (a), and a, respectively, from the circumference. In other words, if a is the radius of the log and r is the distance from the center or axis to the isothermal region at which the temperature is computed, then $(a - r)$ is the distance from the surface to the point at which the temperature is given. The ratio $\left(\frac{a-r}{a}\right)$ is therefore equal to 0.10, 0.25, 0.50, 0.60, and 1.0 for the curves shown. In the last case, $r = 0$; hence the curve for this distance from the circumference shows the temperature variation along the axis from the end to the mid-length of the timber. The distance from the circumference to the point on the radius at which the temperature is computed is evidently equal to the numerical value of $\left(\frac{a-r}{a}\right)$ multiplied by the radius. For example, if the radius is 12 in. and $\left(\frac{a-r}{a}\right) =$

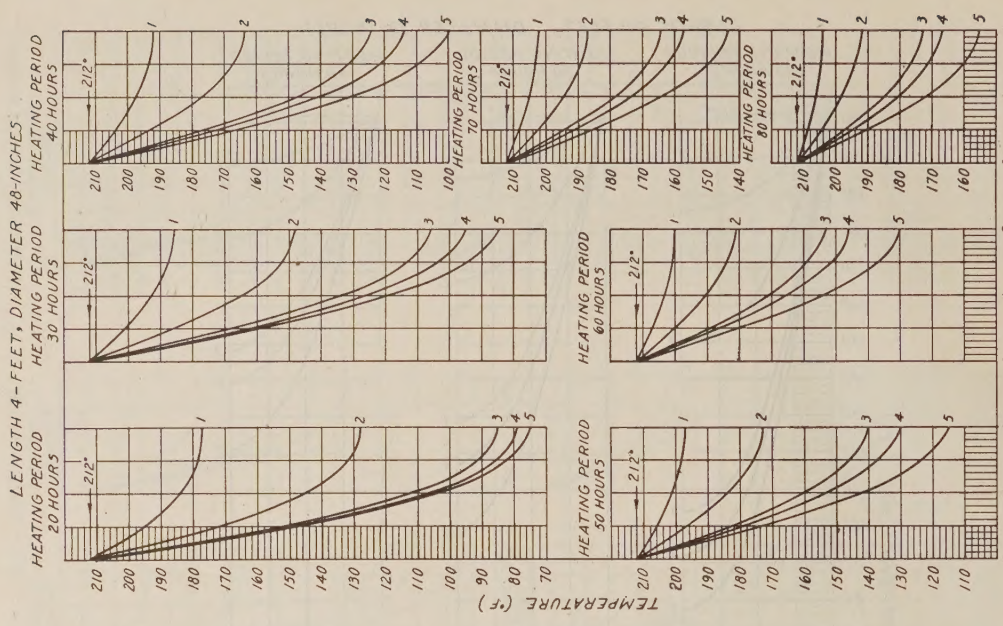

FIG. 8 TEMPERATURES OBTAINED AT DIFFERENT DISTANCES FROM END OF LOG 4 FT LONG AND 48 IN. DIAM

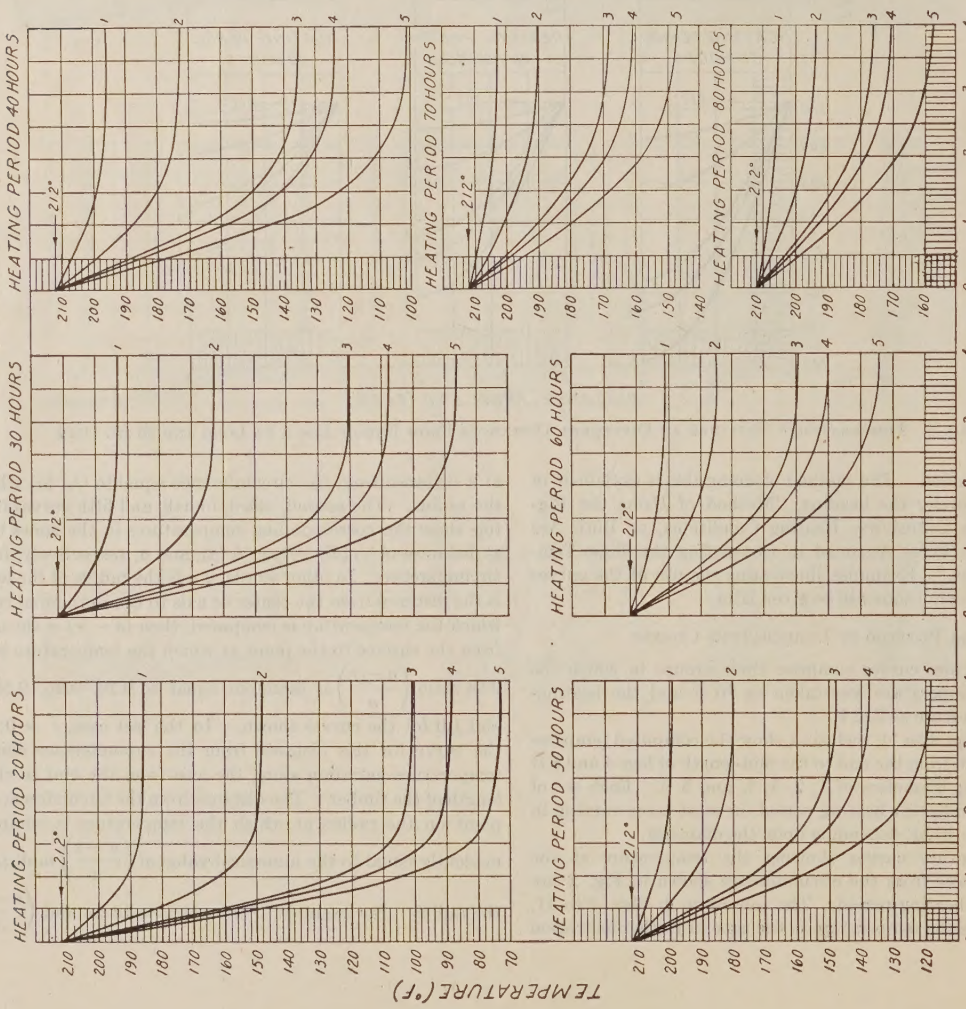

FIG. 7 TEMPERATURES OBTAINED AT DIFFERENT DISTANCES FROM END OF LOG 8 FT LONG AND 36 IN. DIAM

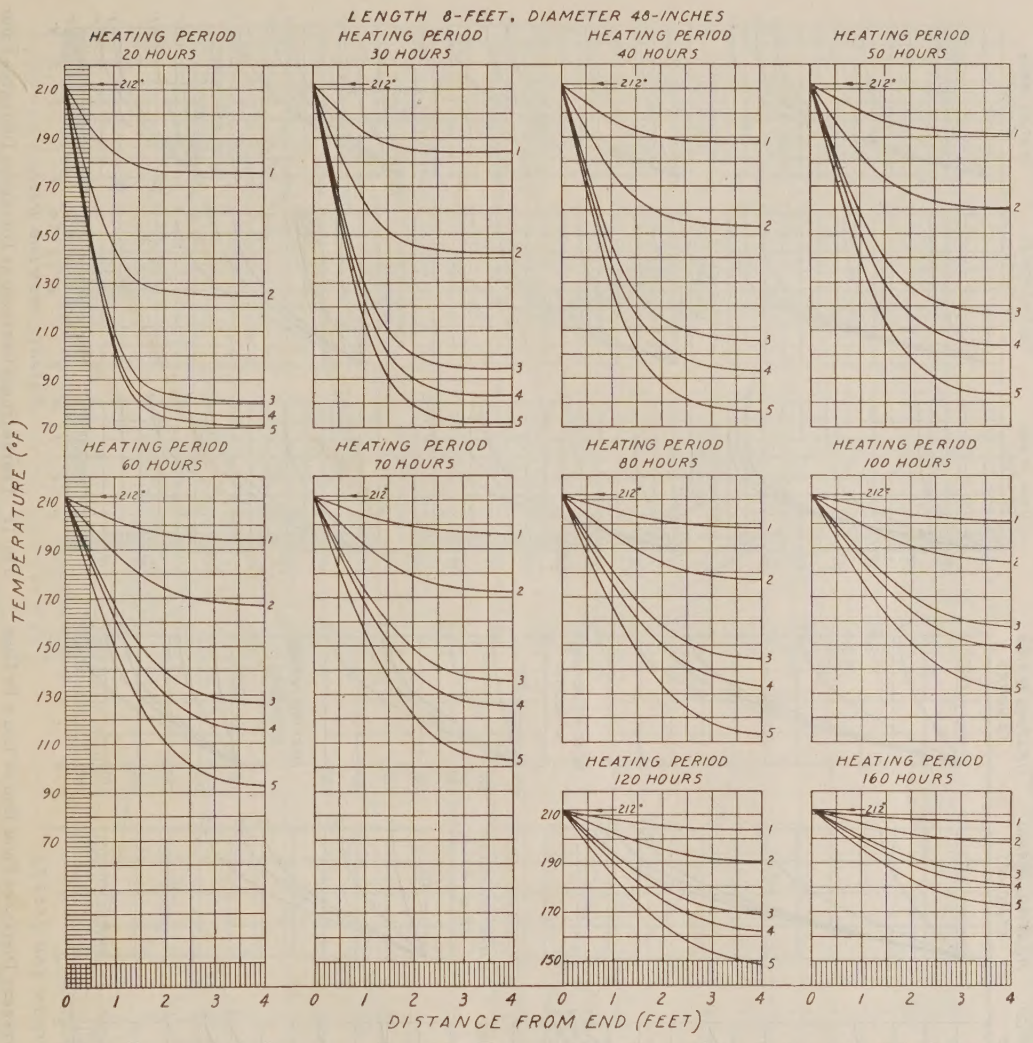

FIG. 9 TEMPERATURES OBTAINED AT DIFFERENT DISTANCES FROM END OF LOG 8 FT LONG AND 48 IN. DIAM

0.10, the distance from the surface is 12(0.10) or 1.2 in. The curves are shown for only one half the length since the rate of temperature change is assumed to be the same from either end.

Group 2. Figs. 12 to 14, inclusive, show the computed temperature distribution for various heating periods at all distances from the circumference to the center at the transverse mid-section of logs 4 and 8 ft long, for diameters of 1, 2, 3, 4, and 5 ft. Similar curves could be prepared for a transverse section at any distance from the end surface by plotting the temperature data from the curves shown in group 1 as was done in preparing the curves in group 2. The temperature at the transverse mid-section, however, is generally of most interest, since the lowest temperatures are obtained in this region. The curves given in group 2 (Figs. 12 to 14, inclusive) show the temperatures obtained at the end of 5- to 10-hr heating periods, except for particularly long heating periods or when the rate of temperature change was very slow. Under conditions in which this rate was unusually slow, somewhat longer time differences were used.

The time required to obtain a given temperature (which is found between any two time-temperature curves) can be determined with sufficient accuracy for practical purposes from the proportional distance on the vertical line intersecting the two curves between which the temperature is found. This assumes that the change in temperature between any two time-temperature curves is directly proportional to the time heat is applied during this time interval. For example, assume the required temperature is 170 F at 8 in. from the surface of a log 36 in. diam and 8 ft long. In this case $\left(\frac{a-r}{a}\right) = \frac{8}{18}$ or approximately 0.45. The vertical line from 0.45, Fig. 13*B*, intersects the horizontal line from 170 F at a point between the temperature curves for heating periods of 60 and 70 hr. The temperature after heating for 60 hr is 164 F, and that after heating for 70 hr is about 173 F, or an increase of 9 deg in 10 hr. When the proportional change in temperature is assumed to be the same as the proportional change in time of heating the temperature ratio is $\frac{170-164}{173-164} =$ $^6/_9$ or $^2/_3$. Since the time interval is 10 hr, the time is found from the relation, $2:3 = x:10$ and x (the time that is required to in-

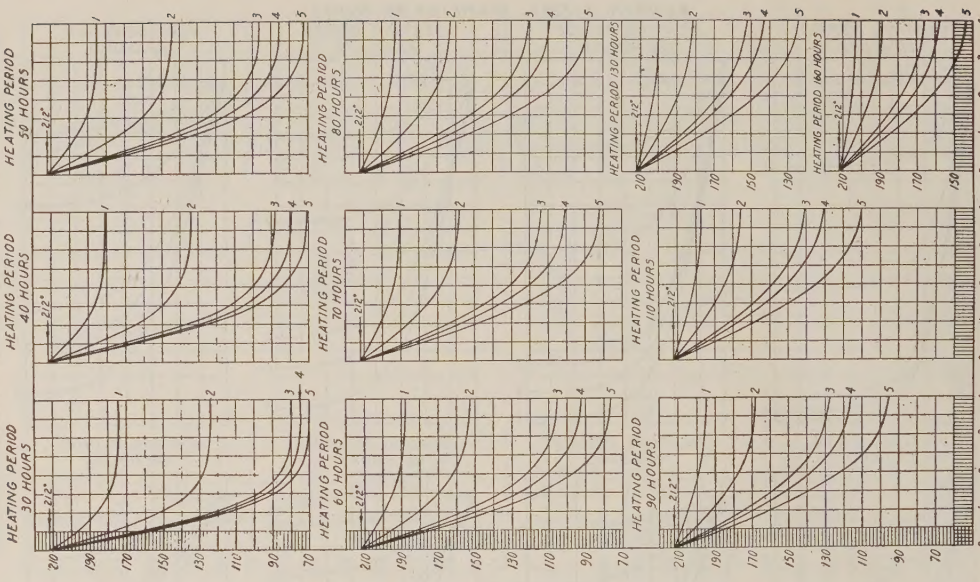

FIG. 11 TEMPERATURES OBTAINED AT DIFFERENT DISTANCES FROM END OF LOG 8 FT LONG AND 60 IN. DIAM

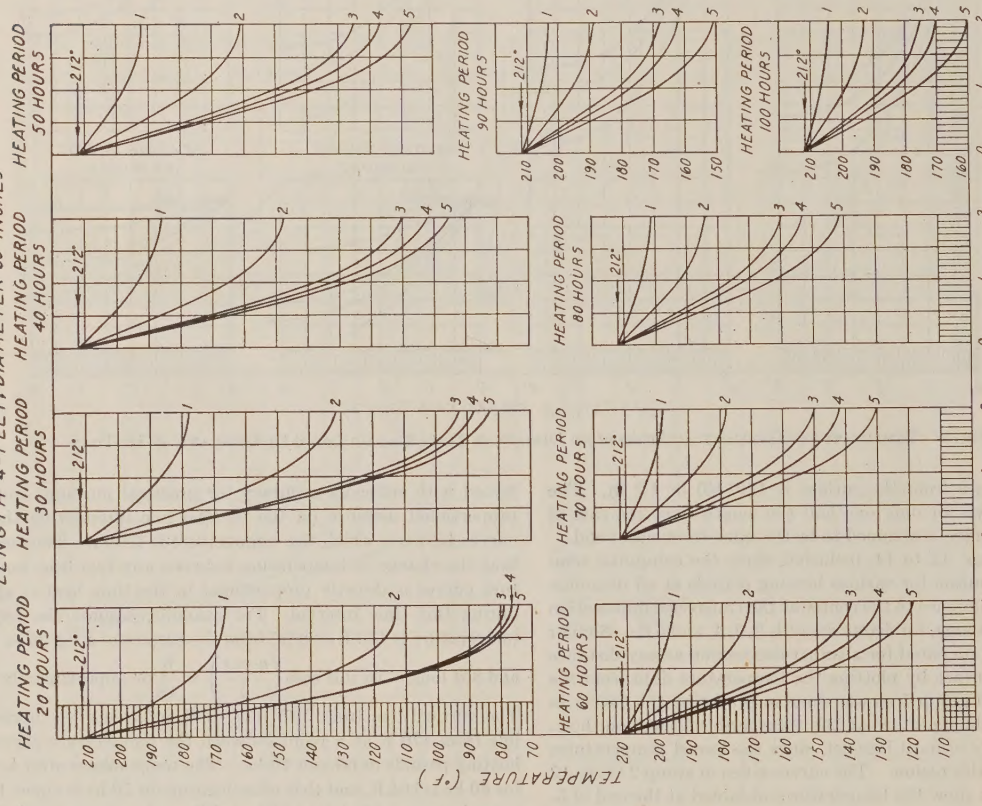

FIG. 10 TEMPERATURES OBTAINED AT DIFFERENT DISTANCES FROM END OF LOG 4 FT LONG AND 60 IN. DIAM

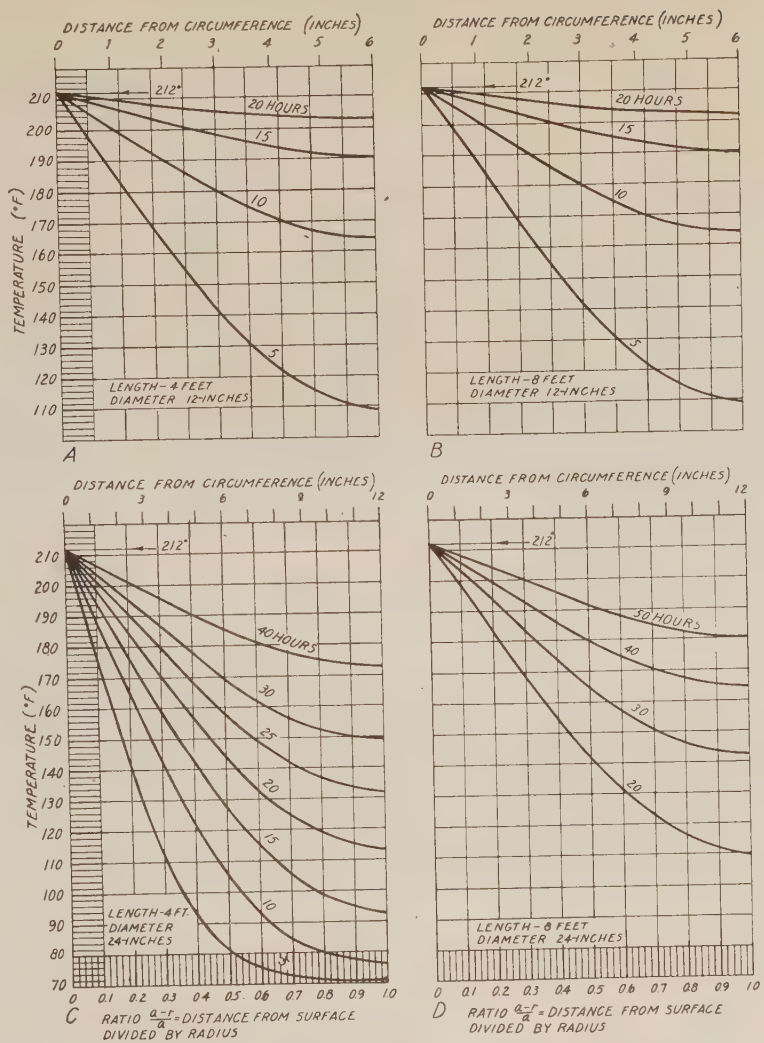

FIG. 12 TEMPERATURE DISTRIBUTION FROM CIRCUMFERENCE TO CENTER OF MID-SECTION; LOGS 4 AND 8 FT LONG AND 12 AND 24 IN. DIAM

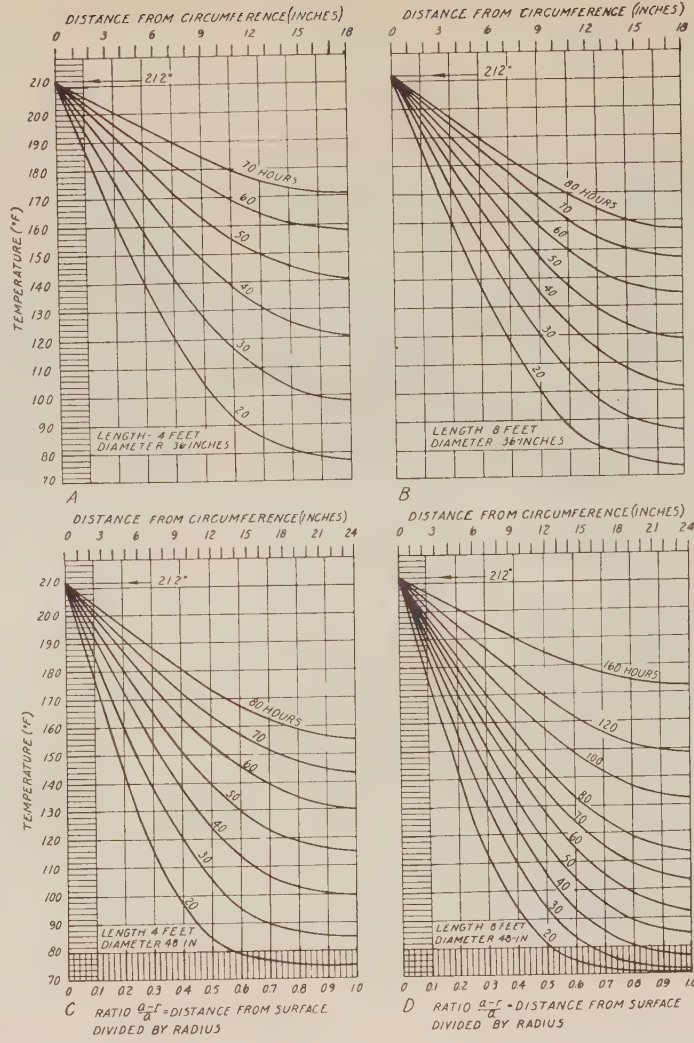

FIG. 13 TEMPERATURE DISTRIBUTION FROM CIRCUMFERENCE TO CENTER OF MID-SECTION; LOGS 4 AND 8 FT LONG AND 36 AND 48 IN. DIAM

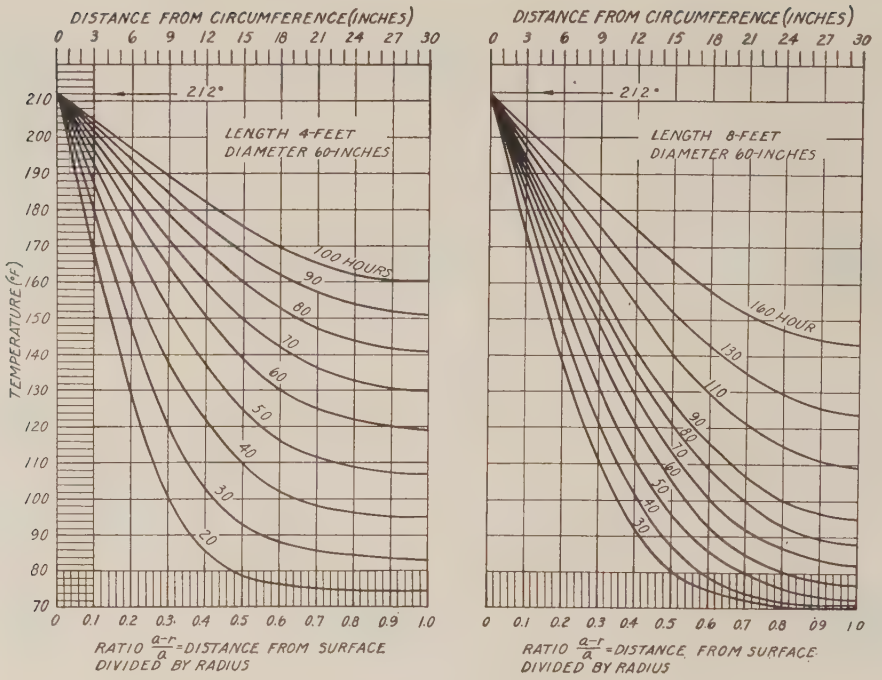

FIG. 14 TEMPERATURE DISTRIBUTION FROM CIRCUMFERENCE TO CENTER OF MID-SECTION; LOGS 4 AND 8 FT LONG AND 60 IN. DIAM

crease the temperature from 164 F to 170 F) is (2/3) 10 or 6 2/3 hr. The total time necessary to reach a temperature of 170 F is then 60 + 6.7 = 66.7 hr.

The same method would be used in finding the corresponding temperature when the heating period is known. If, for example, the heating period is 23.5 hr, and it is desired to find from Fig. 12*D* the temperature obtained at a point in the log half way between the axis and circumference, the figure shows that after 20 hr heating the temperature is 142 F, and after 30 hr heating it is 164 F, or an increase of 22 deg in 10 hr. The temperature increase above 142 F is then computed by the proportion (23.5 — 20):10 = x:22, from which it is found that the temperature change $x = \left(\frac{3.5}{10}\right) 22 = 7.7$ deg F. The temperature obtained after heating for 23.5 hr is then obtained by adding 7.7 deg to 142 F and is approximately 150 F.

If desired, the temperatures can be plotted against heating periods for any particular point in the timber, as for example at the center. Such curves would furnish a convenient method for reading directly the temperature obtained in a given time, or the corresponding heating period required to reach a definite temperature.

Group 3. In order to obtain curves that would show the temperature at various distances from the circumference at the mid-length of logs of any diameter between 12 and 60 in., data used in plotting the curves in group 2 were also used in preparing the curves shown in Figs. 15 and 16. Each curve in Figs. 15 and 16 was prepared by plotting the temperatures for each heating period for the logs of different diameters. Curves were then drawn through these plotted points for the same heating period. For heating periods over 50 hr, data were plotted only for timbers 36 in. or more in diameter.

Temperatures plotted in group 3, Figs. 15 and 16, are for points at distances from the circumferential surface of 1/4, 1/2, and 3/4 the radius, and for the center or where $\frac{a-r}{a} = 1$. When the required heating period or temperature is found between two time-temperature curves, the heating period or temperature can be found by using the proportional relation as explained for the curves in group 2.

The data show that it is not feasible to heat the large-diameter timbers at a considerable distance from the surface because of the extremely long heating periods required. For example, under the conditions assumed in making the temperature computations, Fig. 15*B* shows that if a temperature of 150 F is desired at a distance of 12 in. from the circumference of a log 4 ft diam, the heating period would be nearly 58 hr or 2.4 days. In such cases it would probably be better to heat to the minimum required temperature at a shorter distance from the circumference. After cutting to this depth the log could be reheated and with the reduced diameter the rate of heating would be much faster. This procedure would also avoid overheating the wood near the surface and at the ends.

The temperature curves shown in group 3 will be particularly useful for general purposes, since they show the relation of temperature and heating period for all diameters between 12 and 60 in. If it is desired to find the temperature at distances from the circumference that are intermediate between $\frac{a-r}{a} = 0.25, 0.50,$ 0.75, and 1.0, which are the distances shown in this group of curves, the data for any distance required may be found in the figures for group 2. These temperatures can then be plotted for the different diameter timbers as was done in preparing the curves for group 3. Temperatures for these four points can also be plotted against the proportional distance from the surface (as in Figs. 12 to 14, inclusive) for any diameter and any heating period. Smooth curves drawn through these plotted points will

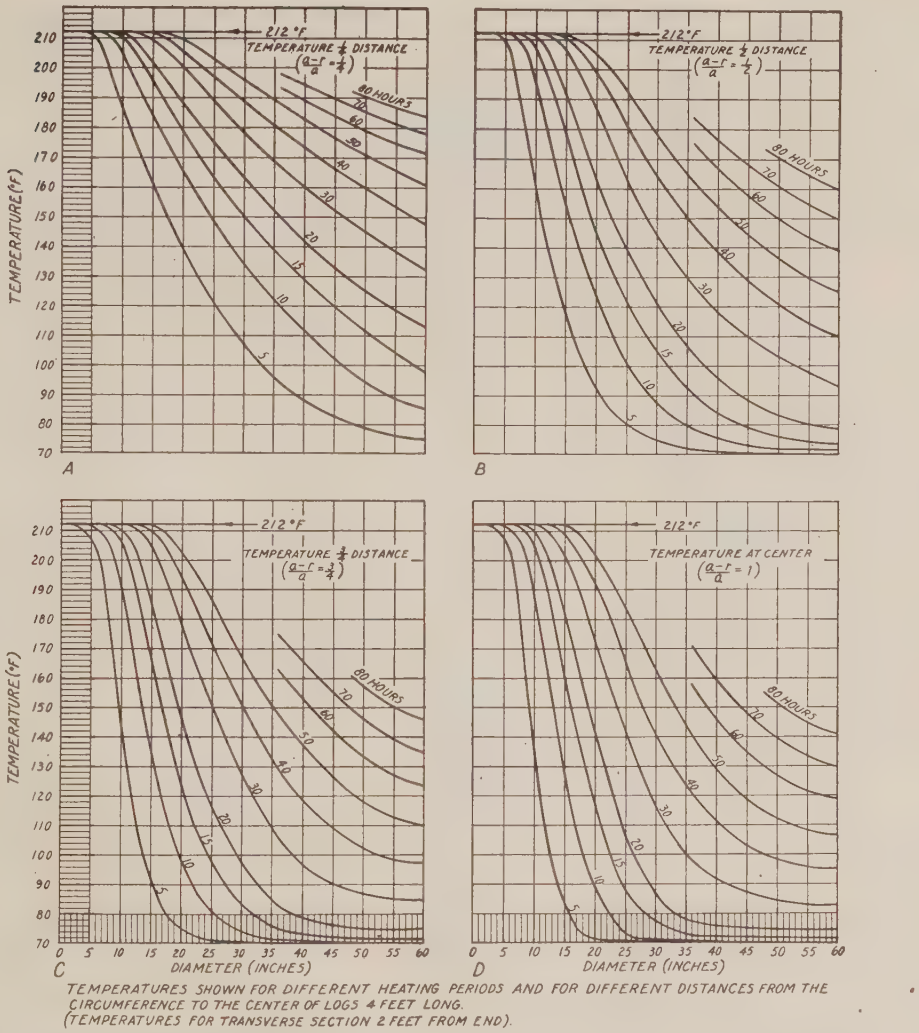

FIG. 15 TEMPERATURES OBTAINED AT DISTANCES OF 1/4, 1/2, AND 3/4 RADIUS AND AT CENTER OF LOGS 4 FT LONG

then show the approximate temperature for all distances from the surface to the center or axis of the timber.

Method of Using Fig. 3. Fig. 3 is a chart that furnishes a convenient method for finding the corresponding wood temperature when the heating conditions are different from those assumed in computing the temperature curves shown in the different groups.

The initial wood temperature U_a and the temperature U_x obtained in the wood after any given heating period are read on the left vertical scale, while the heating-medium temperature U_b is read on the right vertical scale. Values of U, the corresponding computed wood temperatures found from the figures, are given on the bottom scale.

In using Fig. 3, it is merely necessary to place a straightedge connecting the initial wood temperature U_a on the left scale with the heating-medium temperature U_b on the right scale. This is illustrated by the line connecting the initial wood temperature U_a = 50 F on the left scale with the heating temperature U_b = 180 F on the right scale. Assume, for example, that with the foregoing temperature conditions it is desired to find the corresponding computed temperature U (see Appendix for definition of symbols) at a point in the timber when the required temperature U_x is 148 F. This is found as follows:

Pass horizontally from 148 F on the left scale to the point of intersection with the line joining 50 and 180 F. Directly below this point of intersection U is found on the horizontal scale to be 177 F. The procedure is shown by the dotted line from 148 F. Again, let it be assumed that data from one of the charts shows that a temperature U of 133 F is obtained after heating for a period of T hr, and it is desired to find the temperature U_x that would be obtained at the same point, in the same time, and in the same timber when the initial wood temperature U_a is 50 F and the heating-medium temperature U_b is 180 F, instead of 70 and 212 F, the temperatures assumed in computing the data used in plotting the curves.

The temperature U_x is found in this case by passing vertically from U = 133 F on the horizontal scale to the line connecting 50 and 180 F. Directly across on the left scale U_x is found to be 108 F. These steps are shown in Fig. 3 by a dotted line connecting the temperature U = 133 F, and U_x = 108 F. This, is simply reversing the procedure for finding $U$when U_x is known.

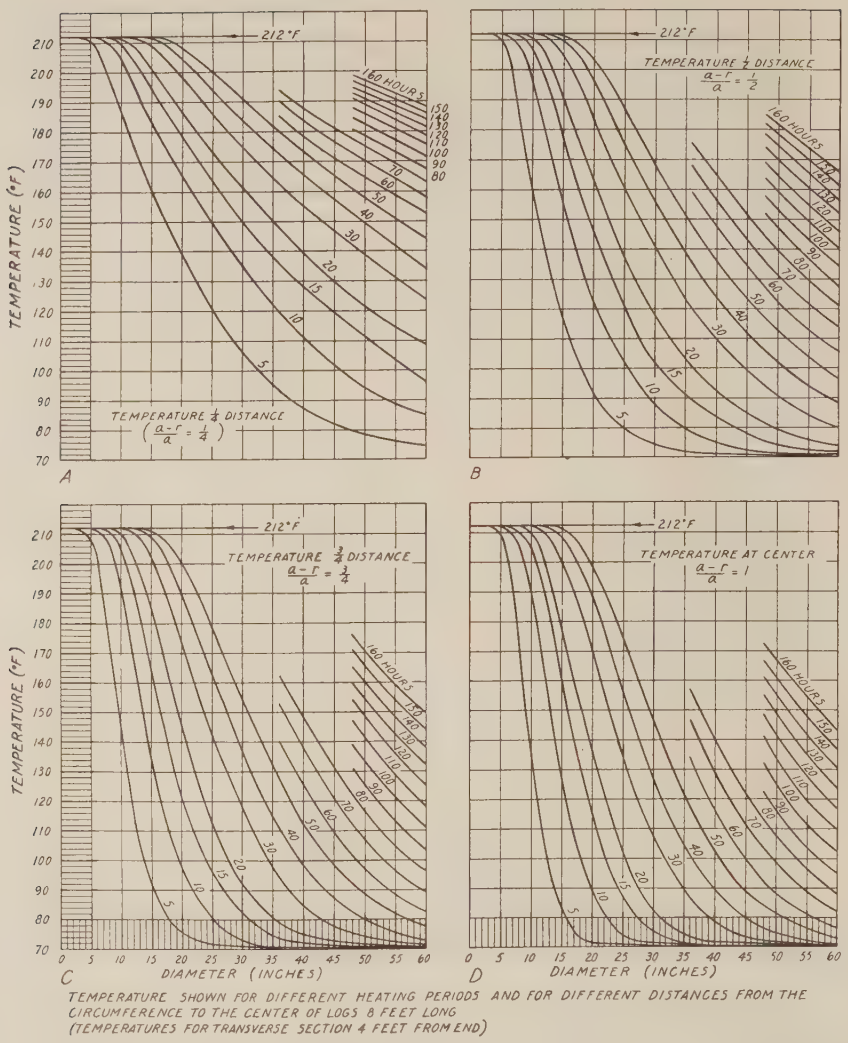

FIG. 16 TEMPERATURES OBTAINED AT DISTANCES OF 1/4, 1/2, AND 3/4 RADIUS AND AT CENTER OF LOGS 8 FT LONG

Fig. 3 is convenient to use in finding how the wood temperatures vary when different heating conditions are employed. For example, in the illustrations given, heating under the lower temperatures assumed for U_a and U_b the wood temperature will be (177 — 148) or 29 deg F lower at the point under consideration, than if the initial wood temperature had been 70 F, and the heating-medium temperature had been 212 F, which were the temperatures assumed in computing the curves. Similarly when any point is at a temperature U of 133 F (with the temperature conditions assumed in computing the curves), when heating under the lower temperature with U_a = 50 F and U_b = 180 F, the same point would be at a temperature of 108 F or 25 deg F lower. This chart can be used for finding either U_x or U instead of computing these temperatures from Equations $[B_1]$ and $[C_1]$ in the Appendix.

In general, problems relating to temperature changes will be either:

1 To find the time T_b required to obtain a specified temperature U_x at some particular point in a timber; or

2 To determine the temperature U_x that will be obtained when the time T_b and temperature U are known. In any problem the following variables are involved: Variables found by means of the temperature charts are U and T, and variables relating to the timber in question are U_a, U_b, U_x, and T_b. The relation between T and T_b is shown by Equation $[A]$ (Appendix), which is $T_b h_x^2 = T(0.00027)$

When U_a, U_b, and U_x are assumed, U is found from Equation $[C_1]$ (Appendix) or from Fig. 3. The corresponding time T required to obtain the temperature U can then be found from the proper chart, and the time T_b can be determined from Equation $[A]$.

When T_b, U_a, and U_b are given, T is found from Equation $[A]$, and the corresponding temperature U can be found from the proper chart. The temperature U_x can then be determined by means of Equation $[B_1]$ (Appendix) or from Fig. 3.

EXAMPLES SHOWING HOW CHARTS ARE USED[3]

Example 1. Data are as follows: Diameter of log = 22 in.;

[3] Refer to Appendix for definitions of symbols used.

length of log = 8 ft; species, yellow birch; heating medium, water; water temperature during heating period = 180 F = U_b; and initial wood temperature = 50 F = U_a.

Required to find the heating period (T_b) needed to obtain a temperature of 140 F (U_x) halfway between the circumference and center at the mid-length. In this case $\frac{a-r}{a} = \frac{1}{2}$. Therefore, for a log of this diameter, the distance from the surface = $^1/_2$ (11) = 5.5 in.

From Table 1 the average specific gravity of yellow birch (based on weight when oven-dry and volume when green) is found to be 0.55, and the diffusivity h_x^2 found in Fig. 1 for this specific gravity is about 0.000249 when the heating medium is water. In this example U_a, U_b, and U_x are given, while U, T, and T_b are to be determined.

The first step is to find U, using Equation [C_1] (Appendix), or Fig. 3. From Equation [C_1]

$$U = 212 - \left[\frac{(180-140)(142)}{(180-50)}\right] = 168 \text{ F}$$

This can be found readily from Fig. 3 by placing a straightedge connecting 50 F on the left scale with 180 F on the right scale, as shown by the straight line on this figure. Passing horizontally from 140 F on the left scale to this line the temperature U is found directly below on the lower scale to be 168 F, which is the temperature found by using Equation [C_1].

The second step is to find from Fig. 16(B) the time T required to reach a temperature of 168 F in a timber 22 in. diam and 8 ft long. Passing from 168 F in Fig. 16(B) to a point directly over the diameter of 22 in. shown on the abscissa, it is found that this point is between the curves for heating periods of 20 and 30 hr. The temperature after heating for 20 hr is found to be 153 F, and after heating for 30 hr is 174 F, or a temperature difference of 21 deg F. The proportion of the vertical distance between the two curves for the temperature of 168 F is then computed as $\frac{168-153}{174-153} = \frac{15}{21}$; and since the time interval is 10 hr, the time T is computed as $\left[20 + \frac{15}{21}(10)\right]$ or about 27.1 hr.

This is the time that would be required if the diffusivity were the same as that assumed in computing the temperature curves; but since the diffusivity for yellow birch was found to be about 0.000249, the time T_b must be computed from the relation shown by Equation [A] (Appendix) that gives

$$T_b = \frac{T(0.00027)}{0.000249} = (27.1)(1.084)$$

or 29.4 hr, which is the time to be determined.

If steam at 212 F were used as the heating medium, the diffusivity as indicated in Fig. 1, would be about 0.000276. With U_a = 50 F, U_b = 212 F, and the required temperature U_x = 140 F, the corresponding temperature U is determined from Equation [C_1] (Appendix) or from Fig. 3 to be 149 F. From Fig. 16(B), the time T required to reach a temperature of 149 F in a log 22 in. diam is found to be about 19 hr, and the required heating period T_b is $\frac{19(0.00027)}{0.000276} = 18.6$ hr.

Example 2. With the same data as given for example 1 find the temperature that would be obtained at $^1/_4$ the distance from the circumference to the center when the heating period T_b is 25 hr. In this example, $\frac{a-r}{a} = {}^1/_4$, and the distance from the circumference = $^1/_4$ (11) = $2^3/_4$ in. instead of $5^1/_2$ in. as in example 1. In this example U_a, U_b, and T_b are given, and T, U, and U_x are to be found.

First, find T from Equation [A] (Appendix). In this case

$$T = \frac{T_b(h_x^2)}{h^2} = \frac{25(0.000249)}{0.00027} = 23 \text{ hr, approximately}$$

Next, find U for this heating period. From Fig. 16(A) the temperature U is found to be about 185 F, after heating for 23 hr.

Then find the temperature U_x from Equation [B_1] (Appendix), or from Fig. 3.

Using Equation [B_1]

$$U_x = 180 - \left[\frac{(180-50)(212-185)}{142}\right] = 155 \text{ F}$$

which is the temperature to be determined. This temperature U_x can also be found from Fig. 3 by placing a straightedge on 50 F on the left scale and on 180 F, right scale. Reading up from 185 F on the bottom scale to the line connecting 50 F and 180 F, and directly across to the left scale, the temperature U_x is found to be about 155 F as computed from Equation [B_1] (Appendix).

If steam at 212 F were used as the heating medium the diffusivity would be 0.000276 (as found for example 1), and T would be $\frac{25(0.000276)}{0.00027} = 25.6$ hr. The temperature U for this heating period is found from Fig. 16(A) to be about 188 F. When U_a = 50 F, and U_b = 212 F, the corresponding temperature U_x is found from Equation [B_1], or from Fig. 3, to be about 185 F.

Example 3. Data are as follows: Diameter of log = 48 in.; length of log = 8 ft; species, Coast Douglas fir; heating medium, water; water temperature during heating period = 190 F = U_b; and initial wood temperature = 60 F = U_a.

Required to find the temperature U_x obtained at a distance of 15 in. (Z) from the end surface and at a distance from the circumference equal to $^1/_4$ the radius when the log section has been heated for 30 hr (T_b). In this example $\frac{a-r}{a} = {}^1/_4$; hence the distance from the circumference = $^1/_4$ of 24 or 6 in. In this example U_a, U_b, and T_b are given, and T, U, and U_x are to be determined.

From Table 1 the average specific gravity of green Coast Douglas fir is found to be 0.45, and from Fig. 1 the corresponding diffusivity for heating in water is found to be about 0.000293 = h_x^2.

The first step is to find the heating period T using Equation [A] (Appendix)

$$T = \frac{T_b(h_x^2)}{0.00027} = \frac{30(0.000293)}{0.00027} = 32.6 \text{ hr}$$

Because of the higher diffusivity of the Douglas fir, in comparison with the diffusivity of 0.00027 used in computing the temperature curves, the Douglas fir heats $\frac{(0.000293-0.00027)}{0.00027}100 = 8.5$ per cent faster, and the temperature attained in 30 hr at the point under consideration would be the same (for the same heating conditions) as that reached after 32.6 hr heating when the wood has a diffusivity of 0.00027.

The second step is to find the temperature U in Fig. 9. From this figure the temperature U is found to be 155 F $\left(\text{for } Z = 15 \text{ in. and } \frac{a-r}{a} = \frac{1}{4}\right)$ after a heating period of 30 hr, and to be 169 F when the heating period is 40 hr. After 30 hr heating, the temperature at the point given would then be computed as

$$\left[155 + \left(\frac{32.6 - 30}{10}\right)(169 - 155)\right] = 159 \text{ F approximately}$$

This is the temperature U, or the temperature that would be obtained if $U_a = U_0 = 70$ F and $U_b = U_1 = 212$ F; but since U_a is assumed as 60 F, and U_b as 190 F, U_x is determined by using Equation [B_1] (Appendix), or from Fig. 3, and is found to be about 141 F which is the temperature to be determined.

This is similar to example 2, except that the point under consideration is between the end surface and the transverse mid-section, and the data are obtained from temperature curves shown in group 1.

Example 4. With the data given in example 3 find the heating period T_b required to obtain a temperature of $U_x = 160$ F for the same point in the log. In this example U_a, U_b, and U_x are given, and U, T, and T_b are to be determined.

The first step is to find the corresponding temperature U when $U_a = 60$ F, $U_b = 190$ F, and $U_x = 160$ F. From Equation [C_1] (Appendix), or from Fig. 3, U is found to be about 179 F.

Fig. 9 shows that when the distance from the end = 15 in. and the distance from the circumference $(a - r) = 6$ in. or $^1/_4$ the radius, the temperature of 179 F is between the temperature curves for heating periods of 50 and 60 hr. After heating for 50 hr, the temperature is 177.5 F, and after heating for 60 hr, it is about 184 F. The heating period required to reach 179 F would then be computed as

$$\left[\left(\frac{179 - 177.5}{184 - 177.5}\right)10 + 50\right] = 52.3 \text{ hr}$$

Since this is the time T required when the diffusivity is 0.00027 the time T_b is as follows

$$T_b = \frac{52.3(0.00027)}{0.000293} = 48.2 \text{ hr}$$

This is similar to example 1 except that the point at which the temperature is to be determined is between the end surface and transverse mid-section.

BIBLIOGRAPHY

1 "Studies of Heat Conduction in Wood—Results of Steaming Green Round Southern Pine Timbers," by J. D. MacLean, Proceedings of the American Wood Preservers' Association, 1930, pp. 197–217.

2 "Studies of Heat Conduction in Wood—Part II—Results of Steaming Green Sawed Southern Pine Timber," by J. D. MacLean, Proc. American Wood Preservers' Association, 1932, pp. 303–329.

3 "Temperatures in Green Southern Pine Timbers After Various Steaming Periods," by J. D. MacLean, Proc. American Wood Preservers' Association, 1934, pp. 355–373.

4 "Temperature and Moisture Changes in Coast Douglas Fir," by J. D. MacLean, Proc. American Wood Preservers' Association, 1935, pp. 77–103.

5 "Average Temperature and Moisture Reduction Calculations for Steamed Round Southern Pine Timbers," by J. D. MacLean, Proceedings of the American Wood Preservers' Association, 1936, pp. 256–279.

6 "Relation of Wood Density to Rate of Temperature Change in Wood in Different Heating Mediums," by J. D. MacLean, Proc. American Wood Preservers' Association, 1940, pp. 220–248.

7 "Thermal Conductivity of Wood," by J. D. MacLean, *Heating, Piping and Air Conditioning*, vol. 13, 1941, pp. 380–391. Same in Trans. American Society of Heating and Ventilating Engineers, vol. 47, 1941, pp. 323–354. Abstract in *Mechanical Engineering*, vol. 63, 1941, pp. 734–736.

8 "Rate of Temperature Change in Wood Panels Heated Between Hot Plates," by J. D. MacLean, Forest Products Laboratory Mimeo. No. R1299, 1942.

9 "Method of Computing the Rate of Temperature Change in Wood and Plywood Panels When the Two Opposite Surfaces Are Maintained at Different Temperatures," by J. D. MacLean, Forest Products Laboratory Mimeo. No. R1406, 1943.

10 "Rate of Temperature Change in Laminated Timbers Heated in Air Under Controlled Relative Humidity Conditions," by J. D. MacLean, Forest Products Laboratory Mimeo. No. R1434, 1943.

Appendix

Method of Computing Temperatures in Round Timbers of Short Length Where End Heating as Well as Heating in the Radial Direction Must Be Taken Into Consideration

In order to derive an equation for computing the temperature U at any point r inches from the axis and Z inches from one of the end surfaces, it is necessary to solve the following partial differential equation

$$\frac{\delta U}{\delta T} = \left[h^2\left\{\frac{\delta^2 U}{\delta r^2} + \frac{1}{r}\frac{\delta U}{\delta r}\right\} + q^2\frac{\delta^2 U}{\delta Z^2}\right] \quad \ldots\ldots\ldots [1]$$

In this equation h^2 is the diffusivity factor for heating in the radial direction and q^2 is the diffusivity factor for heating in the longitudinal direction.

Equation [1] must be solved, subject to the following boundary conditions: Let $\theta = (U - U_1)$, where U_1 is the temperature of the heating medium and U is the temperature at the point under consideration at any time T.

Let U_0 = initial wood temperature; a = average radius of log, and L = length in inches.

If $\theta = (U - U_1)$, $U = U_0$ and $\theta = (U_0 - U_1)$ when $T = 0$

$$\left.\begin{array}{l}\theta = 0 \text{ when } r = a \\ \qquad\qquad Z = 0 \\ \qquad\qquad Z = L\end{array}\right\} \quad \text{and } T > 0$$

$\theta = f(r,Z)$ when $T = 0$

Substituting θ in Equation [1]

$$\frac{\delta\theta}{\delta T} = \left[h^2\left\{\frac{\delta^2\theta}{\delta r^2} + \frac{1}{r}\frac{\delta\theta}{\delta r}\right\} + q^2\frac{\delta^2\theta}{\delta Z^2}\right] \quad \ldots\ldots\ldots [1a]$$

A solution of differential Equation [1a] to meet the boundary conditions gives

$$\theta = \sum_{m=1}^{m=\infty}\sum_{n=1}^{n=\infty} Am,ne^{-T\left(h^2\lambda_n^2 + \frac{q^2\pi^2m^2}{L^2}\right)}\sin\frac{m\pi Z}{L}J_0(\lambda_n r). \quad [2]$$

where

$$Am,n = \frac{4}{a^2L[J_1(\lambda_n a)]^2}\int_0^a dr\int_0^L rf(r,\mu)J_0(\lambda_n r)\sin\frac{m\pi\mu}{L}\,d\mu$$

When $f(r,\mu)$ is a constant and equal to $(U_0 - U_1)$, as in this case

$$Am,n = \frac{4(U_0 - U_1)}{a^2L[J_1(\lambda_n a)]^2}\int_0^a dr\int_0^L rJ_0(\lambda_n r)\sin\frac{m\pi\mu}{L}\,d\mu$$

$$= \left[\frac{4(U_0 - U_1)}{L\lambda_n aJ_1(\lambda_n a)}\right]\left(\frac{L}{m\pi}\right)(1 - \cos m\pi)$$

$$= \frac{8(U_0 - U_1)}{m\pi\lambda_n aJ_1(\lambda_n a)} \text{ when } m \text{ is odd, and } = 0 \text{ when } m \text{ is even}$$

Substituting the value

$$\frac{8(U_0 - U_1)}{m\pi\lambda_n aJ_1(\lambda_n a)}$$

for Am,n and the temperature difference $(U - U_1)$ for θ, Equation [2] may be written

$$U - U_1 = 8(U_0 - U_1) \sum_{m=1}^{m=\infty} \sum_{n=1}^{n=\infty} \frac{1}{m\pi\lambda_n a J_1(\lambda_n a)} \sin\frac{m\pi Z}{L} J_0(\lambda_n r) e^{-T\left(h^2\lambda_n^2 + \frac{\pi^2 q^2 m^2}{L^2}\right)} \quad \ldots\ldots\ldots [3]$$

In the foregoing equations T is the time in seconds, $J_0(\lambda_n r)$ and $J_1(\lambda_n a)$ are Bessel functions of the zeroth and first order, respectively, and $(\lambda_n r) = x$ in $J_0(x)$ and $J_1(x)$.[4] Term λ_n is a root of $J_0(\lambda_n a) = 0$ and e is the base of the Napierian logarithms.

Writing the first few terms of Equation [3]

$$\begin{aligned} U = U_1 + (U_0 - U_1)\frac{8}{\pi}\Bigg[& \frac{1}{\lambda_1 a J_1(\lambda_1 a)} \sin\frac{\pi Z}{L} J_0(\lambda_1 r) e^{-T\left(h^2\lambda_1^2 + \frac{\pi^2 q^2}{L^2}\right)} \\ & + \frac{1}{\lambda_1 a J_1(\lambda_1 a)} \frac{1}{3} \sin\frac{3\pi Z}{L} J_0(\lambda_1 r) e^{-T\left(h^2\lambda_1^2 + \frac{9\pi^2 q^2}{L^2}\right)} \\ & + \frac{1}{\lambda_1 a J_1(\lambda_1 a)} \frac{1}{5} \sin\frac{5\pi Z}{L} J_0(\lambda_1 r) e^{-T\left(h^2\lambda_1^2 + \frac{25\pi^2 q^2}{L^2}\right)} + \ldots \\ & + \frac{1}{\lambda_2 a J_1(\lambda_2 a)} \sin\frac{\pi Z}{L} J_0(\lambda_2 r) e^{-T\left(h^2\lambda_2^2 + \frac{\pi^2 q^2}{L^2}\right)} \\ & + \frac{1}{\lambda_2 a J_1(\lambda_2 a)} \frac{1}{3} \sin\frac{3\pi Z}{L} J_0(\lambda_2 r) e^{-T\left(h^2\lambda_2^2 + \frac{9\pi^2 q^2}{L^2}\right)} + \ldots \\ & + \frac{1}{\lambda_3 a J_1(\lambda_3 a)} \sin\frac{\pi Z}{L} J_0(\lambda_3 r) e^{-T\left(h^2\lambda_3^2 + \frac{\pi^2 q^2}{L^2}\right)} \\ & + \frac{1}{\lambda_3 a J_1(\lambda_3 a)} \frac{1}{3} \sin\frac{3\pi Z}{L} J_0(\lambda_3 r) e^{-T\left(h^2\lambda_3^2 + \frac{9\pi^2 q^2}{L^2}\right)} + \ldots \\ & + \frac{1}{\lambda_4 a J_1(\lambda_4 a)} \sin\frac{\pi Z}{L} J_0(\lambda_4 r) e^{-T\left(h^2\lambda_4^2 + \frac{\pi^2 q^2}{L^2}\right)} \\ & + \frac{1}{\lambda_4 a J_1(\lambda_4 a)} \frac{1}{3} \sin\frac{3\pi Z}{L} J_0(\lambda_4 r) e^{-T\left(h^2\lambda_4^2 + \frac{9\pi^2 q^2}{L^2}\right)} + \ldots \Bigg]. \quad [4] \end{aligned}$$

The number of terms that must be used in making temperature calculations will depend to a considerable extent upon the value of the negative exponent of the Napierian log base e. Since this exponent involves the time T and the dimensions of the timber (as well as the diffusivity factors h^2 and q^2), the series converges more rapidly as the time T increases, and as the diameter and length of the timber decrease, since the values of λ vary inversely with the radius, and the second term of the negative exponent varies inversely as the square of the length L.

[4] Tables of Bessel's functions for different values of x and roots of $J_n(x) = 0$ are given in "Smithsonian Physical Tables," Smithsonian Institute, Washington, D. C., and in "Fourier Series and Spherical Harmonics," by W. E. Byerly, Ginn and Co., 1893, New York, N. Y.

Method of Using Figures When Diffusivity, Heating Conditions, or Both, Are Different From Those Assumed in Computing the Time-Temperature Curves

Equation [A] which follows, shows the relation of time and diffusivity, and Equations [B] and [C] show the method of finding the corresponding wood temperatures when the heating conditions are different from those assumed in computing the data for the temperature curves shown in the figures.

Symbols applying to computed data in figures are as follows:

U_0 = initial wood temperature, assumed as 70 F
U_1 = heating-medium temperature, assumed as 212 F
h^2 = diffusivity in radial direction = 0.00027 sq in. per sec
q^2 = diffusivity in longitudinal direction = $2.52(h^2)$ = 0.00068
U = temperature obtained in given time T at some particular distance from surface. Values of U are temperatures within wood at distance from surface shown by figure
T = time of heating (in hours) necessary to obtain temperature U. This period is found from figure for diameter and length under consideration

Symbols, applying to temperature computations when the diffusivity, heating conditions, or both, are different from those used in computing the data plotted in the figures, are as follows:

U_a = any initial wood temperature
U_b = any heating-medium temperature
h_x^2 = any value of diffusivity for transverse direction, sq in. per sec

Since the diffusivity in the longitudinal direction (q^2) is taken as approximately $2\frac{1}{2}$ times the diffusivity in the transverse direction for the calculated temperatures, only values of h_x^2 need to be considered.

U_x = temperature obtained at definite point in timber when initial wood temperature U_a, heating temperature U_b, or both, are different from U_0 = 70 F, and U_1 = 212 F, the initial wood and heating-medium temperatures assumed in computing curves shown in figure
T_b = time of heating (in hours) required to obtain temperature U_x when either diffusivity h_x^2, initial wood temperature U_a, the heating-medium temperature U_b, or all three variables are different from corresponding values used in computing data for curves

Relation of Heating Period and Diffusivity. The relation of the heating period T and the heating period T_b is shown by the equation

$$T_b(h_x^2) = T(0.00027) \ldots\ldots\ldots\ldots [A]$$

In this equation T_b is the heating period assumed or to be determined when the wood has a diffusivity h_x^2, and T is the heating period found from the figure for the timber in question. Values of h_x^2 for green wood of any given specific gravity can be found in Fig. 1, when either water or steam is used as the heating medium. Specific-gravity values for different woods, based on weight when oven-dry and volume when green, are given in Table 1.

Relation of Initial Wood Temperature, Heating-Medium Temperature, and Temperatures Obtained in Wood. A simple proportional relation exists between the temperatures obtained under any given heating conditions. For example, the relation of the temperatures obtained when the initial wood temperature U_a, the heating-medium temperature U_b, or both, are different from those assumed in making temperature computations are expressed by the equation

$$\frac{(U_b - U_x)}{(U_b - U_a)} = \frac{(U_1 - U)}{(U_1 - U_0)}$$

When U_a, U_b, and U are known it is necessary to determine U_x, the wood temperature obtained when U_a, U_b, or both are different from U_0 and U_1. Solving for U_x in terms of U_b, U_a, U_1, U_0, and U gives

$$U_x = U_b - \left[\frac{(U_b - U_a)(U_1 - U)}{(U_1 - U_0)}\right] \ldots\ldots\ldots [B]$$

When U_x, U_a, and U_b are known it is necessary to solve for U to find the heating period T from the proper figure. Solving for U in terms of U_a, U_b, U_x, U_0, and U_1 gives

$$U = U_1 - \left[\frac{(U_b - U_x)(U_1 - U_0)}{(U_b - U_a)}\right] \ldots\ldots\ldots [C]$$

If the values of $U_0 = 70$ F and $U_1 = 212$ F (the initial wood and heating-medium temperatures assumed in making the computations) are substituted in Equations $[B]$ and $[C]$

$$U_x = U_b - \left[\frac{(U_b - U_a)(212 - U)}{142}\right] \ldots\ldots\ldots [B_1]$$

$$U = 212 - \left[\frac{(U_b - U_x)(142)}{(U_b - U_a)}\right] \ldots\ldots\ldots [C_1]$$

Values of U_x and U can also be determined by means of Fig. 3, as explained in the text.

(Owing to travel emergency conditions existing when this paper was presented, discussion will be accepted until February 10, 1946)

Flame-Temperature Measurements in Internal-Combustion Engines

By O. A. UYEHARA,[1] P. S. MYERS,[2] K. M. WATSON,[3] and L. A. WILSON[4]

The theory, development, and calibration of an electro-optical pyrometer, capable of determining instantaneous true temperatures of luminous flames, are described. A description is also given of auxiliary apparatus used with the electro-optical pyrometer to obtain simultaneous values of pressure, temperature, and crank position in an internal-combustion engine. Typical data obtained with this instrumentation as applied to a Diesel engine are included.

THE need for instantaneous and continuous temperature data throughout the combustion process in internal-combustion engines has long been recognized. Combustion rates, chemical equilibria, fuel vaporization, ignition lag, and heat transfer are all affected by temperature. Measurement of high temperatures in internal-combustion engines is complicated by the rapidity of temperature fluctuations and by variations in flame thickness and emissivity.

About two years ago the chemical-engineering and mechanical-engineering departments of the University of Wisconsin initiated a co-operative Diesel-fuel research program, the objectives of which could best be achieved if precise combustion temperature and pressure data were obtainable. A study of methods used by previous investigators to measure combustion temperatures showed that thermocouples (1, 2, 3),[5] the sodium-line reversal method (4, 5, 6), the total-radiation method (7 8), and the "two-wire" method (9) are obviously not adaptable to instantaneous and continuous measurements. The "additive" method, as reported by Graff (10), is instantaneous, but it is useless when radiation from carbon particles becomes appreciable; and, in addition, the transformation of radiation to temperature is laborious and involves the use of some questionable assumptions.

Hottel and Broughton (11) employed an optical pyrometer with filters, using two different wave lengths of radiation to measure the temperature of a steady luminous flame, and established the validity of the two-color principle. Although the Hottel-Broughton pyrometer was not directly applicable to the proposed combustion-engine research, the two-color principle appeared to be feasible. This led to the development of an electro-optical pyrometer which is instantaneous in response to flame-temperature variations and will determine the temperature at every point in the combustion process for an individual cycle of the engine. Auxiliary instruments were also developed for the measurement of combustion-chamber pressures, injection-nozzle opening, and the indication of completion of combustion, all in relation to crank position. It is believed that this instrumentation may prove useful in a variety of applications, particularly where rapidly fluctuating high temperatures and pressures are encountered.

[1] Department of Chemical Engineering, University of Wisconsin, Madison, Wis.

[2] Department of Mechanical Engineering, University of Wisconsin, Madison, Wis. Jun. A.S.M.E.

[3] Professor of Chemical Engineering, University of Wisconsin, Madison, Wis.

[4] Professor of Mechanical Engineering, and Chairman, Department of Mechanical Engineering, University of Wisconsin, Madison, Wis. Mem. A.S.M E.

[5] Numbers in parentheses refer to the Bibliography at the end of the paper.

Contributed by the Oil and Gas Power Division and presented at a meeting of the Cleveland Section, Cleveland, Ohio, May, 1945, of The American Society of Mechanical Engineers.

The Electro-Optical Pyrometer

The relationship between the intensity of monochromatic radiation from a black body, the wave length of the radiation, and the temperature of the black body is expressed by Wien's law

$$J = C_1\lambda^{-5}e^{\frac{-C_2}{\lambda T}} \quad \text{.....[1]}$$

where

J = intensity of radiation at wave length λ
C_1, C_2 = known constants
λ = monochromatic wave length
e = base for Naperian logarithms
T = absolute black-body temperature

A graphical representation of Equation [1] is shown in Fig. 1.

For a nonblack body, it is necessary to introduce a new factor (E_λ) called the monochromatic emissivity, which is defined as the ratio of the intensity of radiation from a nonblack body to that from a black body at the particular temperature and wave length involved. Thus, for a nonblack body

$$J = E_\lambda C_1\lambda^{-5}e^{\frac{-C_2}{\lambda T}} \quad \text{.....[2]}$$

The intensity of radiation from a nonblack body may also be represented mathematically by

$$J = C_1\lambda^{-5}e^{\frac{-C_2}{\lambda T_A}} \quad \text{.....[3]}$$

where T_A is the apparent temperature and is defined as the temperature at which a black body would have the same monochromatic intensity of radiation as the nonblack body.

Equating [2] and [3]

$$E^\lambda = e^{\frac{-C_2}{\lambda}\left(\frac{1}{T_A}-\frac{1}{T}\right)} \quad \text{.....[4]}$$

or

$$\ln E_\lambda = -\frac{C_2}{\lambda}\left(\frac{1}{T_A}-\frac{1}{T}\right) \quad \text{.....[4a]}$$

This is the form of equation that is generally used to correct optical pyrometers for departure from black-body conditions where the monochromatic emissivity is known. These relations are shown graphically in Fig. 1, where the dotted line represents a nonblack body at 4000 deg R. The apparent temperature at λ_A would be 3000 deg R, and at λ_B 2500 deg R. If the monochromatic emissivity E_λ were the same at all wave lengths, Equation [4a] might be written for each of two different wave lengths, λ_A and λ_B, and the monochromatic emissivities equated. Then, by determining the apparent temperatures at λ_A and λ_B,

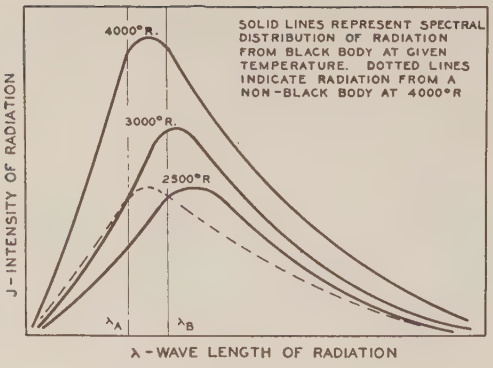

FIG. 1 GRAPHICAL REPRESENTATION OF WIEN'S LAW

the true temperature of a nonblack body might be calculated without knowing its emissivity.

In general, monochromatic emissivities are not equal at different wave lengths. It has been shown by Hottel and Broughton (11) that the monochromatic emissivity of a luminous flame is expressed by an equation of the form

$$E_\lambda = 1 - e^{\frac{-KL}{(\lambda)^\alpha}} \quad \ldots\ldots\ldots\ldots\ldots\ldots [5]$$

where

K = absorption constant per unit flame thickness and is independent of wave length
L = flame thickness
α = constant for limited wave-length range

It was also shown by Hottel and Broughton (11) that the true temperature of a flame could be determined by using this relationship between the monochromatic emissivities and measuring the apparent temperature at the two wave lengths involved. Following the development of Hottel and Broughton, substitution of Equation [5] into Equation [4*a*] gives

$$\ln\left(1 - e^{\frac{-KL}{\lambda^\alpha}}\right) = \frac{-C_2}{\lambda}\left(\frac{1}{T_A} - \frac{1}{T}\right) \quad \ldots\ldots\ldots [6]$$

Writing Equation [6] in exponential form and rearranging

$$e^{\frac{-KL}{(\lambda)^\alpha}} = 1 - e^{\frac{-C_2}{\lambda}\left(\frac{1}{T_A} - \frac{1}{T}\right)} \quad \ldots\ldots\ldots\ldots [7]$$

Taking the logarithm of each side and rearranging

$$-KL = (\lambda)^\alpha \ln\left[1 - e^{\frac{-C_2}{\lambda}\left(\frac{1}{T_A} - \frac{1}{T}\right)}\right] \quad \ldots\ldots\ldots [8]$$

Two such equations may be written for two different wave lengths, denoted by the subscripts 1 and 2. Equating the two KL terms, which are equal over a limited wave-length range, and rearranging, gives the following

$$\left[1 - e^{\frac{-C_2}{\lambda_1}\left(\frac{1}{T_{A1}} - \frac{1}{T}\right)}\right]^{\frac{(\lambda_1)^{\alpha_1}}{(\lambda_2)^{\alpha_2}}} = \left[1 - e^{\frac{-C_2}{\lambda_2}\left(\frac{1}{T_{A2}} - \frac{1}{T}\right)}\right] \quad [9]$$

If λ_1, λ_2, α_1, and α_2 are known, and the two apparent temperatures are measured, the true flame temperature T is the only unknown in Equation [9]. Once the true temperature is determined the term KL may be evaluated, thus giving an indication of the flame emissivity. Thus true flame temperatures may be obtained from two optical pyrometers which simultaneously record apparent temperatures corresponding to different wave lengths of radiation.

Apparatus. In the use of this method for measuring true flame temperatures, substantially monochromatic radiation of two different wave lengths must be obtained. Although filters have generally been used, a system of lenses and prisms was adopted in this work. This method does not require a division of the radiation as would the use of filters. Furthermore, the lenses and prisms are not affected by temperature and humidity changes. To obtain sufficient dispersion two prisms were used.

A schematic diagram of the electro-optical pyrometer is shown in Fig. 2. The radiation from the combustion chamber is focused by a lens system on a limiting diaphragm which has an opening somewhat smaller than the image of the source of radiation. Thus vibration or other small movements of the source of radiation do not cause a variation in the light permitted to pass through the limiting diaphragm. After the radiation passes the diaphragm it is paralleled by a lens, dispersed by the two prisms, and again focused by another lens. A barrier containing two slits is situated at the focal point of this lens. A phototube is located behind each slit in such a position that it is actuated by the radiation passing through the slit. A vacuum-type phototube with a caesium-oxide-silver surface was chosen because of its instantaneous response, its electrical stability, and its spectral response curve. The outputs from the phototubes are amplified and impressed on the vertical plates of two single-beam cathode-ray tubes. For this particular application the cathode rays are displaced horizontally in proportion to the engine crank position. In this manner a graph of apparent temperature as ordinates and crank angle as abscissas is repeatedly traced on each cathode-ray screen.

The amplifiers are of the direct-coupled type designed for use with vacuum-type phototubes and have a practically flat frequency response curve from 0 to approximately 15,000 cycles per sec. Two stages of amplification are required for the desired sensitivity. Batteries are used in the first-stage amplifiers to insure stability of operation. Voltage for the second-stage push-pull amplifiers is supplied from a voltage-regulated power pack.

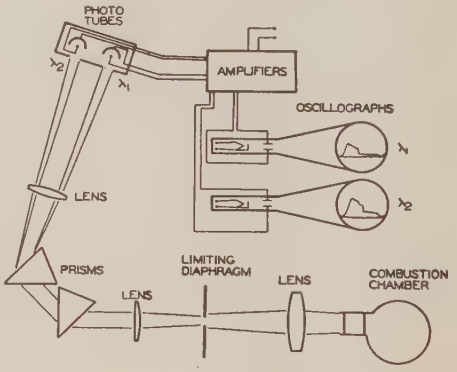

FIG. 2 SCHEMATIC DIAGRAM OF ELECTRO-OPTICAL PYROMETER

Black-Body Calibration. Care was necessary to insure an accurate calibration of the electro-optical pyrometer since the method depends on the measurement of two apparent temperatures of nearly equal values and the use of this small temperature difference in calculating the true temperature. Two methods of calibration were considered; (*a*) calibration by the use of a broad-ribbon tungsten lamp with known emissivity values and, (*b*) calibration by sighting directly upon a black body.

A search of the literature on the emissivity of tungsten (12, 13, 14) revealed wide disagreement both as to the values to be used for emissivities and as to their variation with temperature and with wave length. Accordingly, the black body was used for

calibration purposes and the broad-ribbon tungsten lamp was retained as a secondary standard. Its use in this connection is described later.

Black-body conditions were established by drilling a hole with a conical bottom in a graphite block. The graphite block was heated in the crucible of an induction furnace, and an optical pyrometer with a lamp calibrated by the Bureau of Standards was used to determine the black-body temperature.

Above 2800 F, the formation of smoke from impurities in the graphite began to cause a departure from black-body conditions. In order to eliminate this difficulty the graphite block was blanketed with an atmosphere of inert nitrogen. This prevented the formation of smoke until a temperature of about 3100 F was reached.

The procedure during the calibration process was as follows: The current to the induction furnace was adjusted and when the black body had reached a constant temperature a reading was then taken with the standard optical pyrometer. The electro-optical pyrometer was then placed in position viewing the black body. The corresponding cathode-ray deflections at the two wave lengths were measured by means of dividers and a steel scale graduated in hundredths of an inch. The electro-optical pyrometer was then removed from its position viewing the black body, and another reading of the black-body temperature was taken with the standard optical pyrometer. The average of the temperatures as measured by the standard optical pyrometer was taken as the correct temperature corresponding to the deflections noted. The foregoing procedure was repeated at various temperatures until the entire temperature range, representing zero to maximum deflection on the cathode-ray tubes had been covered. These data are shown in Fig. 3.

After the final calibration of the electro-optical pyrometer had been completed, it was used to calibrate the broad-ribbon tungsten lamp which was to be employed as a secondary standard. A rigid holder for the tungsten lamp was necessary to obtain reproducible results since the temperature of the filament was not uniform over its various portions. The resulting graph of deflection versus current is shown in Fig. 4. Since these data are from several different runs, the reproducibility of results is clearly established.

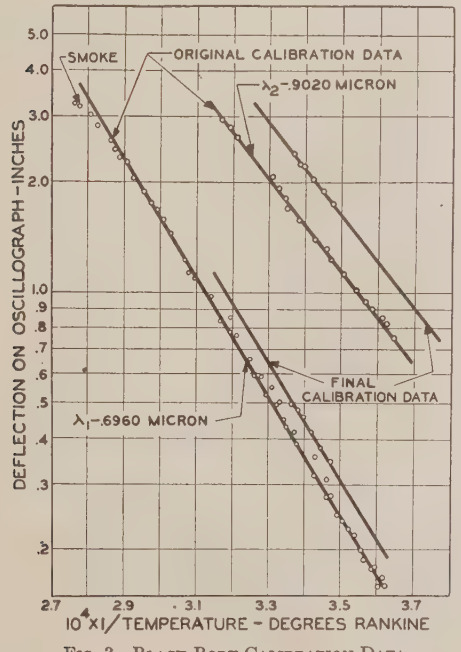

FIG. 3 BLACK-BODY CALIBRATION DATA

The original tungsten lamp proved defective and the filament broke after a short period of use. Consequently, it was necessary to repeat the black-body calibration at a few temperatures in order to standardize a second tungsten lamp. No effort was made to reproduce the original calibration and since the calibration data plot as straight lines in Fig. 3, the entire temperature range was not covered.

Determination of Equation Constants. In order to calculate true temperatures from Equation [9] it was necessary that λ_1 and λ_2 and the constants α_1 and α_2 be evaluated.

Two factors had to be considered in choosing the wave lengths to be used. Approximately equal oscillograph deflections were desired for accuracy in scaling. Assuming equal electronic amplification, the deflection is a function of the spectral sensitivity of the phototube and the intensity of radiation at the temperature and wave length involved. Rassweiler and Withrow have shown (15, 16) that in the range of wave lengths below 0.5 micron a small amount of spectral energy from intermediate products of combustion is present and might cause a departure from the relationships established between the monochromatic emissivities of a luminous flame. There is also a number of strong water-vapor absorption and emission bands (17, 18, 19) from 0.190 micron to 0.36 micron, and from 0.95 micron to 314 microns, and strong CO_2 bands (18, 19) in the region of 14 to 16 microns. However, Rassweiler and Withrow (15, 16), Graff (10), and Landen and Blanc (20) found that black-body spectral distribution existed in the flames studied at wave lengths above 0.6 micron. Accordingly, the phototubes were placed in the region of 0.6 to 1.0 micron and experimentally shifted in this region to obtain approximately equal responses under engine operating conditions.

It was first attempted to determine the values of the wave lengths used by means of a sodium-vapor lamp and a mercury-vapor lamp. The locations of the sodium and mercury lines were easily identified in the visible region of the spectrum by inspection and by the response of the phototube. However, one of the phototubes was located in the infrared region of the spectrum where it was necessary to identify the spectral lines by the response of the phototube alone. Difficulty was experienced in identifying positively the reference lines because of the fact that the response of the phototube varied considerably in the infrared region. Hence, the wave lengths determined by the phototube alone were considered unreliable.

A second method of wave-length determination utilized data obtained during the black-body calibration of the electro-optical pyrometer. Assuming constant amplification from the electronic equipment, the calibration data, when plotted as in Fig. 3, should plot as a straight line of slope $\frac{C_2}{\lambda}$, where C_2 is a known constant. From the slope of the calibration curve a value of 0.696 micron was obtained for the shorter wave length. This is in close agreement with the value of 0.699 micron determined by the use of the sodium and mercury lines. However, the value for the longer wave length of 0.902 micron was not in agreement with 0.860 micron estimated by the use of the mercury and sodium lines. Since the latter value was in doubt, and since the values obtained during the black-body calibration are "effective" wave lengths, the black-body values were taken as correct.

The range and relative intensities of the wave lengths permitted to pass through each of the two barrier slits, Fig. 2, to the phototubes are of interest since the narrowness of the peaks of the relative-intensity curves are an indication of the monochromacity of the radiation reaching the phototubes. The

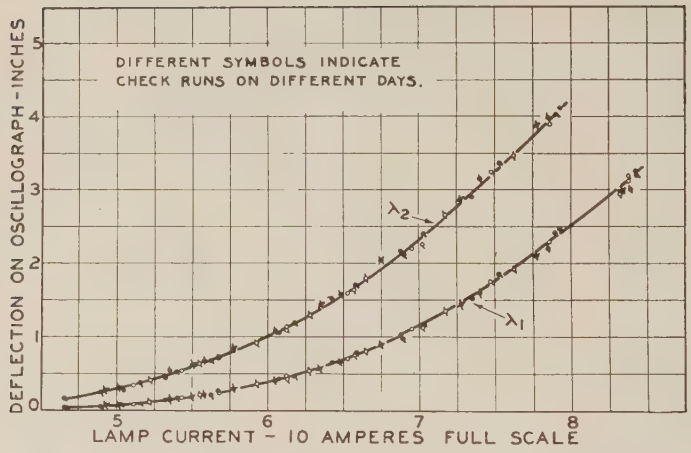

FIG. 4 CALIBRATION DATA FOR SECONDARY-STANDARD TUNGSTEN LAMP

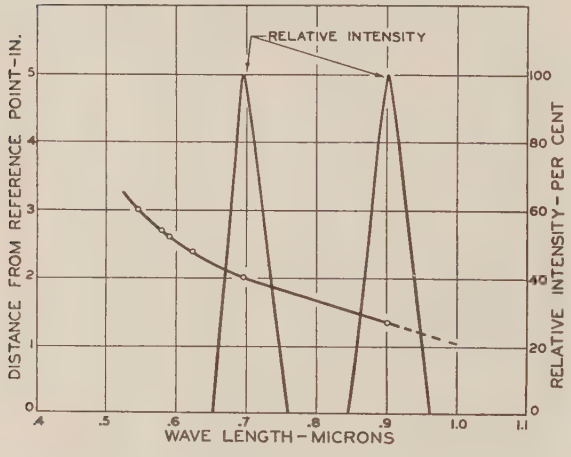

FIG. 5 RELATIVE INTENSITY AND WAVE-LENGTH RANGE DETERMINATION

following method was used to construct the relative-intensity curves shown in Fig. 5:

Data obtained during the wave-length determination were plotted showing the distances from a reference point to the points where known wave lengths were intercepted by the barrier. By measuring the distance from the two edges of the slit to the reference point, and using the curve of Fig. 5, the range of wave lengths permitted to pass through each barrier slit was obtained.

To obtain the relative intensity of the wave lengths passing through the barrier slits, the size of the image of the limiting diaphragm was measured at the barrier with monochromatic radiation entering the electro-optical pyrometer. The wave length at the center of each slit was determined from Fig. 5, and that portion of the radiation at this wave length permitted to pass through the barrier slit was calculated from the width of the slit and the dimensions of the limiting-diaphragm image. This procedure was then repeated for thirteen equidistant points across the width of each barrier slit. If the intensity of radiation is assumed to be the same for the wave lengths represented at the various points taken, the relative intensities for the wave lengths passing through each barrier slit are then given by the ratio of the respective portions of the monochromatic radiation passing through each barrier slit. The results of the analysis outlined are shown graphically by the relative-intensity curves in Fig. 5. The accuracy of the equal-intensity assumption is discussed in the next section.

The values to be used for α_1 and α_2 in Equation [9] depend on the wave lengths λ_1 and λ_2. It was suggested by Hottel and Broughton (11) that the range of wave lengths ordinarily used might be covered by two constant values of α. The values recommended are 1.39 for the range from 0.3 to 0.8 micron, and 0.95 for the range from 0.8 to 10 micron. These values were obtained by plotting experimental transmissivity data in such a manner that the slope of the line represented α. Inspection of the data indicated that each of the recommended values corresponds to the average slope of a portion of the transmissivity curve. Inasmuch as the wave lengths employed in the electro optical pyrometer had been evaluated, it was considered more accurate to determine α values by measuring the slope of the curve at the points corresponding to these particular wave lengths. The values so determined are $\alpha_1 = 1.32$ and $\alpha_2 = 1.05$. The effect of any error in these constants is discussed in the following section.

Accuracy. Since this method requires very accurate measurements of two apparent temperatures, the effect of all possible experimental errors must be minimized. One possible source of error is the electronic equipment. Direct-coupled amplifiers with two stages of amplification, batteries, and a voltage-regulated power pack were used. At first, slight inconsistencies were observed, but after waxing resistors and connections, "burning-in" resistors, etc., reproducible results were obtained as shown by the close agreement of the data in Fig. 4.

A small error is possible in measuring deflections on the cathode-ray tubes since the spot is of finite size. Measurements taken by various individuals differed by a maximum of only 0.02 in. on a 5-in. cathode-ray tube. This error was minimized by measuring each time from a given point on the spot, and by using the average of several readings.

In measuring the black-body temperature with the standard optical pyrometer observations by various individuals differed by a maximum of 15 F. Maximum deviation of the final calibration data from a straight line when plotted, Fig. 3, was only 10 F.

The effect of errors in evaluating α is discussed in reference (11), where calculations are presented showing that the error in true temperature due to a change in α from 1.7 to 1.39 is only 13.7 deg F for moderately thick flames. Thus a small error in determining α will not seriously affect the calculated temperature.

Forsythe (21) discusses the magnitude of the errors involved in assuming that the effective wave length of radiation used remains constant with changes in temperature, and he states that for most work the correction to be applied is negligible, amounting approximately to 4 deg at 5400 deg R.

The fundamental accuracy of this method of determining true flame temperatures has been demonstrated convincingly by Hottel and Broughton (11). However, in order to verify both the calibration and the calculations, a steady high-temperature flame was set up so that its temperature as determined by the electro-optical pyrometer might be compared to that measured by a standard method.

In order that the required high temperatures might be reached a burner was constructed to use acetylene, with air and oxygen supplied in any desired proportions. The experimental flame was approximately $^1/_4$ in. $\times$ 1 in. in cross section. The burner was set up inside a water-cooled jacket in order to simulate the conditions in the engine. Two peepholes were provided through which the flame might be observed.

The method used to determine the true temperature of the experimental flame was as follows: A broad-ribbon tungsten lamp of controllable brightness was placed behind the flame in the line of sight of the standard optical pyrometer. Due to the partial transparency of the flame, the standard pyrometer could "see" the tungsten lamp. The temperature of the tungsten lamp was adjusted until there was only a small difference between the reading of the standard optical pyrometer when sighted through the flame onto the tungsten lamp and when sighted directly on the tungsten lamp. Graphical interpolation of the readings taken in this manner permitted estimation of the temperature at which the apparent temperature of the tungsten lamp and the true temperature of the flame were equal.

The results of the determination of the true flame temperatures are given in Table 1. It was found that the flame temperature varied as much as 100 F over various portions of the flame visible through the peepholes; therefore, care was exercised to sight on the same portion of the flame with the standard optical pyrometer as with the electro-optical pyrometer.

To determine the effect of flame thickness on the electro-optical pyrometer temperature readings, the burner was rotated 90 deg so that the flame thickness was approximately 1 in. The lens aperture opening in the electro-optical pyrometer was stopped down so that the oscillograph deflections were not more than full scale. The data in Table 2 were then obtained.

The foregoing experimental evidence was accepted as satisfactory proof of the accuracy of the method and apparatus for the proposed internal-combustion-engine studies.

Working Charts. Since the solution of Equation [9] is a tedious process, a chart was constructed to express true temperature as a function of cathode-ray deflections. This chart was derived from the following rearrangement of Equation [9]

$$\frac{1}{T_{A1}} = \frac{1}{T} - \frac{\lambda_1}{C_2} \ln \left\{ 1 - \left[1 - e^{\frac{-C_2}{\lambda_2}\left(\frac{1}{T_{A2}} - \frac{1}{T}\right)} \right]^{\frac{(\lambda_2)\alpha_2}{(\lambda_1)\alpha_1}} \right\} \quad \ldots [10]$$

In the solution of this equation values were selected for T and for T_{A2} and the equation was solved for T_{A1}. By means of Fig. 3,

TABLE 1 DETERMINATION OF TRUE FLAME TEMPERATURES

I	First Comparison	
	Standard Optical Pyrometer (thin axis of flame):	
	Temperature of lamp through flame (average of two readings), deg R	4025
	Temperature of lamp (average of two readings), deg R	4025
	Electro-optical pyrometer readings (thin axis of flame):	
	Deflection at λ_1, in.	1.84
	Deflection at λ_2, in.	2.84
	True temperature, deg R	4020
II	Second Comparison	
	Standard Optical Pyrometer (thin axis of flame):	
	First trial:	
	Temperature of lamp through flame (average of three readings), deg R	4075
	Temperature of lamp, deg R	4145
	Second trial (lower lamp current):	
	Temperature of lamp through flame (average of three readings), deg R	4025
	Temperature of lamp, deg R	4005
	Using a graphical interpolation, the temperature of the lamp when sighted through the flame equals the temperature of the lamp at 4035 deg R	
	Electro-Optical Pyrometer Readings (thin axis of flame):	
	Deflection at λ_1, in.	1.86
	Deflection at λ_2, in.	2.85
	True temperature, deg R	4020

TABLE 2 ELECTRO-OPTICAL PYROMETER READINGS (THICK AXIS OF FLAME)

Deflection at λ_1, in.	2.3
Deflection at λ_2, in.	3.6
True temperature, deg R	4020

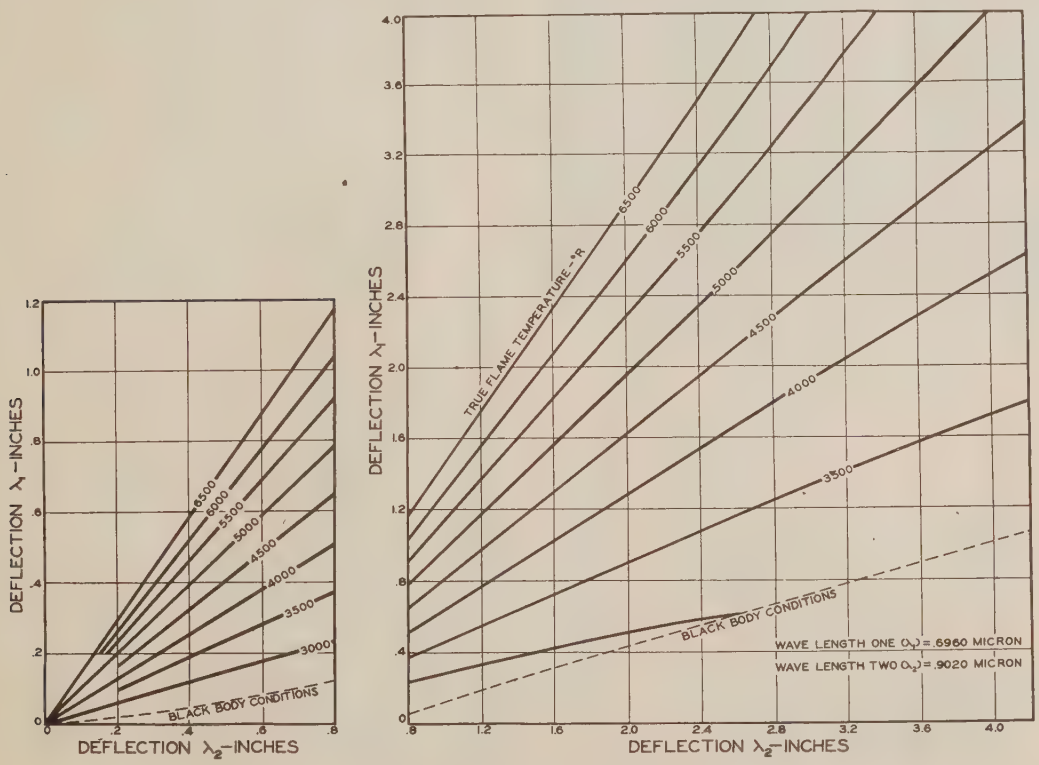

Fig. 6 True Temperature Working Chart

values of T_{A1} and T_{A2} were translated into inches of deflection on the oscillographs. The completed chart is shown in Fig. 6.

Since a knowledge of the variations in the KL factor is of interest, a similar chart, Fig. 7, was constructed, showing lines of constant KL factor.

Quartz Windows. Quartz was chosen as a suitable material to transmit combustion radiation because of the uniformity of its transmissivity over the range of wave lengths used in the electro-optical pyrometer (22). A polished quartz rod is fitted into a cylindrical steel holder which screws into one of the openings to the combustion chamber. To hold the rod against explosion pressures, a shoulder, forming a hole slightly smaller than the quartz rod, was machined at the outer end of the holder. The quartz was cemented in with litharge and glycerine to prevent leakage.

Periodically it is necessary to remove carbon deposits from the inner end of the quartz rod because the vertical deflections of the cathode rays vary with the intensity of the radiation transmitted through the quartz window. However, since the presence of a coating of carbon has the same effect as a reduction in flame emissivity, the true temperature value obtained is affected only to the extent that the scaling accuracy is impaired by the reduction in deflection.

Auxiliary Equipment Used With Electro-Optical Pyrometer

Sweep and Timing Arrangement. The two apparent temperatures to be used in calculating the instantaneous true temperature of a rapidly fluctuating flame must of necessity be measured at precisely the same instant. In the conventional internal-combustion engine this is best accomplished by an arrangement whereby the rotation of the engine controls the horizontal motion of the cathode rays and simultaneously provides timing marks at frequent intervals corresponding to known crank positions. In addition, it should be readily adjustable so that any small portion of the combustion process can be expanded to reveal minute details which are not clearly discernible when the entire process is shown on the cathode-ray screen, and it should function equally well at all engine speeds without alteration. These features were incorporated in the sweep and timing arrangement designed for use with the electro-optical pyrometer.

The sweep and timing arrangement was built as a separate unit and coupled to the end of the dynamometer shaft by an Oldham-type coupling. The characteristics of this type of coupling are such that the angular velocity of the driven shaft is the same at every instant as that of the driving shaft, even if the shafts are not in perfect alignment.

The arrangement of the working parts of the unit is shown in Fig. 8. Secured to the shaft are two cam-shaped disks, H and I. One of these disks has a constant increase in radius per degree for 330 deg, while the other has the same total increase in 90 deg. The remainder of the periphery in each case is at a constant radius until finally a radial decrease in diameter reduces the radius to the minimum value. Using either disk, light from a source A is projected through a radial slit C, behind which the edge of the rotating disk gradually cuts off the beam of light. A mirror E reflects the remaining light into a phototube D. Thus the amount of light reaching the phototube at any instant is directly related to the position of the disk at that instant. The phototube is connected to a direct-coupled two-stage amplifier, and the output voltage is impressed on the horizontal plates of all the cathode-ray tubes. Inasmuch as the voltage required to sweep the cathode rays a given distance is not the same for all tubes, potentiometers were installed as a means of making compensatory adjustments. Since the horizontal movement of the cathode rays is controlled by the variation in radius of a disk, the sweep is directly related to engine rotation during the period corresponding to K in Fig. 8. After a pause occasioned by the

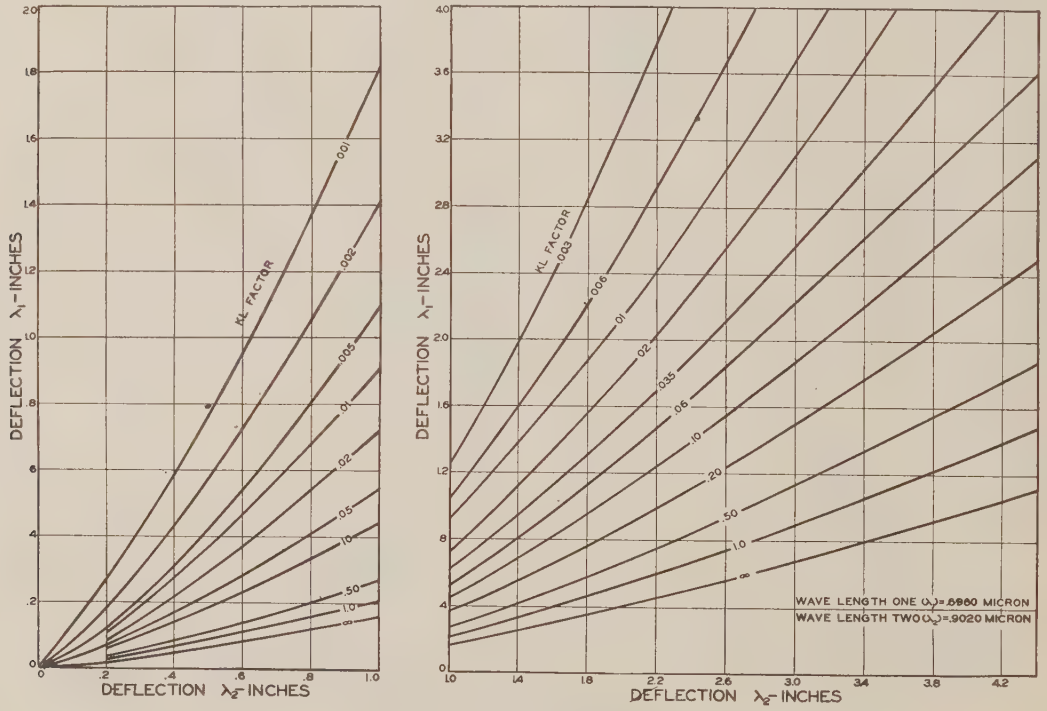

Fig. 7 *KL* Factor Working Chart

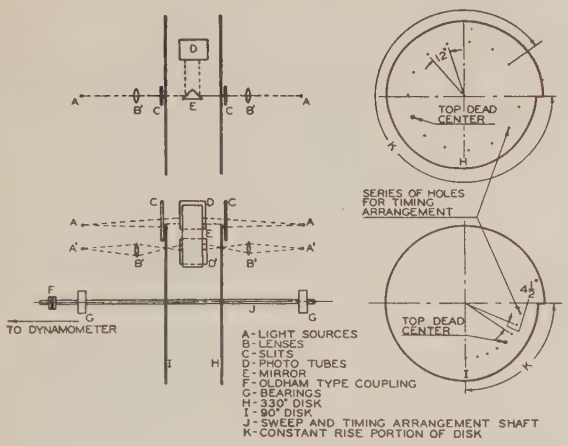

FIG. 8 SCHEMATIC DRAWING OF SWEEP-AND-TIMING ARRANGEMENT

constant-radius part of the disk, the abrupt decrease in radius instantaneously returns each ray to the opposite side of its screen to begin another sweep cycle.

The portion of the combustion process viewed on the cathode-ray screen can be varied, either by changing from one disk to the other by switching lights *A*, or by varying the intensity of the light. Using the first method, the horizontal sweep of the cathode rays can be made to correspond either to 330 deg of crank rotation, or to 90 deg, depending on which of the lights *A* is illuminated. With equal ease, the total sweep of the cathode rays can be adjusted at will by varying the intensity of the light source *A* by means of a rheostat. These adjustments permit as much or as little of the combustion process as desired to be spread across the fluorescent screens of the cathode-ray tubes. The range, in degrees of crankshaft rotation, may be any amount from 9 to 330 deg. The 9-deg range is particularly advantageous where pressure and temperature changes occur most rapidly.

The timing device is integral with the sweep arrangement. Using a milling-machine head, small holes were drilled in each disk on an arc 5 in. from the center of rotation and extending over that portion of the disk where the constant increase in radius occurs. The holes are $4^1/_2$ deg apart in the 90-deg disk, and 12 deg apart in the 330-deg disk. The center hole of the series was drilled slightly larger than the others.

A light source *A'*, a lens *B'*, the mirror *E*, and a phototube *D'*, Fig. 8, are so placed that light reaches the phototube intermittently through the holes in the disk as the disk rotates. The phototube is connected through amplifiers to the vertical plates of one of the cathode-ray tubes. This arrangement causes the cathode ray to be deflected vertically at intervals corresponding to the spacing of the holes in the disk. The position of each disk on the shaft was fixed in assembling so that the large hole passes light to the phototube when the engine is exactly at top center, causing a higher deflection which clearly marks the top-center position.

In order to bring into view portions of the cycle outside the normal range, the holder for the lights, lenses, mirror, and phototubes was made movable about the axis of the shaft, and a ring graduated in degrees was mounted adjacent to the holder. When the holder is shifted from its normal position the long timing mark on the screen no longer corresponds to the top-center position. However, since all the timing marks are shifted the same number of degrees as the holder, the position on the screen corresponding to top center can readily be found by means of the graduated ring.

It was found necessary to balance the disk-and-shaft assembly dynamically and to mount the entire assembly on a heavy cast-iron block insulated from floor vibration. It was also found necessary to use bronze bearings rather than ball bearings since the latter, when tried, set up vibrations of a magnitude sufficient to cause noticeable distortion of the cathode-ray diagrams. The entire unit is painted black and inclosed in a lightproof housing to prevent stray light from reaching the two phototubes. The unit is shown in Fig. 9.

Pressure Indicator. An electro-optic pressure indicator developed by Robertson (23) at the University of Wisconsin is employed to obtain pressure data. A schematic diagram of the pressure pickup unit is shown in Fig. 10, in which light from source *A* is made parallel by lens *B*, then is reflected by a mirror *C* through a limiting diaphragm *D* onto a highly polished pressure diaphragm *E*, which is screwed into an opening in the wall of the combustion chamber. Pressure variations in the combustion chamber cause the diaphragm *E* to change shape, dispersing the light reflected back by the polished surface. A portion of this light passes through perforations in the reflecting surface of the mirror *C*, and through a limiting diaphragm *F* to a phototube *G*. The output of the phototube is amplified and impressed on the vertical plates of a cathode-ray tube. The cathode ray is actuated horizontally by the sweep circuit previously described. Since the intensity of the light reaching the phototube is varied by changes in pressure, the cathode ray traces a pressure versus crank-angle diagram on the tube screen.

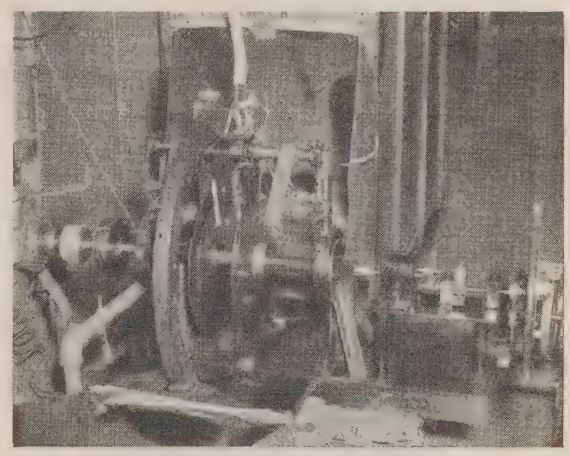

FIG. 9 THE SWEEP-AND-TIMING ARRANGEMENT

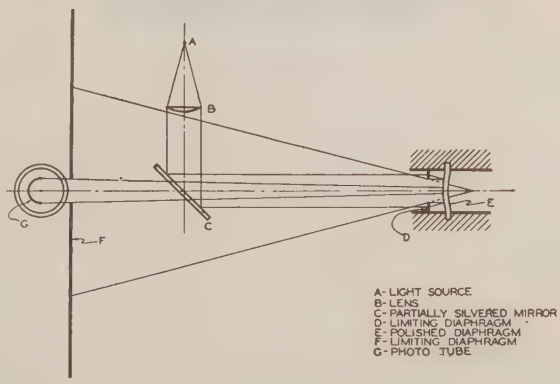

FIG. 10 SCHEMATIC DRAWING OF PRESSURE INDICATOR

The electro-optic pressure indicator was calibrated in place on the engine under actual operating conditions by using a supplementary balanced-diaphragm indicator. This method eliminates the possibility of errors due to changes in the modulus of elasticity of the polished diaphragm, or in the reflectivity of its surface, when exposed to high-temperature conditions. The balanced-diaphragm indicator was similar to one developed by the Bureau of Standards, but was modified slightly to avoid any change in the engine-clearance volume when it was screwed into an opening normally occupied by a quartz window. A tank of compressed nitrogen was connected to the outer side of the diaphragm to balance the engine pressure, and a calibrated pressure gage was used to measure the applied pressure. When the engine pressure exceeded the nitrogen pressure, the diaphragm moved outward, making contact with the electrically insulated center portion of the indicator which was coupled electrically, by a condenser, to the grid of the first-stage amplifier used to amplify the output of the phototube of the electro-optic pressure indicator. Whenever this contact was made or broken, the cathode ray was temporarily displaced, producing a jog in the pressure diagram. A reproduction of a pressure diagram taken with the balanced-diaphragm indicator in operation is shown in Fig. 11. The effect of engine vibration on the condenser coupling is visible in this picture. Nevertheless, the point at which the diaphragm made contact is clearly indicated. By varying the pressure supplied to the outside of the balanced diaphragm and measuring the corresponding deflections, a calibration curve of deflection versus pressure was obtained as shown in Fig. 12. The intake pressure was taken as atmospheric since the error in this assumption was negligible.

Since the magnitude of the deflections obtained depended on the light intensity as well as the pressure variations, it was found necessary to supply closely regulated direct current to the light source. This was accomplished by the use of storage batteries which were constantly charged at a rate slightly higher than the current required for the light source. By the use of this method to obtain constant light intensity, results reproducible within the limits of measuring accuracy were obtained.

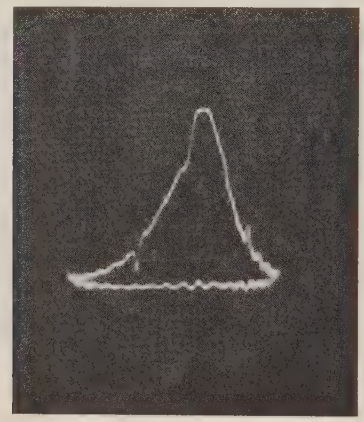

FIG. 11 PRESSURE-INDICATOR DIAGRAM SHOWING CALIBRATION MARKS

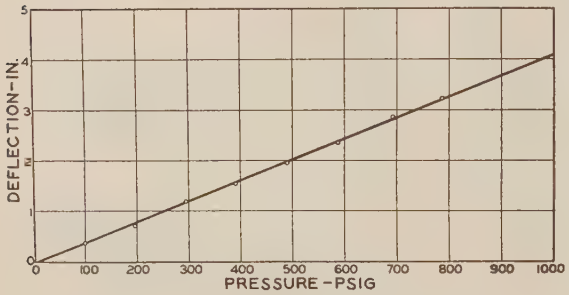

FIG. 12 PRESSURE-INDICATOR CALIBRATION DATA

Injection Indicator. The engine is equipped with a Bosch solid-injection system with the conventional commercial method of varying the time of injection. A shutter is attached to the nozzle plunger so that when the nozzle valve is lifted from its seat and injection started, the amount of shutter opening is increased. A light on one side of the shutter actuates a phototube on the other side whenever the shutter opening changes. The output of the phototube is amplified and impressed on the vertical plates of one of the cathode-ray tubes. This cathode ray is actuated horizontally by the sweep circuit previously described. Thus the beginning of injection is indicated by a vertical deflection of the cathode ray, and the end of injection is indicated by the return of the cathode ray to its original position. In addition, any pressure waves of sufficient magnitude to move the nozzle plunger and shutter are shown.

End-of-Combustion Indicator. The end of combustion occurs either in the precombustion chamber or in the main chamber, depending on the load on the engine and the point at which injection occurs. One of the quartz windows is located in the cylinder head so that combustion in the main chamber can be viewed through it. By observation, it was found that at light engine loads combustion apparently does not carry over from the precombustion chamber into the main chamber. Therefore, at light loads, the end of combustion is indicated by the electro-optical pyrometer. Under heavy-load conditions combustion carries over into the main chamber. Accordingly, a phototube was placed in such a position that it is actuated by the radiation from the quartz window viewing the main chamber. The output of this phototube is amplified and impressed on the vertical plates of one of the cathode-ray tubes. This cathode ray is actuated horizontally by the sweep circuit. Thus the end of combustion can be determined regardless of where combustion ceases.

Camera-Shutter Synchronizer. A permanent record of the data is obtained by photographing simultaneously all of the oscillographs while all the devices which activate the cathode rays are in operation. In order that single cycles with their cyclic pressure and temperature fluctuations can be studied, as well as general trends of numerous cycles, photographs of single cycles are desired.

In order to photograph these single cycles, a shutter synchronizer is required which will open and close the shutter at the proper crank position regardless of engine speed, and which will do so one time only without being reset.

The device, shown in Fig. 13, was developed to meet these requirements. A wooden disk *I* is coupled to the end of the sweep-and-timing mechanism shaft through reduction gears having a ratio of 40 to 1. Two small blocks *A* are attached to one side of the disk to form an adjustable cam. This cam actuates a follower *C* which closes the breaker points *D*, permitting current to flow through the solenoid *F* which opens the camera shutter. When the cam leaves the follower the breaker points open the solenoid circuit and the camera shutter closes. The combined length of the two blocks forming the adjustable cam corresponds to one engine cycle. Therefore the camera shutter remains open for one cycle, the point at which it opens and closes being determined by the location of the adjustable blocks on the disk. A manually operated switch *H* in the solenoid circuit is closed when a picture is desired and opened immediately after the shutter closes. Thus one combustion cycle is photographed at a time,

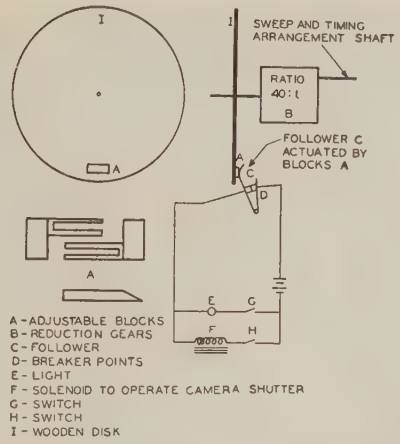

FIG. 13 SCHEMATIC DIAGRAM OF CAMERA-SHUTTER SYNCHRONIZER

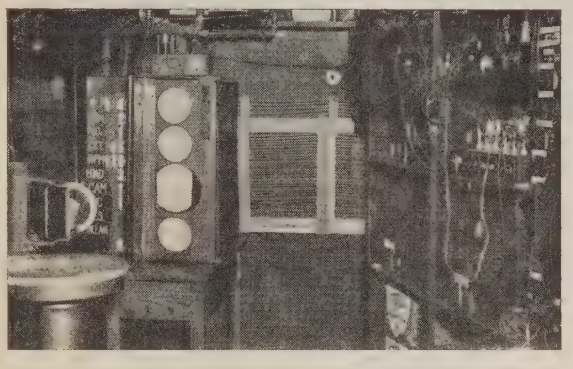

FIG. 14 CATHODE-RAY TUBES, ASSOCIATED ELECTRONIC EQUIPMENT AND CAMERA

and as many additional photographs as desired can be taken by repeating the operation with fresh film. To prevent the inadvertent closing of this switch when the breaker points are already closed, a light *E* is connected in parallel with the solenoid.

In order to obtain compact and complete photographic records of original data, the cathode-ray tubes were placed in a vertical row beside a black title board on which pertinent identifying data are shown by white letters. A view of this arrangement is shown in Fig. 14. The board is illuminated when taking photographs. Also, two small illuminated holes, 10 in. apart, to be used for alignment and enlargement purposes, were provided adjacent to the bank of cathode-ray tubes and are photographed simultaneously with the oscillographs. Before photographs are taken, the horizontal travel of the cathode rays is adjusted by means of the potentiometers so that, at any time, a vertical line through all the cathode-ray "spots" is parallel to the two illuminated holes. When the image of the oscillographs is projected onto a ground-glass screen with the proper enlargement, the alignment "dots" are 10 in. apart. The deflections corresponding to particular crank positions are determined by projecting lines from the corresponding timing marks parallel to the two dots. A 35-mm camera fitted with an f 1.9 lens is used to photograph the oscillographs.

Engine and Auxiliary Apparatus. The engine to which the previously described apparatus is attached is a commercial-model Diesel engine, the specifications of which appear in Table 3. It has a high-turbulence precombustion-chamber type of head which has openings as shown in Fig. 15. The engine is coupled to an electric dynamometer. A view of the engine with the electro-optical pyrometer, the pressure indicator, the injection indicator, and the end-of-combustion indicator in position is shown in Fig. 16.

The length of time necessary for the engine to consume a predetermined amount of fuel, and the total revolutions during that time, are automatically measured by means of an electromagnetic tripping device.

As part of the energy balance, the heat loss to the jacket cooling water is measured by means of calibrated thermometers, a direct-connected positive-displacement pump, and a calibrated $^3/_8$-in. sharp-edged stainless-steel orifice.

In order to determine the average air-fuel ratio, the air consumption is measured by means of a thin-plate orifice constructed according to the A.S.M.E. Code. Air pulsations are smoothed out by volumes and pressure drops as recommended by the Code.

Two smoke meters are attached to the exhaust line, one a continuous-flow type and the other a sampling type.

A Bureau of Mines gas-analysis apparatus is used to analyze the exhaust gases for oxygen, carbon dioxide, and carbon monoxide. The remainder is assumed to be nitrogen.

PRELIMINARY RESULTS

The engine head, as shown in Fig. 15, has a radial opening and a tangential opening in the precombustion chamber through

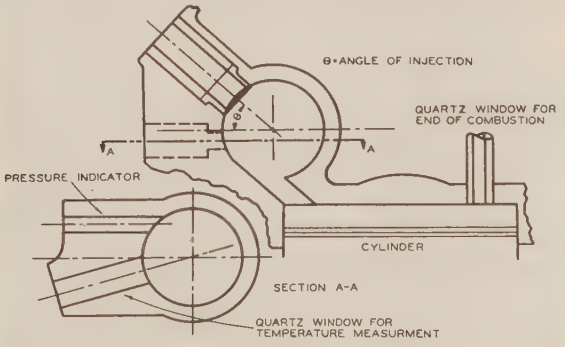

FIG. 15 SCHEMATIC DRAWING OF ENGINE HEAD

which temperature observations could be made. In order to determine which one would be best suited for temperature measurements, quartz windows were installed and observations were made through each of these openings. The procedure for obtaining comparative data for the two openings was as follows: The engine was run at rated speed and load until equilibrium conditions were reached. Then the engine was momentarily stopped, the quartz windows cleaned and reinserted, and the engine started and allowed to run for about 5 min in order to again reach equilibrium conditions. Temperature observations were then made by sighting alternately the electro-optical pyrometer through the two windows, and photographing the oscillographs of apparent temperature variations.

The temperatures determined through the tangential window

TABLE 3 SPECIFICATIONS OF TEST DIESEL ENGINE

Manufacturer	Fairbanks-Morse & Co.
Model no.	36A
Number of cylinders	1
Bore, in.	$4^1/_4$
Stroke, in.	6
Rated rpm	1200
Rated bhp	10
Compression ratio	14.5
Strokes per cycle	4

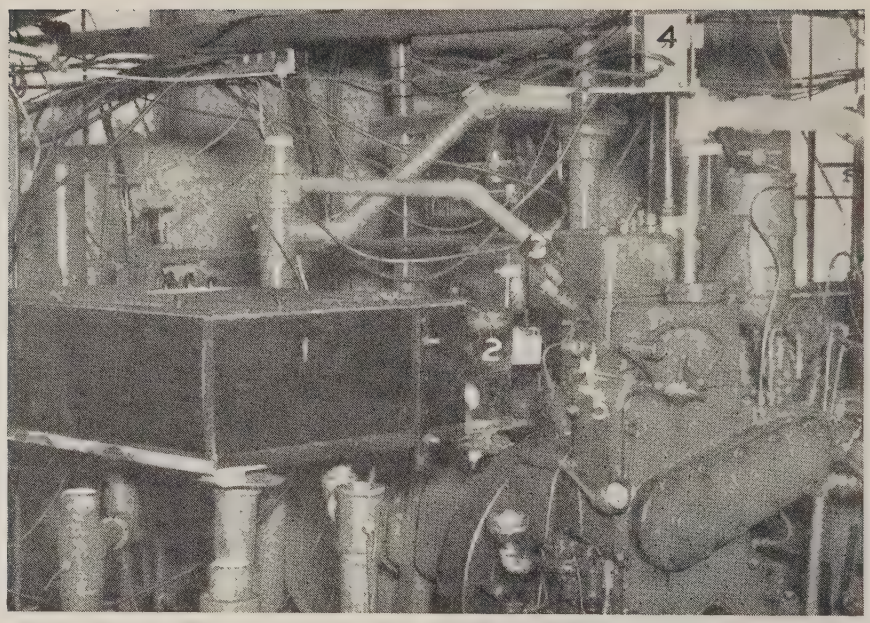

FIG. 16 DIESEL ENGINE AND ASSOCIATED EQUIPMENT
(1 Electro-optical pyrometer; 2 Pressure indicator; 3 Injection indicator; 4 End-of-combustion indicator; 5 Quartz window.)

were slightly lower than those determined through the radial window, particularly during the first part of combustion. This was undoubtedly a result of the cooling effect of the combustion-chamber walls. During the last half of combustion the two temperatures were found to be nearly equal.

At light loads, rapid variations in flame emissivity, with a consequent rapid variation in the apparent temperatures, were observed when the electro-optical pyrometer was sighted on the opening which views the precombustion chamber tangentially. At full load these variations in flame emissivity tended to decrease both in rapidity and in magnitude. The flame-emissivity variations observed through the radial opening were always less rapid and of smaller magnitude than those viewed through the tangential opening.

The analysis of the photographic records from the two openings failed to show any appreciable difference in ignition lag.

After consideration of these factors, the quartz window for temperature measurements was left in the radial opening and the pressure indicator was inserted in the tangential opening, as indicated in Fig. 15.

Having settled on a suitable location for the quartz window, and having previously established the reproducibility of temperatures measured with the electro-optical pyrometer, Fig. 4, the cyclic reproducibility of engine temperatures under constant operating conditions was next investigated. Some of the results of this investigation are shown in Fig. 17. These data show that the average trend is reproduced, but the temperature at any particular point in the cycle is not necessarily reproduced from cycle to cycle. Data taken on different days under the same operating conditions showed similar temperature fluctuations, but the average trend was the same as shown in Fig. 17. The pressure measurements showed closer agreement.

As a preliminary to investigating the effects of fuel composition on the combustion process, tests were in progress at the time this paper was prepared to establish for a single fuel the effect of different operating conditions on the temperatures during the combustion process. Operating variables such as engine speed, engine load, point of injection, jacket-water temperature, etc., are individually varied while the other operating variables are maintained constant.

For the preliminary tests reported in this paper, the operating variable was the point of injection, which was adjusted to occur at top center, at 18 deg before top center, and at 24 deg before top center, rated speed and load being maintained in each case. Photographs were taken with the horizontal scale expanded different amounts, so that particular portions of the combustion process might be studied in detail. The photographs were analyzed in the manner previously described.

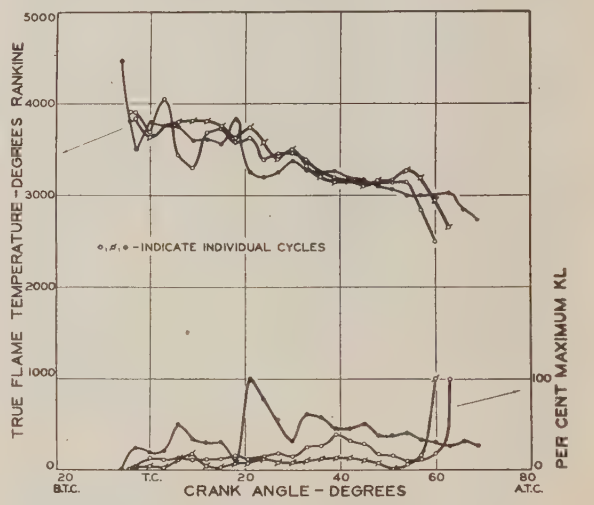

FIG. 17 TEMPERATURE AND *KL* FLUCTUATIONS UNDER CONSTANT OPERATING CONDITIONS

FIG. 18 OSCILLOGRAM OF ENTIRE COMBUSTION PROCESS WITH INJECTION AT 24 DEG BEFORE TOP CENTER

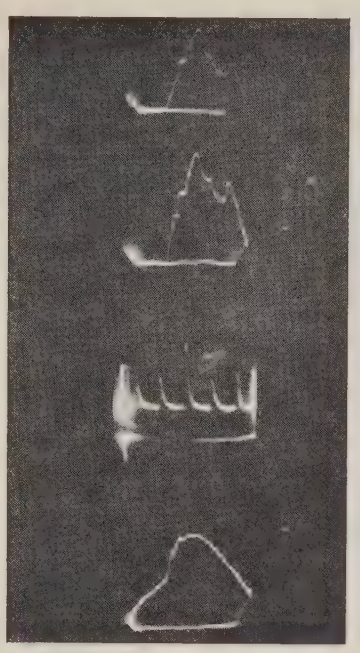

FIG. 19 OSCILLOGRAM WITH INJECTION AT 24 DEG BEFORE TOP CENTER AND HORIZONTAL SCALE EXPANDED

FIG. 20 OSCILLOGRAM WITH INJECTION AT 24 DEG BEFORE TOP CENTER AND HORIZONTAL SCALE EXPANDED

FIG. 21 OSCILLOGRAM OF ENTIRE COMBUSTION PROCESS WITH INJECTION AT TOP CENTER

Views taken during the run with injection occurring at 24 deg before top center are shown in Figs. 18, 19, and 20. In Fig. 18 the horizontal scale is compressed so that the whole combustion process is shown. The timing marks are 12 deg apart, the high mark indicating top center. The effect of expanding the horizontal scale by increasing the light intensity passing through the slit is shown in Fig. 19. The timing marks are still 12 deg apart. The 90-deg disk was in use when the photograph reproduced in Fig. 20 was taken, consequently the timing marks in this picture are $4^1/_2$ deg apart. Fig. 21 shows the effect of late injection. The alignment dots are visible on the right-hand side of all the photographs.

The true temperature, pressure, and KL factor fluctuations, as recorded on the illustrations Figs. 18 and 21, are shown in Fig. 22, together with data for a single cycle with injection occurring at 18 deg before top center. Each of the dotted lines in Fig. 22 was obtained by analyzing 10 cycles, similar to Figs. 18, 19, and 20, for each point of injection and drawing average curves for these data.

The data in Fig. 22 are presented at this time primarily to show that the electro-optical pyrometer is capable of following and recording the temperature variations inside the cylinder of an internal-combustion engine. Not enough data have been obtained to explain the cyclic temperature fluctuations or the variations in temperature with point of injection. However, additional tests are now in progress to establish more completely the effect upon the temperature of varying the point of injection, as well as the effect of the other operating variables and the fuel composition. The results of these tests will be reported at some future time.

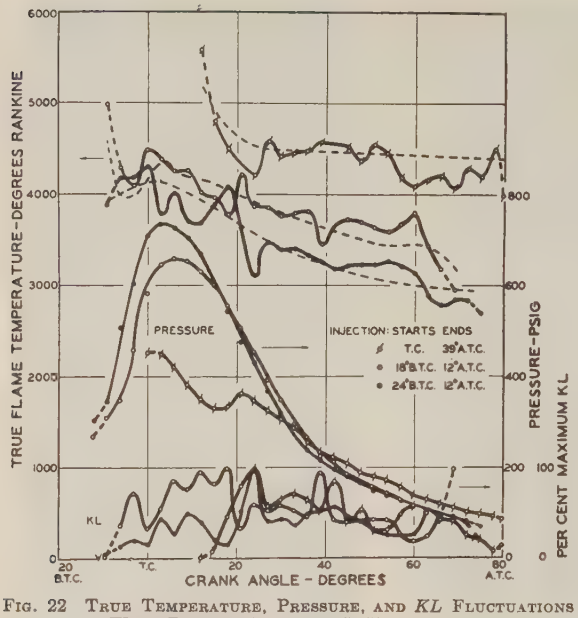

FIG. 22 TRUE TEMPERATURE, PRESSURE, AND *KL* FLUCTUATIONS WHEN POINT OF INJECTION IS VARIED

ACKNOWLEDGMENT

The work reported herein was made possible by financial support granted by the Wisconsin Alumni Research Foundation and by the University of Wisconsin College of Engineering. To these organizations, and to the many students and members of the faculty who have rendered valuable assistance and encouragement, the authors desire to express their sincere gratitude.

BIBLIOGRAPHY

1 "Second Report to the Gas-Engine Research Committee," by F. W. Burstall, Proceedings of The Institution of Mechanical Engineers, parts 3–5, 1901, pp. 1031–1154.

2 "On the Measurement of Temperatures in the Cylinder of a Gas Engine," by H. L. Callendar and W. E. Dalby, Proceedings of the Royal Society of London, England, vol. 80, series A, 1907–1908, pp. 57–74.

3 "Cyclical Changes of Temperature in a Gas-Engine Cylinder," by E. G. Coker and W. A. Scoble, Proceedings of The Institution of Civil Engineers, vol. 196, Part 2, 1913–1914, pp. 1–74.

4 "Flame Temperatures in an Internal-Combustion Engine, Measured by Spectral Line Reversal," by A. E. Hershey and R. F. Paton, University of Illinois, Engineering Experiment Station, Bulletin No. 262, Urbana, Ill., Oct., 1933.

5 "Flame Temperatures Vary With Knock and Combustion-Chamber Position," by G. M. Rassweiler and L. Withrow, *S.A.E Journal*, vol. 36, 1935, Trans. section, pp. 125–133.

6 "The Measurement of Flame Temperatures in a Petrol Engine by the Spectral Line-Reversal Method," by S. S. Watts and B. J. Lloyd-Evans Proceedings of the Physical Society, vol. 46, 1934, pp. 444–449.

7 "Flame Radiation and Temperature Measurements on an Internal-Combustion Engine," by A. E. Hershey, *Industrial and Engineering Chemistry*, vol. 24, 1932, pp. 867–870.

8 "Measurement of Gas Temperatures in an Internal-Combustion Engine," by A. E. Hershey, Trans. A.S.M.E., vol. 58, 1936, paper PRO-58-2, pp. 195–201.

9 "Measurement of Fluctuating Temperature of Working Gas in Internal-Combustion Engines," by A. Kobayashi, Trans. Society of Mechanical Engineers of Japan, vol. 3, no. 11, May, 1937, pp. 192–197.

10 "Gas Temperature Measurements in Internal-Combustion Engines," by. H. Graff, *Zeitschrift des Vereines deutscher Ingenieure*, vol. 86, no. 29–30, July 25, 1942, pp. 461–466.

11 "Determination of True Temperature and Total Radiation From Luminous Gas Flames," by H. C. Hottel and F. P. Broughton, *Industrial and Engineering Chemistry*, Analytical Edition, vol. 4, 1932, pp. 166–175.

12 "Spectral Radiant Intensities of Some Tungsten Filament Incandescent Lamps," by W. E. Forsythe and B. T. Barnes, *Journal of the Optical Society of America*, vol. 26, 1936, pp. 313–315.

13 "The Properties of Tungsten and the Characteristics of Tungsten Lamps," by W. E. Forsythe and A. G. Worthing, Abstract, Bulletin of Lamp Development Laboratory, Incandescent Lamp Department of General Electric Company, vol. 2, January, 1930, pp 6–12.

14 "Positive and Negative Thermionic Emission From Tungsten," by H. B. Wahlin and L. V. Whitney, *Physical Review*, vol. 50, 1936, pp. 735–738.

15 "Emission Spectra of Engine Flames," by G. M. Rassweiler and L. Withrow, *Industrial and Engineering Chemistry*, vol. 24, 1932, pp. 528–538.

16 "Spectroscopic Studies of Engine Combustion," by L. Withrow and G. M. Rassweiler, *Industrial and Engineering Chemistry*, vol. 23, 1931, pp. 769–776.

17 "Properties of Ordinary Water-Substance," by N. Ernest Dorsey, Reinhold Publishing Corporation, New York, N. Y., 1940, pp. 128–130 and 150.

18 "Measurement of Radiant Energy," by W E. Forsythe, McGraw-Hill Book Company, Inc., New York, N. Y., 1937, pp. 181–182.

19 "Infrared Radiation From Explosions in a Spark-Ignition Engine," by C. F. Marvin, Jr., F. R. Caldwell, and S. Steele, Report no. 486, National Advisory Committee for Aeronautics, 1934, pp. 223–234.

20 "Instrumentation in the Study of Diesel Combustion," by E. W. Landen and L. A. Blanc, Trans. A.S.M.E., vol. 65, 1943, pp. 121–125.

21 Ref. (18), pp. 382–383.

22 "Sapphire and Other New Combustion-Chamber Window Materials," by George Calingaert, S. D. Heron, and Ralph Stair, *S.A.E. Journal*, vol. 39, 1936, Trans. section, pp. 448–450.

23 "An Electro-Optic Pressure Indicator," by A. F. Robertson, *Review of Scientific Instruments*, vol. 12, 1941, pp. 142–148.

Discussion

H. B. NOTTAGE.[6] As a tribute to experimental ingenuity and skill in tackling a difficult problem of practical interest, this paper is of outstanding merit. Even with slight imperfections, just so they would be consistent and recognized, the results of a comprehensive engine study with the author's equipment should fundamentally advance our recognition of the perverse idiosyncracies of combustion in an engine.

It is admittedly difficult to make a paper of this nature complete in its coverage of all details of technique. A further word from the authors would be appreciated concerning the extent to which this equipment is independent of the diagnostic and manipulative sensitivities of the individuals who have made it work. What pitfalls would await the uninitiated adventurer following in their path?

Is the present form of the equipment the first one assembled? What further improvements are needed or expected? What is the useful life of the mechanical parts? How quickly do the photocells deteriorate? How frequently must the photocells be recalibrated? Are separate means advisable to check on the interchangeability of the photocells? How high an engine speed would this equipment stand with maintained accuracy? What maximum and minimum pressure and temperature limits can be handled? Will this equipment show up detonating frequencies independent of "hash?"

Is it worth while to consider building in a differentiating circuit to determine the rates of pressure and temperature variations?

How much of the lack of reproducibility between cycles might be due to the engine-operating controls themselves? How long is the engine run in before data are taken? Is ordinary commercial injection equipment believed to be satisfactory here? An-

[6] Project Engineer, Pratt & Whitney Aircraft, East Hartford, Conn. Jun. A.S.M.E.

other oscillogram of fuel injections rate versus time might be imagined as an additional complication.

Then, from an analytical viewpoint, are there believed to be any limitations on Equation [5], as applied to an engine combustion chamber? What is the magnitude of the monochromatic transmissivity of the flame? What would be the corresponding reflectivity and absorptivity of the combustion-chamber surfaces in operation? What kind of temperature does one measure along a radiant beam passing through a gas mass in violent physical and chemical agitation? Has this temperature been employed to calculate the radiant component of the heat transfer to the combustion-chamber walls?

Further data are most certainly awaited with keen interest.

J. P. Megroot.[7] In studies such as the author has made, the apparatus involves a small window inset in a cylinder. Beyond doubt the coolest part of the cylinder is the wall. The question then arises, can a really good idea of the temperature inside the cylinder be obtained from measurement through such a window?

Why was the measurement of pressure taken with the presented method instead of with the piezo-electric crystal method in which the indicating parts are inertia-free and therefore more correct?

Hans Bohuslav.[8] How many pictures could be taken before the window had to be removed and cleaned? Were the measurements influenced by the radiation of the combustion-chamber walls? Was it possible to measure the combustion-chamber-wall temperature and determine the effect of an increase in such temperatures on the cleanliness of combustion and flame temperature? It is commonly known that after an engine has run for a while and is properly warmed up, the combustion becomes cleaner; therefore, the temperature of the combustion-chamber wall would have an influence on the speed of combustion and temperature of the flame.

L. R. Turner.[9] What is the possibility of using this method to measure the temperature of gases which have no radiant particles in them? In their experiments, have the authors used additives in sufficient quantities such that the radiation is along one wave length? It is the writer's understanding that a method has been worked out but he is unfamiliar with the quantities required to get black-body conditions at one wave length.

Leopold Strauss.[10] The authors' illustrations show the precombustion chamber as spherical. What would be the effect of a differently shaped chamber on the temperature measurements? Also, what effect does turbulence within the chamber have on temperature measurement?

Authors' Closure

The discussion submitted by H. B. Nottage includes several pertinent questions which one thoroughly conversant with the technical theories and principles involved might naturally raise. The authors welcome the opportunity to discuss these questions at this time but not all of them can be answered conclusively until after further experience and experimentation.

The authors believe that the equipment is quite independent of the personal element, once the operators become familiar with the basic principles and technique. The equipment is still in its original form except for a few minor changes. Simplification is possible and certainly would be necessary before it could be used successfully by nontechnical operators.

Probably the most desirable improvement in the electro-optical temperature indicator would be realized if the equations involved were solved electronically so as to produce true temperatures directly on a single oscillograph screen. This would eliminate the laborious, time-consuming routine inherent in the present arrangement and should improve the accuracy. Needless to say, some means of attaining this objective is vigorously being sought.

The mechanical parts are few and not subject to rapid wear or deterioration. The phototubes are used at low light levels, and at moderate voltages, consequently they should be usable for a long period of time. The original phototubes are still in use and show no appreciable deterioration after many hours of service. Any change that might occur in the characteristics of the phototubes, occasioned by deterioration or replacement, is taken care of by strict adherence to the practice of checking the calibration of the apparatus each time it is used.

The authors are of the opinion that the instrumentation will operate successfully at any speeds employed in present-day reciprocating engine practice if proper precautions are observed in designing the electrical circuits and the mechanical auxiliaries. Since there are no mechanical connections between the engine and the electronic indicators, these instruments should follow accurately, without interference from engine vibrations, any frequency up to the limit of frequency response of the amplifiers.

As a matter of possible interest, the electro-optical temperature indicator was once sighted toward the sun and the temperature thus obtained checked the generally accepted value very closely.

If, as is hoped, the true flame temperature can be indicated directly on a single oscillograph screen as a function of crank angle, temperature rate curves will definitely be of interest. With the present equipment, however, apparent temperature rate curves do not seem to be in order as both flame emissivity and temperature variation affect the rate.

Lack of cycle reproducibility is believed to be inherent in the combustion process, since the injector rack is usually locked in a fixed position while data are being obtained. This conclusion seems reasonable because of the manner in which ignition originates and combustion is propagated in a Diesel engine, and more particularly so in the high turbulence, precombustion-chamber type used in the present investigation.

The engine is run at the desired operating conditions for a period of approximately one hour before data are taken. Special injection equipment may prove useful, but the final answer to this question must await further experimental work. The use of injection rate diagrams has been considered. While such additional data would undoubtedly contribute useful information, the necessary equipment has not been developed as far as the authors are aware and consequently this improvement must await future development work.

The authors consider that Equation [5] is just as applicable to luminous flames in engine combustion chambers as it is to open flames. The equation must fail, however, when a luminous flame becomes nonluminous and the radiation becomes discontinuous with respect to wave length. In the present experiments the luminosity of the Diesel flame is of such magnitude that the equation is considered applicable. Further experimental work will be necessary to establish its validity in the case of the less luminous Otto-cycle flames.

The monochromatic transmissivity varies between wide limits. As yet, the authors have made no attempt to separate the transmissivity of the flame and that of the sooty quartz window. KL values for the flame-window combination range from 0.001 to 1.0. The corresponding absorptivity of the combustion-chamber

[7] Engineer Consultant, Cleveland, Ohio.

[8] Vice-President in Charge of Engineering, Sterling Engine Company, Buffalo, N. Y. Mem. A.S.M.E.

[9] National Advisory Committee for Aeronautics, Cleveland Airport, Cleveland, Ohio.

[10] Sterling Engine Company, Buffalo, N. Y. Jun. A.S.M.E.

walls is unknown but must be quite high due to the surface coating of soot. It should be noted that the temperature obtained with the electro-optical pyrometer is exponentially weighted toward the highest temperature existing in the radiant particles visible to the instrument. This fact, together with the high turbulence and the suspected lack of thermal equilibrium, may be largely responsible for the lack of reproducibility.

Separation of the flame absorptivity and the window absorptivity would be necessary before the radiant heat transfer could be calculated. A new type of quartz window is now being employed which may make such separation feasible.

With respect to Mr. Megroot's question concerning the effect of window temperature, it is unlikely that radiation from the window itself can appreciably alter the electro-optical pyrometer readings because the window temperature is far less than the flame temperatures, and the exponential averaging previously mentioned tends to nullify minor radiation effects.

Experience with the piezo-electric pressure indicator in previous combustion studies at the University of Wisconsin indicated that it does not hold to its calibration well. The electro-optical pressure indicator has proved entirely satisfactory in that respect. Furthermore, the natural frequency of the diaphragm used in the electro-optical pressure indicator is approximately 200,000 cycles. Since the ability of the diaphragm to respond to rapid changes in pressure is determined by its natural frequency, the response is satisfactory up to the limit of the frequency response of the amplifiers used.

Replying to Hans Bohuslav's questions, the frequency with which the quartz window must be cleaned is a function of the engine-operating conditions, with a minimum of about 15 minutes. Since the paper was presented, a self-cleaning window has been developed which apparently remains clean indefinitely. No attempt has been made in the present investigation to measure combustion-wall temperatures. In view of the exponential averaging, previously mentioned, radiation from the relatively cool wall is negligible as far as flame-temperature measurement is concerned.

Concerning the discussion submitted by Mr. Turner, since the method in question measures the temperature of the soot particles in the flame it is not applicable to nonluminous flames. Inasmuch as the Diesel flame is luminous, there has been no occasion to employ additives in the present investigation. The possibility of additives affecting the combustion characteristics would seem to make their use undesirable if it can be avoided. The authors have not experimented with the amount of additives required to approach black-body conditions, nor do they know of any reference to experiments of this nature. Reference (10) describes a method whereby the spectral radiation of an additive was used to measure flame temperatures, but black-body conditions were not approximated.

The question by Leopold Strauss concerning the effect of combustion-chamber shape must await further experimentation because, as yet, the apparatus has been employed on only one type of combustion chamber. Turbulence should have no effect upon the temperature measurements if thermal equilibrium exists. Lacking thermal equilibrium, however, temperature variations would be indicated if "hot" and "cold" masses were swept alternately in front of the combustion-chamber window.

The authors wish to express their appreciation to those who contributed to the discussion of the paper.

Polar Diagram for Tuning of Exhaust Pipes

By TROELS WARMING,[1] MILWAUKEE, WIS.

In this paper is shown how a simple polar diagram, not requiring any higher mathematics, can be used for calculation of the natural frequency of the exhaust system on a Diesel engine. In general this diagram can be used for determination of all the natural frequencies of any system consisting of gases or fluids in containers of complex form.

CURRENTLY there seems to be an increasing interest in tuning of exhaust pipes on Diesel engines, see, for instance, a paper by P. H. Schweitzer;[2] and it may therefore be of advantage to have an easy method to determine the natural frequencies of such systems. A polar diagram, similar to the diagram developed some years ago by F. M. Lewis[3] for calculation of crankshaft systems, may be used for this purpose. It will be found, however, that gas systems are much simpler to deal with than shaft systems.

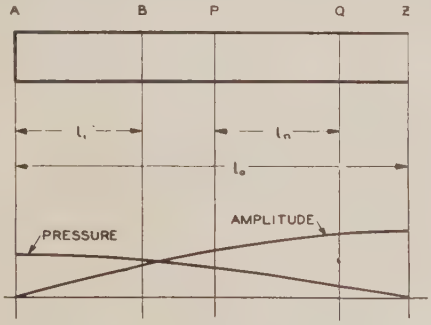

FIG. 1 OSCILLATION IN PIPE OPEN AT ONE END

Consider first the system shown in Fig. 1, consisting of a pipe with constant area and open at one end. The natural frequency of this system is

$$N = \frac{v}{4\,l_0} \cdot 60 = \frac{15\,v}{l_0} \text{ vibrations per min} \quad \ldots\ldots [1]$$

where l_0 is the length of the pipe in inches, and v the sound velocity in inches per second. The exhaust from a Diesel engine may with good approximation be considered as atmospheric air for which the sound velocity is

$$v = 585\sqrt{t + 460} \text{ in. per sec} \quad \ldots\ldots [2]$$

where t is the temperature in degrees F.

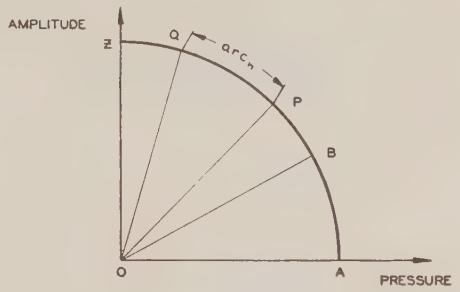

FIG. 2 POLAR DIAGRAM FOR SYSTEM IN FIG. 1

When the air in this pipe oscillates, amplitude and pressure at the various points are given by a sine and a cosine curve, Fig. 1. Amplitude and pressure at a point B in the pipe are therefore the co-ordinates for the corresponding point B on the circle shown in Fig. 2, where

$$\text{arc } AB = \frac{l_1}{l_0} \cdot 90 \text{ deg}$$

The scales used in this polar diagram are of no importance for the determination of natural frequencies since only the relative values are needed. Amplitude and pressure are therefore both measured in inches on the diagram. It is of importance, however, that these scales are not influenced by the area of the pipe.

Consider now length $PQ = l_n$ of the pipe. The corresponding circle arc $PQ = \text{arc}_n$ is

$$\text{arc}_n = \frac{l_n}{l_0} \cdot 90 \text{ deg} \quad \ldots\ldots [3]$$

Substituting l_0 from Equation [1]

$$\text{arc}_n = \frac{6\,N\,l_n}{v} \text{ deg} \quad \ldots\ldots [4]$$

The air particles between P and Q oscillate independently of what takes place in the rest of the pipe, with the exception that at P and Q certain pulsating pressures are supplied and certain volumes of air are pumped in and out. If these pressures and volumes were provided by oscillation at the same frequency but in pipes of different diameter, the oscillations between P and Q would not be affected.

This makes it possible to treat more complicated systems, Figs. 3 and 4. Each length of pipe with constant area will have a corresponding arc of a circle determined by Equation [4]. Where two pipes of different area are connected, the pressure does not change, but the two amplitudes, a_n and a_{n+1}, at the point of connection are inversely proportional to the areas, S_n and S_{n+1}

$$\frac{a_{n+1}}{a_n} = \frac{S_n}{S_{n+1}} \quad \ldots\ldots [5]$$

It may be added that the condition is different from that of constant flow, in which case the pressure changes where the area changes. This pressure change is necessary to accelerate the air passing to a different velocity. In a vibratory system, as con-

---

[1] Mechanical Engineer, Nordberg Manufacturing Company. Jun. A.S.M.E

[2] "Improving Engine Performance by Exhaust-Pipe Tuning," by P. H. Schweitzer, *Journal of the American Society of Naval Engineers*, vol. 56, May, 1944, p. 185.

[3] "Torsional Vibration in the Diesel Engine," by F. M. Lewis, Trans. Society of Naval Architects and Marine Engineers, vol. 33, 1925 p 109.

Contributed by the Oil and Gas Power Division and presented at a meeting of the Cleveland Section, Cleveland, Ohio, May, 1945, of THE AMERICAN SOCIETY OF MECHANICAL ENGINEERS.

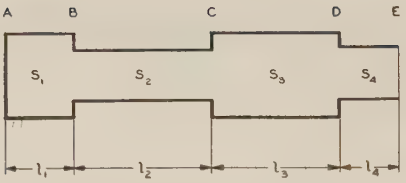

FIG. 3 MORE COMPLICATED SYSTEM
(Letters S indicate pipe areas.)

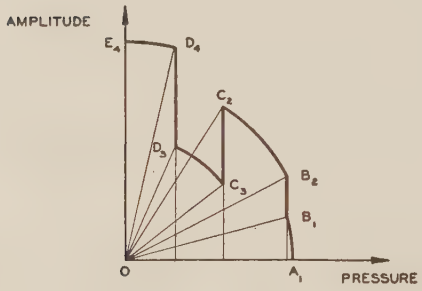

FIG. 4 POLAR DIAGRAM FOR SYSTEM IN FIG. 3

sidered here, the air in the whole pipe is accelerated simultaneously, thus not causing any sudden pressure changes at any point in the system.

CONSTRUCTION OF POLAR DIAGRAM

In order to explain the construction of the polar diagram in Fig. 4, it is first assumed that the natural frequency N of the system is known. The first point A_1 of the diagram is chosen arbitrarily on the abscissa axis because it gives the condition at the closed end A of the system where the amplitude is zero. Point B_1, which gives the condition at the end B of the first pipe, is located on a circle arc through A_1 determined by Equation [4] and with center in point O. Point B_2 gives the condition at the beginning of the second pipe, where the pressure is the same as at B_1, while the amplitude is determined by Equation [5]. Point B_2 is therefore found by simply multiplying the ordinate for B_1, as measured on the diagram, by this proportion. The circle arc B_2C_2 has center in point O and is determined by Equation [4].

The construction is continued through all the steps of the system, but, with atmospheric pressure at the open end, the last point must fall on the ordinate axis. However, if the diagram had been drawn for a frequency different from the natural frequency of the system, the last point would not have fallen on this axis. We have therefore in the polar diagram a method of checking whether a given frequency is the natural frequency.

It is added that the diagram may be drawn just as well by first choosing point E_4 arbitrarily on the ordinate axis and then proceeding the other way through the system. If point A_1 then falls on the abscissa axis, the frequency used was the natural frequency.

So far only the fundamental vibration of the system has been considered, but for higher frequencies the polar diagram, instead of 90 deg, will go through 270 deg, 450 deg, etc. For a system closed at both ends, the diagram will go through 180 deg (or 360 deg, 540 deg, etc.) thus beginning and ending on the abscissa axis. If the system is open at both ends, the diagram will begin and end on the ordinate axis.

Before calculating the natural frequency of an actual exhaust system, it must be simplified to a system of pipes with constant area, see, for instance, Figs. 3, 5, or 7. Parts of complicated shape are changed so that they keep the same volume and the same length, the length being measured as the distance the gases flow. Exhaust pots and mufflers are thus considered as short pipes with large area. At the open end of a pipe is added a length equal to 0.4 times the pipe diameter in order to provide for the fact that the air particles just outside the pipe take some part in the vibration.

A frequently used exhaust system has a pipe, with constant area S and length l, and some additional volume V as, for instance, valves or exhaust pots, near the closed end. If $V/S < l/2$, the system may be calculated as one straight pipe, Fig. 1, of length $l_0 = V/S + l$. The error involved is less than 3 per cent.

CALCULATING NATURAL FREQUENCY

As an example, the natural frequency will be calculated of the system shown in Fig. 5, assumed filled with exhaust gas at an average temperature of 500 F. The sound velocity, Equation [2], then is

$$v = 585\sqrt{500 + 460} = 18{,}100 \text{ in. per sec}$$

A rough estimate of the natural frequency is obtained from Equation [1] by considering the system as one straight pipe

$$= \frac{15v}{l} = \frac{15 \cdot 18{,}100}{160} = 1700 \text{ vibrations per min}$$

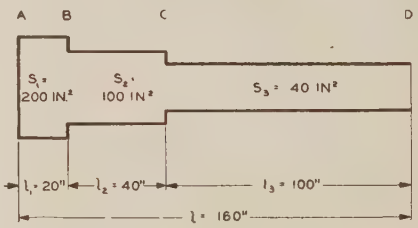

FIG. 5 EXHAUST SYSTEM CALCULATED IN EXAMPLE

The first polar diagram in Fig. 6 is drawn for this frequency. The angle of the circle arcs, all of which have center in point O, is from Equation [4]

$$\text{arc}_n = \frac{6Nl_n}{v} = \frac{6 \cdot 1700 \cdot l_n}{18{,}100} = 0.564 \cdot l_n \text{ deg}$$

where l_n is the corresponding pipe length.

Point A_1 is chosen somewhere on the abscissa axis. Point B_1 is found by

$$\text{arc } A_1B_1 = 0.564 \cdot l_1 = 0.564 \cdot 20 = 11.28 \text{ deg}$$

Point B_2 is found by multiplying the ordinate for B_1 by

$$\frac{S_1}{S_2} = \frac{200}{100} = 2$$

Point C_2 is found by

$$\text{arc } B_2C_2 = 0.564 \cdot l_2 = 0.564 \cdot 40 = 22.56 \text{ deg}$$

Point C_3 is found by multiplying the ordinate for C_2 by

$$\frac{S_2}{S_3} = \frac{100}{40} = 2.5$$

Point D_3 is found by

$$\text{arc } C_3D_3 = 0.564 \cdot l_3 = 0.564 \cdot 100 = 56.4 \text{ deg}$$

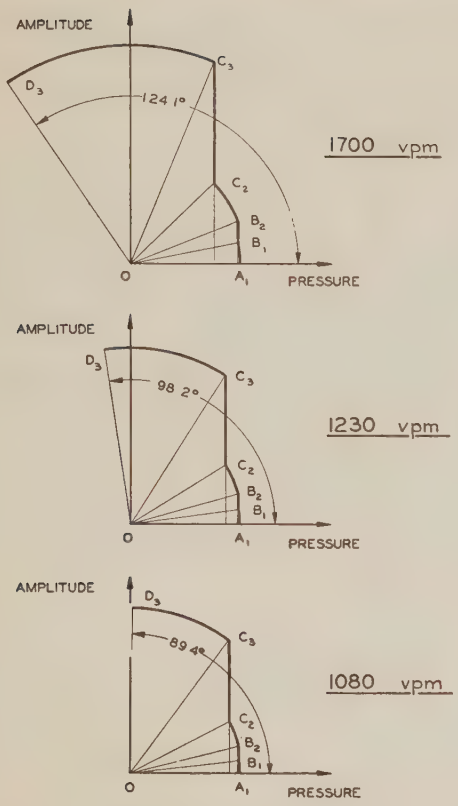

FIG. 6 POLAR DIAGRAMS FOR SYSTEM IN FIG. 5

The diagram shows that the estimate of 1700 vibrations per min was too high since the total angle described is 124.1 deg instead of 90 deg. A second estimate is therefore made

$$N = \frac{90}{124.1} \cdot 1700 = 1230 \text{ vibrations per min}$$

For this frequency a new polar diagram is constructed with the angle of the circle arcs

$$\text{arc}_n = \frac{6 \cdot 1230 \cdot l_n}{18{,}100} = 0.407 \cdot l_n \text{ deg}$$

The procedure is the same as before and the result this time is a total described angle of 98.2 deg.

By extrapolation from the first two estimates is found

$$N = 1230 - \frac{1700 - 1230}{124.1 - 98.2}(98.2 - 90)$$

$$= 1080 \text{ vibrations per min}$$

A polar diagram for this frequency has a total described angle of 89.4 deg which is quite close to 90 deg. However, by interpolation between the last two tries will be found

$$N = 1080 + \frac{1230 - 1080}{98.2 - 89.4}(90 - 89.4) = 1090 \text{ vibrations per min}$$

which is the natural frequency of the system with good accuracy.

During the construction of the polar diagram, difficulties may arise with points falling either outside the paper or too close to the center to give an accurate construction. The following rule will then be helpful: Any point in the diagram may be moved on a radius, closer to or away from the center, and the construction may then be continued from the new location.

BRANCHED SYSTEMS

Branched systems need a separate polar diagram for each branch and for the main pipe, all diagrams using the same frequency, Figs. 7 and 8. The diagrams for the branches are begun at the end of the branch and worked toward the junction. At this point the pressure p must be the same in both branches so the diagram for one of them, in this case branch II, is reduced accordingly. The diagram for the main pipe now can be drawn beginning at the junction point. The pressure p must be the same as in the branches, and the amplitude a_7 is determined by

$$a_7 \cdot S_7 = a_4 \cdot S_4 + a_6 \cdot S_6$$

where a_4, a_6, and a_7 are measured in inches on the diagram, and S_4, S_6, and S_7 are pipe areas. The diagram is then completed and, if the last point falls on the ordinate axis, we have the natural frequency of the branched system.

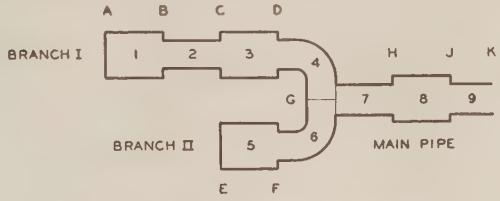

FIG. 7 BRANCHED EXHAUST SYSTEM

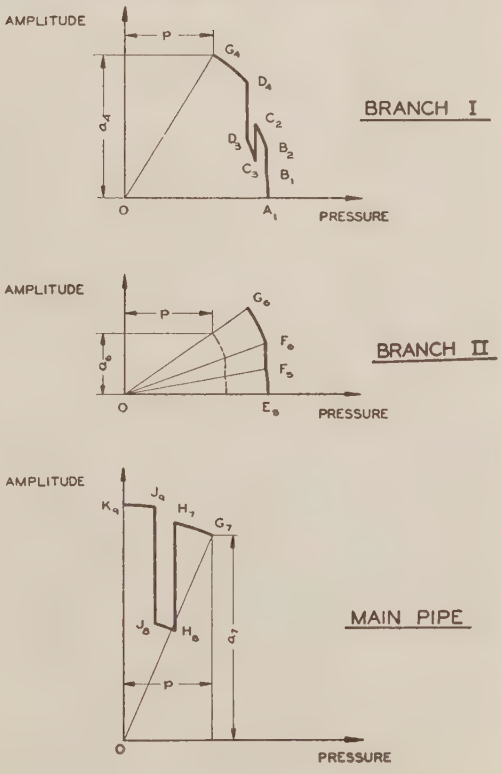

FIG. 8 POLAR DIAGRAMS FOR SYSTEM IN FIG. 7

Discussion

T. M. Robie.[4] What is the effect of discharging into a concrete pit and taking the exhaust pipe out somewhere before the end of the pit? In other words, supposing the exhaust pipe enters the pit horizontally at one end and leaves the pit vertically at some point before the other end of the pit. Would the vibrations in the pit, due to the exhaust gases hitting the end wall and bouncing back, affect the calculations and if so, what correction should be made?

R. O. Bernauer.[5] The author has been a co-worker with the writer at Nordberg for the past 5 or 6 years and in that time has worked on the critical speeds of crankshafts, parallel operation of synchronous generators, and various other vibration problems. He has always had a way of presenting anything very simply and has used polar diagrams a great deal in solving problems. This paper is his latest application of the polar diagram.

The writer is not going into a technical discussion regarding the use of it. In 1925, Professor Lewis used the polar diagram in the determination of critical speeds of crankshafts and the author is using it in an analogous manner in this paper. In parallel-operations problems he uses vector diagrams which are closely related. The writer congratulates the author on his unique and simple paper and thinks it should be of great value to engineers because of its simplicity. The paper deals with relative lengths from which pressures and amplitudes in any system may be secured.

In his presentation the author did not go into branch or network systems at any length but did give examples in his paper. These are obtained by the confluence of pipes and are very difficult to handle by other methods. His method is important in that it presents a simple way of solving branch or networks problems.

L. R. Turner.[6] In connection with the polar diagrams, what happens where there is a restriction at the end of the pipe?

L. M. Tichvinsky.[7] The determination of natural frequencies even of simple members of a Diesel engine is required in order to obviate a possible condition of resonance. Their calculations are rather lengthy and require accurate procedures.

The simple and elegant method presented by the author for the same purpose invites a question as to its accuracy. It is believed that the method is practical for designers; however, it would be interesting to know the error when comparing the calculated and the graphically obtained values of natural frequencies of a system such as shown in Fig. 7 of the paper.

V. L. Maleev.[8] The writer checked the method described in this paper for an exhaust system connecting several Diesel engines to a common muffler with a long tail pipe. The system contains chambers of various volumes and pipes of various diameters and lengths and it was a tedious job to find by usual calculations the natural frequency of the gases in this system. The polar-diagram method gave a great saving of time without any sacrifice of accuracy. In addition, this method shows very clearly what changes should be made in a system if a certain natural frequency is to be obtained.

The writer believes that, where due to the difficulty of calculating the natural frequency, the latter was often only estimated, with the polar-diagram method available the natural frequency actually will be computed and this will lead to better design. Furthermore, the writer believes that this method will be very helpful not only for tuning exhaust pipes of internal-combustion engines, but also for designing exhaust mufflers which up to date are not too satisfactory, and possibly in designing injection systems of compression-ignition engines.

The only criticism which pertains, however, not to the content of the paper, is in respect to the use of the designation "arc" instead of the word "angle;" 90 deg multiplied by a ratio gives a certain number of degrees and not an arc. In laying out the diagrams, again one uses angles on the protractor and not arcs. The polar diagram itself deals with angles, not arcs.

The paper is written very clearly and will be appreciated by all who have to deal with natural frequencies of gases or fluids in various systems. It constitutes a valuable contribution to the engineering literature.

Author's Closure

Mr. Robie asks about a concrete pit. Usually it will be sufficient to substitute a straight pipe, of the same length as the average path of the gases through the pit, and with an area giving same volume as the pit. If the part of the pit beyond the vertical outlet is very long, it may be necessary to consider it as a branch to the system. This also should be done if higher orders of vibration are considered.

Mr. Bernauer's kind remarks are very much appreciated. The association with him, through the past years, has always been very pleasant.

In reply to Mr. Turner, it can be said that if the open end of a pipe is restricted by a plate with a hole, this hole is considered as the open end. We then must add a pipe, of same diameter d as the hole, and of length $0.4\,d$, on both sides of the plate. It will be found this way, that the smaller the hole, the more effective is the mass in the added pipe, and consequently the lower is the natural frequency.

Mr. Tichvinsky questions whether the simplicity of the polar diagram is at the expense of accuracy. This is not the case. With a careful graphical construction the error should be less than 1 per cent and if that is not satisfactory, it is quite simple to calculate the steps of the diagram, if necessary with logarithms. Usually that does not serve any purpose, however, because the engine does not behave that accurately.

Compared to other published methods, the polar diagram is more accurate because it takes account of the inertia and the compressibility of the air throughout the system. In other methods, the inertia in exhaust pots or other large volumes is disregarded. The error involved is small, but the polar diagram takes care of the inertia automatically.

It is interesting that Professor Maleev has found the polar diagram useful and time-saving. That is what the author hoped to accomplish with this paper.

[4] General Diesel Sales Division, Fairbanks Morse & Company, Chicago, Ill. Mem. A.S.M.E.

[5] Nordberg Manufacturing Company, Milwaukee, Wis.

[6] National Advisory Committee for Aeronautics, Cleveland Airport, Cleveland, Ohio.

[7] Vice-President in Charge of Engineering, American Bearing Corporation, St. Louis, Mo., and Indianapolis, Ind. Mem. A.S.M.E.

[8] Aviation Division, Harvey Machine Company, Inc., Los Angeles, Calif.

Substitution of Lower-Quality Industrial Diamonds in Diamond Dresser Tools

By H. WHITTAKER,[1] CRANFORD, N. J.

A shortage of grinding-wheel dresser diamonds, which threatened the war effort early in 1942, led to an investigation of lower-quality diamonds hitherto not used for dresser tools. According to estimates made available by the British Ministry of Supply to the War Production Board, the supply of those qualities and sizes of industrial diamonds preferred and used in large quantities for truing and dressing abrasive grinding wheels was expected to be critical. The War Metallurgy Committee on the recommendation of the Office of Production Research and Development of the War Production Board undertook a study, as "restricted" Project NRC-507, to determine if lower-quality, more plentiful stones could be substituted for the preferred qualities and sizes for some or all wheel-truing and dressing operations. The investigation was carried out in the Research and Development Laboratories of the Crane Company, Chicago. This paper, based on that work, has been released for publication by the OPRD. In the first part of this investigation, a survey of users of diamond dresser tools established definitely that the higher qualities were preferred and used almost exclusively for dressing grinding wheels. The results of this survey and a review of the literature on the practices and the factors which influence the use of dresser tools were reported in a previous paper.[2] In order to provide positive information on the possibilities of using lower-quality stones, it was necessary to classify the seemingly infinite variety of industrial diamonds according to distinguishing characteristics and to test each type under controlled conditions which simulated grinding practices.

Examination and Classification of Industrial Diamonds

PRACTICALLY the entire production of industrial diamonds is distributed in bulk by the Diamond Trading Company, London, in the form of six general classified assortments. These assortments, from highest to lowest in value, are known commercially as "industrial serie," "finest industrials" "industrial smalls and mine rejections," "industrial cleavages and chips," "better bort" (not distributed in quantity at present), and "crushing bort."

The "industrial serie" contains the better, whole, mostly transparent stones from all producing areas. The stones are classified according to size, color, shape, and quality, and range in size from about 0.25 carat to 7 carat.

The assortment known as "finest industrials" is made up from the production of Consolidated African Selection Trust and Gold Coast fields. It contains whole stones, twinned crystals, called macles, flats, and a fairly large number of chips, or fragmented stones all in small sizes averaging about 0.05 carat, with some stones as large as 0.25 to 0.5 carat.

"Industrial smalls and mine rejections" is roughly 70 per cent C.A.S.T. production with the balance from Forminiere and Angola. The stones are all under 0.1 carat in size down to fine "sand" 60 per carat. Over one half the assortment is made up of chips and fragments dark in color, and the remainder is whole stones transparent to dark colored.

"Industrial cleavages" range from transparent to colored fragments, as opposed to single, whole stones, in all sizes. Darkest colors and frosted and coated fragments are usually not included.

All of the remaining materials from all producing areas not included in the foregoing assortments are lumped together in "crushing bort," which is intended for crushing to powder. The dark-colored coated fragments and stones characteristic of the Belgian Congo predominate in crushing bort; and for this reason the term crushing bort is often used synonymously with Belgian Congo. "Better bort" consists of the single, whole, and sound stones selected from crushing bort.

The main source of dresser-tool stones is the industrial serie. The most plentiful sources, and practically the only sources, of substitutes for dresser-tool stones over 0.25 carat in size to supplement the supply are crushing-bort and better-bort assortments. Samples representing the preferred types of dresser stones and the possible substitutes were obtained for testing. Stones were selected from 15 of the 32 categories in the industrial serie. These categories were second yellow, first and second colored, first gray, first brown, dark and darkest brown, first and second gray brown, second river, and common gray colored rounds, first yellow, first brown, first gray, and second gray shapes. A few samples of "cleavages" were obtained, representative of the classifications known as colored, first and common gray cleavages. A 5000-carat parcel of bort completed the sampling of materials. It was made up of selections from crushing bort and better bort and it covered most of the varieties found in these assortments, such as common coated stones, common coated cleavages, black-bort stones, and colored-bort stones.

Representative samples of each of the different categories were examined with a binocular microscope, a petrographic microscope, and other methods for soundness and distinguishing characteristics. The higher-quality stones in the industrial serie were transparent whole stones of definite crystal habit. Most of the stones contained small inclusions and several stones were fractured internally. The lower-quality stones in the serie were darker in color, of low transparency, and they contained inclusions in fairly large amounts. The crystal habit of the lower qualities was not so well defined, and these stones had more striated and irregular surfaces than had the other qualities. Three quarters of the transparent stones showed fluorescence, which varied in degree from vivid to pale shades of blue and yellow, when the stones were exposed to the light of a mercury-vapor lamp. About one half of the stones exhibited phosphorescence. A majority of the diamonds examined under polarized light showed the presence of internal strain. Density measurements made by the immersion method using carbon tetrachloride on about 50

---

[1] Consulting Engineer. Mem. A.S.M.E.

[2] "Substitution of Lower Quality Diamonds," War Metallurgy Committee Progress Report W-57, Nov. 6, 1943.

Contributed by Special Research Committees on Cutting Fluids and Metal Cutting Data and Bibliography and presented at a Meeting of the Chicago Section, Chicago, Ill., June 18–19, 1945, of The American Society of Mechanical Engineers.

of the larger stones gave values of density ranging from 3.510 to 3.526 on the basis of water at 4 C.

In contrast with the samples from the serie, a majority of the stones examined from the bort assortment were translucent to opaque; the degree of opacity appearing to vary with structure and crystal habit. Most of the stones were well defined in crystal habit. A considerable number of the stones consisted of cleavages, fragments, and aggregated crystal masses. Those stones that were sufficiently translucent to enable internal inspection were observed to contain large areas of inclusions. Only about one fifth of the opaque coated stones examined showed fluorescence of dull intensity, and a few showed phosphorescence. A few of the more opaque stones were radiographed to determine whether internal defects could be detected by this method. The stones were immersed in Russian mineral oil in cellophane containers and exposed for 5 sec at 5 in. focal distance to unfiltered X rays produced by a molybdenum target operated at 20 kv and 18 ma. The resulting shadowgraphs, several of which are given in Fig. 1, indicated that it may be possible to detect flaws and inclusions in opaque stones by this method. However, the detection of small inclusions of foreign elements having low absorption coefficients comparable to carbon is not possible; and thus limitations may be placed on the usefulness of radiography.

It was desirable to supplement the present commercial classification, which is rather loose, with a classification which would make possible closer distinctions among the various types of diamonds for testing purposes. While the physical properties of diamond establish its suitability for wheel dressers, variations in structural characteristics and soundness are the criteria for selection of individual stones.

The structural characteristics and factors to be considered are as follows:

1 Wholeness; whole stones or fragments.
2 Crystal habit; largely determines shape.
3 Opacity; degree of impurities.
4 Homogeneity; continuity of structure.
5 Soundness; number of fractures and cracks.
6 Size.

Compared with the present loose classification, crystal habit is analogous to shape, quality is a combination of wholeness, opacity, homogeneity, and soundness, and color is partially analogous to opacity. Practically all of the industrial serie stones were whole single crystals of definite crystal habit. Of the 5000 carats of better and crushing bort available for this investigation, about 3000 carats were whole stones. Well over 90 per cent of the bort exhibited definite crystal habit. One half of the whole stones were single crystals, 17 per cent were twinned crystals, 30 per cent were aggregated crystal masses, and 3 per cent were of no discernible crystal habit.

It was observed that the stones occurred in one of three crystal forms: Octahedron, dodecahedron, and cube, and combinations of these forms. No other crystal forms were evident except modification to tetrahexahedron. Thirteen classes, grouped under five general headings, illustrated in Figs. 2 and 3, were defined which served to include all of the observed forms and combinations, as follows:

Dodecahedron. Class No. 1, "distorted dodecahedron:" Elliptical, dodecahedron crystals lengthened in the direction of trigonal axis of symmetry with faces more or less modified to tetrahexahedron.

Class No. 2, "normal dodecahedron:" Symmetrical dodecahedron crystals with or without curved faces resulting from tetrahexahedral influence.

Octahedron. Class No. 3, "octahedron - dodecahedron:" Twenty-faced combination octa-dodec crystals with octahedron faces usually curved and shieldlike.

Classes No. 4 and No. 5, "octahedron:" Octahedron crystals with or without rounded faces caused by transparent or glassy growth plates, and giving rise to striated edges. No. 5 is same except growth plates are translucent.

Combination Octahedron, Dodecahedron, and Cube. Classes Nos. 6 to 9 constitute a series between an octahedron and a cube with the sizes of the octahedron faces decreasing as the cube faces increase, the dodecahedron faces varying accordingly: No. 6 octahedron faces large, others small; No. 7 octahedron faces large, other faces larger, but not as large as the octahedron faces; No. 8 equal-sized octa-dodec-cube faces, which configuration produces a spheroidal stone; No. 9 minor octahedron and dodecahedron faces relative to cube faces.

Cube. Class No. 10 and No. 11, "cube:" Six-sided crystals with rough terraced growths on faces. No. 11 has convex, concave, pyramidal, or flat faces.

No Definite Crystal Habit. Classes No. 12 and No. 13, no habit: Crystal habit not evident with glassy or transparent rind. No. 13 has translucent to opaque coating or rind.

Opacity, degree of diaphaneity or ability to transmit light, is a measure of the amount of impurities in the form of dispersed included matter. A scale was set up based on the amount of light transmitted through a stone using a 10-w Mazda lamp contained in a white-walled box covered with a $^1/_8$-in-thick sheet of opal glass. An opaque stone that did not transmit any light under these conditions was assigned a value of 7 and a water-white stone was assigned a value of 1. Five other stones having equal intermediate steps of increasing opacity were selected to serve as standards of comparison to give a complete graded range of opacities.

Homogeneity, or continuity of structure was observed to be related somewhat to crystal habit and opacity. A large number of stones which fell in classes 6 to 9, "combination octahedron-dodecahedron-cube," and which had high opacities 4 to 7, consisted of a transparent octahedron crystal nucleus surrounded by a secondary growth containing large amounts of inclusions, thus giving rise to a discontinuity in structure at the interface between core and rind. The thickness of the secondary growth appeared to be rather definitely related to the width of the dodecahedron face in the ratio of 0.4–0.7 to 1, depending on the extent of rounding of the face. Transparent crystals, classes 1 to 5 in particular, appeared to be built up of layers on a basic octahedron form. The interfacial boundaries in this case do not result in as marked a discontinuity in structure because the primary and secondary growths are about equal in composition.

During the detailed examination of over 5000 carats of bort and higher-quality material, a great deal of evidence was found in support of the theory of diamond-crystal formation stated by Polinard, "one might explain that all forms of diamonds are due to the development and to the piling up of octahedron plates which superimpose themselves on the faces of an octahedral nucleus."

Soundness is used to indicate the number of weaknesses which may be contained in a stone as a result of cracks, fractures, and fissures. The soundness of transparent stones can be judged by inspection with a microscope using suitable lighting. Radiography may be of some assistance in detecting flaws in opaque stones which cannot be inspected by ordinary means. The Norton Company has used an impact test to grade bort for suitability for dresser tools with fair success. That firm has tested samples of most of the classes herein described. According to the results of these tests, the impact resistance of single crystals averaged higher than either twinned or aggregated stones in like classes. Discernible differences in impact resistance were ob-

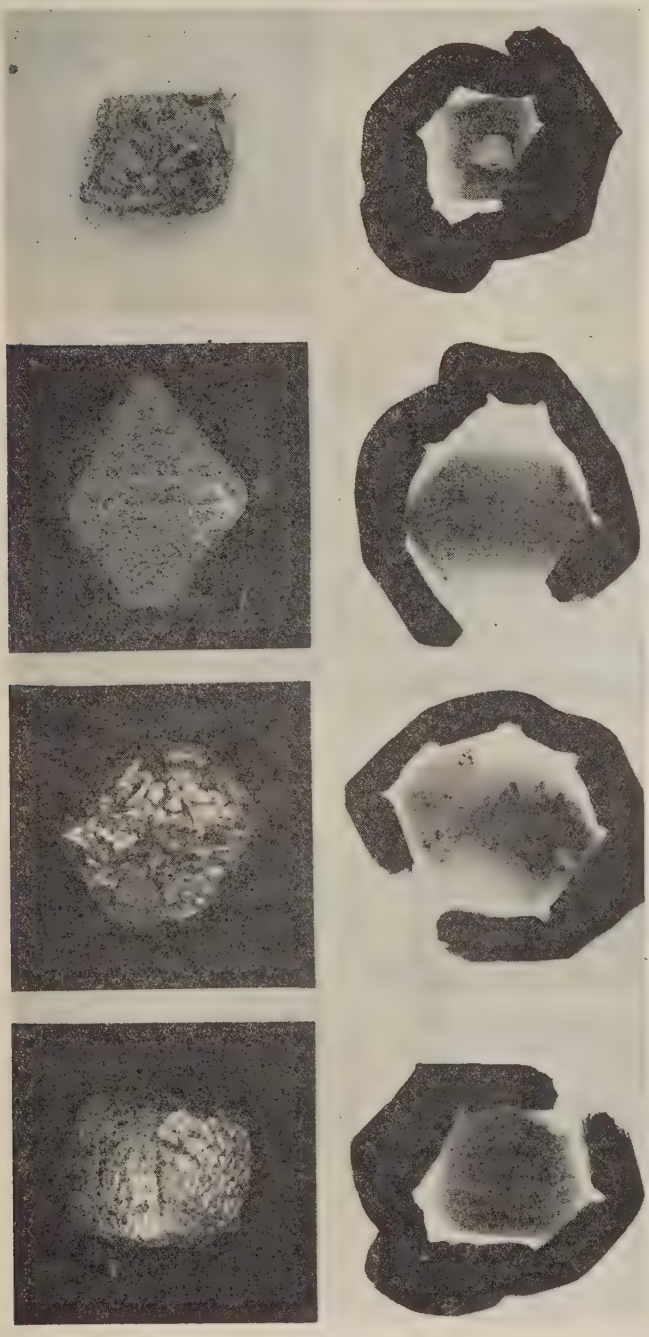

Class No. 11
Opacity—7
Opaque Cube
Diamond inclusion
shown

Class No. 6
Opacity—4
Opaque Combination

Class No. 4
Opacity—5
Opaque Octahedron
Inclusions shown

Class No. 11
Opacity—3
Translucent Cube
No inclusions

FIG. 1 RADIOGRAPHS OF OPAQUE DIAMONDS
(The black outline which surrounds the radiographs is caused by aluminum foil which was used to support the stones.)

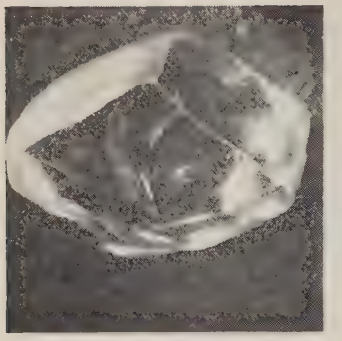

Class No. 1
Opacity—1
Distorted dodecahedron

Class No. 2
Opacity—1
Normal dodecahedron

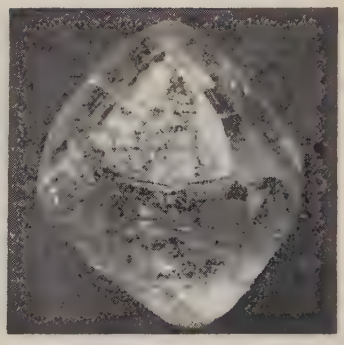

Class No. 3
Opacity—1
Octahedron-dodecahedron

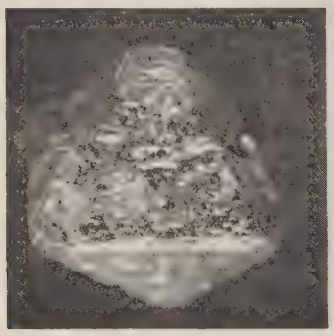

Class No. 4
Opacity—2
Octahedron
Transparent growth

Class No. 5
Opacity—3
Octahedron

Class No. 6
Opacity—4
Combination habit

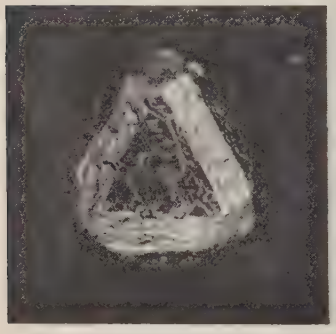

Class No. 7
Opacity—4
Combination habit

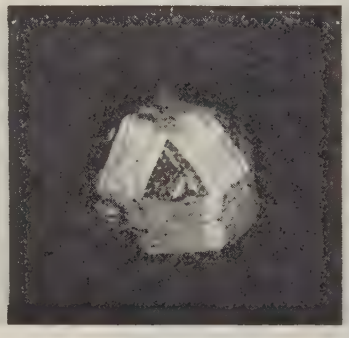

Class No. 8
Opacity—3
Combination habit

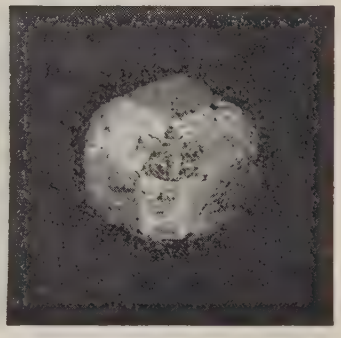

Class No. 9
Opacity—4
Combination habit

FIG. 2 ILLUSTRATIONS OF CLASSES OF DIAMONDS

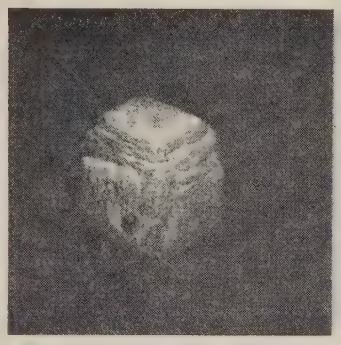

Class No. 10
Opacity—3
Cube

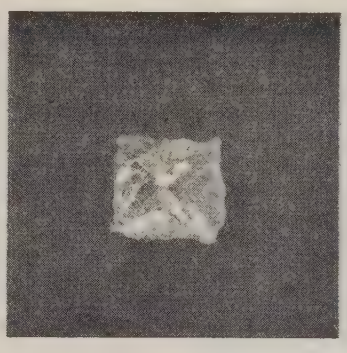

Class No. 11
Opacity—2
Cube

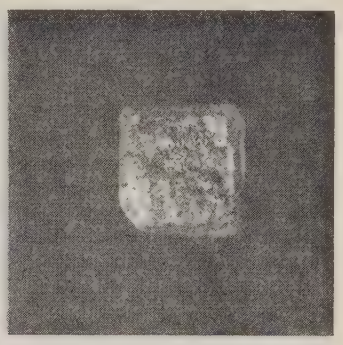

Class No. 11
Opacity—1
Cube

Class No. 11
Opacity—7
Cube

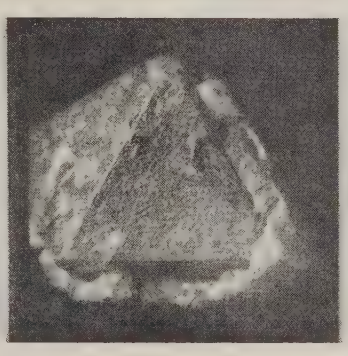

Class No. 6
Opacity—4
Combination habit
Coating broken away

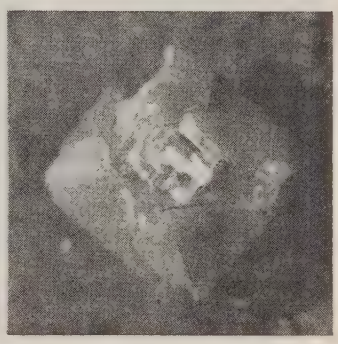

Class No. 6
Opacity—5
Combination habit
Coating broken away

FIG. 3 ILLUSTRATIONS OF CLASSES OF DIAMONDS AND COATED STONES

tained for six classes tested. The more rounded stones exhibited greater resistance to impact than did stones having sharp corners. The classes fell in the following order: Classes Nos. 9, 8, 7, 6, 10, and 11, from 92 per cent unbroken grain to a low of 50 per cent unbroken grain. It may be possible to adjust the impacting force to just destroy flawed and weak stones without damaging sound stones and thus produce a sharper and more efficient separation.

The classification herein proposed and used experimentally on over 5000 carats of industrial diamonds accounts for the most important factors which are thought to influence the utility of industrial diamonds for dressing purposes. Whereas, further refinements may be needed, it is flexible and allows for all possible types and combinations of crystal form, structural differences, and degrees of impurities. The author has examined, in addition to the materials herein described, original parcels of all assortments among which he has not found any stones that could not be fitted into this classification, in particular with respect to crystal habit.

A stone may be completely defined for the purpose by designating (1) the class number, from 1 to 13, which defines its crystal habit and shape; (2) the opacity number, from 1 to 7, which indicates degree of impurities; (3) the extent of flaws; and in addition, (4) by indicating whether a whole stone, a fragment, a twin or an aggregated crystal mass. Industrial-serie materials fall in classes 1 to 4 in the lower opacities, numbers from 1 to 3, with some exceptions; for example, dark-brown rounds having an opacity of 5. The major portion of material in crushing bort falls in classes 6 to 9 and higher opacities, numbers from 3 to 7. Minor amounts fall in classes 3 to 5 and 10 to 13.

GRINDING-WHEEL DRESSER-TOOL TEST METHOD

To compare the different varieties of diamonds as to their relative suitability for dressing grinding wheels, a test method was developed for the rapid quantitative determination of the rate of wear under simulated shop-dressing conditions. The test consisted of the continuous dressing of a 1-in. face-grinding wheel, the periodic measurement of the amounts worn off the diamond and the abrasive wheel, and careful observations of changes in shape and chipping of the diamond point. The essential parts of the test apparatus, shown in Fig. 4, were a heavy tool holder, specially designed to allow for any desired setting of drag, rotation, and traverse angles, mounted on the table of a Brown and Sharpe No. 2 cylindrical grinder with automatic feed, counter, speed control, and fluid system for wet dressing. The diamonds, which ranged from $^1/_2$ to 1 carat, were set by the powder hot-press method in a large-head steel shank. The shank was $^7/_8$ in. long, $^1/_2$ in. diam at the head, and $^1/_4$-in-diam shaft.

To save time and also to enable an inspection of the stone as wear took place, the loss on the diamond was measured by means

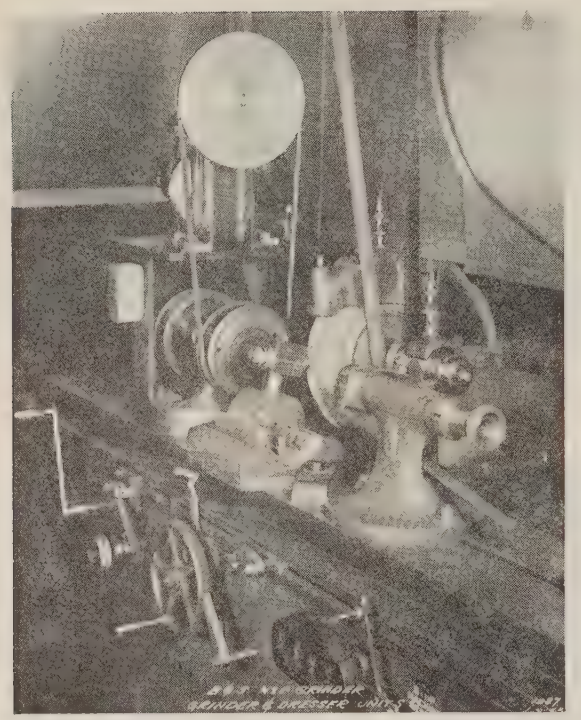

FIG. 4 WEAR-TEST APPARATUS

of a graphical method. The diamond point in its shank was projected on a screen at ×100 magnification and the profile recorded. After testing, a second profile was made in the same position over the first projection. The difference between the two profiles was a measure of the loss in height because of wear. The area of the flat generated on the diamond point was traced at ×100 magnification using a reflection microscope and a reflex camera and was measured with a planimeter. Height loss and area measurements are all that are needed to compute the volume loss, provided the shape of the removed portion is known. The volume loss was then converted to weight loss using 3.52 for the specific gravity of the diamond. The computed weight loss of the diamond in carats was divided by the volume in cubic inches removed from the grinding wheel to give the "unit of wear rate." Since the order of magnitude of the unit of wear rate was ten hundred thousandths of a carat per cubic inch, the notation ct. $\times 10^{-5}$/cu in. was used, that is, the unit was multiplied by 100,000 in order to express the result in terms of whole numbers.

The test procedure had the advantage of savings in time and materials, but precision was sacrificed to some extent. By means of this testing procedure a diamond could be tested under almost any combination of conditions that might be encountered in practice in about a day and a half. To do the same job by weighing would consume 5 times as many test wheels and would take a week, because of the larger amount of diamond that must be worn off to enable an accurate weight determination. The greatest source of error was in the assumption of the shape of the solid removed in making the volume-loss computation.

Since the actual shape of the solid figure removed from the point of the diamond would be some shape between that of a sharp-sided pyramid and a segment of a sphere of equal heights and base areas, depending on how close the assumed shape is to the actual shape, the error can be as great as 20 per cent. This was checked experimentally by testing a number of stones sufficiently to enable accurate weight-loss determinations, and in most cases the wear rates determined by weight and by computed volume were well within the possible error of 20 per cent. Therefore, for purposes of comparison in this investigation, differences less than 25 per cent, roughly 5×10^{-5} ct./cu in. (0.00005) were not considered significant; two stones of 15 and 20 $\times$ 10^{-5} ct./cu in., respectively, would be considered alike in so far as could be determined.

Of interest in the establishment of a set of standard test conditions for comparison of diamonds and also of practical value were the tests that were made to learn the effects of the many factors which may influence the rate of wear of diamond dressers in the dressing operation. These factors had to be controlled in order to place the test results on a comparable basis:

1 One set of factors is determined by the conditions of operation, such as loading of the wheel with metal, wheel speed, rate of traverse, feed, and use of a coolant. In practical grinding operations the grinding wheel is dressed and trued after the wheel has been loaded with metal and the edges are broken down from the grinding of work. No appreciable difference in wear rates was found when a wheel was dressed after it was loaded with metal by grinding a number of pieces of hard tool steel and when the wheel was dressed without loading. Changing wheel speed from 4000 to 6000 fpm had very little effect on wear rate. Nor did varying the rate of traverse between 0.001 and 0.003 in. per revolution affect rate of wear to any great extent. Contrary to expectations, a 0.001-in. feed caused $1^1/_2$ times the wear rate of a 0.005-in. feed. However, it will be noted that for each pass a 5 times greater volume of grinding wheel is removed with a 0.005-in. feed. Thus the average loss per pass was 3 times as great for the 0.005-in. cut as for the 0.001-in. cut. Observations on the durability of diamond dressers in the shop are usually based on the number of dressings. The feed used would have an important bearing on the comparisons. A considerable difference in wear rate was observed between wet and dry dressing. The average rate of wear on nine stones when the wheel was dressed dry was 20×10^{-5} ct./cu in. and was only one fifth as great, 4×10^{-5} ct./cu in., when the tools were flooded with water at the rate of 7200 cc/min. The difference tended to become slightly greater as grit size was decreased. Average values obtained for 36, 60, and 120-grit vitreous wheels were 27, 18, and 8 for dry dressing and 6, 4, and less than 1 for wet dressing, respectively (all $\times 10^{-5}$ ct./cu in.).

2 Another set of factors is introduced by the variations in types of grinding wheels. The grinding-wheel factors are grit size, grade, type of bond, type of abrasive, and size. The rate of wear may be affected as much as tenfold over the range of types of grinding wheel. The rate of wear increased as grit size increased. A soft grade (Norton 60I5BE) wheel abraded the test diamond at the rate of 7; a medium grade (Norton 60M-5BE) at 11; and a hard grade (Norton 60P5BE) at 13, $\times 10^{-5}$ ct./cu in. Of all factors in the wheel, the type of bond had the greatest effect on wear rate; for example, vitreous-bonded wheels are up to 10 times as abrasive to the diamond as are resin-bonded wheels. The effect is less marked for fine grits, soft grades, and wet dressing, but is still of the order of fivefold. The two types of abrasive aluminum oxide and silicon carbide have similar effects on wear rate. That the size of the grinding wheel influences wear on the diamond was apparent from the results of tests on a 20-in. × 6-in. wheel. The average wear rate of 10 stones was 19×10^{-5} ct./cu in. as opposed to 4×10^{-5} ct./cu in. obtained on a 12-in. × 1-in. wheel, both dressed wet. The increase in wear rate with size of wheel is due, possibly, to the increased time of continuous contact of the wearing surfaces, and the

TABLE 1 DIAMOND-DRESSER SHOP TESTS ON HEAVY AND LIGHT GRINDERS

Tests made by	Crane Company		Buick Aviation Plant	
Tool no.	6689	6690	103	72
Initial weight, carats	3.1	3.9	0.725	0.688
Final weight, carats	2.59	3.83	0.720	0.685
Loss in weight, carats	0.51	0.07	0.005	0.003
Make of grinder	Cincinnati	Mattson	Heald	Heald
Type of grinder	Centerless	Surface	Internal	Internal
Wheel size, in.	20 × 6	20 × 3	3½ × 2	3½ × 2
Wheel grit size	36	36	60–	60–
Number of dressings	1532	243	810	516
Passes per dressing	2	2	3 and 1	3 and 1
Depth of cut, in.	0.0025	0.002	0.003 and 0.001	0.003 and 0.001
Volume of wheel removed	2514	184	141	90
Wear rate, ct. × 10^{-5}/cu in.	20.1	38	3.6	3.3
Work ground	Valve stems	Toggle-valve links	6-In. gears	6-In. gears

tendency of the area of the wearing surface of the diamond to increase, both resulting in higher temperatures on the stone. The effect of wheel size was further demonstrated in results of shop tests given in Table 1. These results also served to indicate that the order of magnitude of wear rate under the test conditions was the same as under shop conditions.

Thus it appears that the rate of wear of diamond dressers is considerably influenced by the conditions of use. The tests, while preliminary, served to establish in a general way the wide range of wear rates that may be encountered. The wear rate may vary between 1 and 40 × 10^{-5} ct./cu in. depending upon the combination of conditions and may be as high as 100 × 10^{-5} ct./cu in. under particularly severe conditions. For most dressing operations the average combination of conditions produces a wear rate of 15–25 × 10^{-5} ct./cu in., and this would be a good figure to keep in mind, or about 20 × 10^{-5} carat per dressing, since between ½ to 1 cu in. is removed per dressing from medium-sized wheels. Consumption of one half of a 1-carat stone should produce about 2500 dressings. To produce a reasonable number of dressings per tool, the size of the stone must bear some relation to the rate of wear for the conditions of use. This does not mean that for double the rate of wear, the stone should necessarily be doubled in size, but a certain minimum size is required. However, factors other than the rate of wear must be considered in determining the proper size to be used.

Another factor which has received very little attention is the effect of the shape and size of the stone on the finish imparted to the wheel for different classes of grinding wheels and work. Also, the size and shape of the stone are important in connection with form-grinding. When these effects are known more precisely, size and shape specifications can be developed which should lead to more efficient and economical use of diamond dressers. Of interest in this connection was the observation that in the dressing operation the wear on the diamond progresses across the flat in the form of a ridge as the diamond is traversed across the wheel, starting at the point of first contact with the wheel (see Fig. 5). The ridge may be compared with the broad cutting edge of a chipping tool. Thus the main working area of diamond is roughly the length of the developed ridge, which extends across the flat, × the width of the ridge, which usually measures less than 1 mm. The remaining areas do, however, maintain some rubbing contact. Recognition of this mechanism of cutting and wear involved may lead to improved designs of dresser tools.

Wear Tests on Varieties of Industrial Diamonds

Representative samples of the various classes of industrial diamonds were tested under controlled standard conditions designed in conformity with the foregoing findings to reproduce average shop conditions. A 1-in-wide by 12 in. to 7-in-diam, 60-mesh-grit medium-grade vitreous-bonded aluminum-oxide grinding wheel was dressed dry; the speed of the wheel was maintained at 5000 fpm; and the tools were traversed, with a

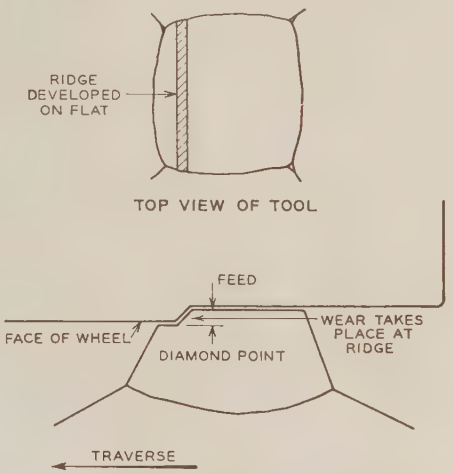

Fig. 5 Diagram Showing Contact Between Diamond Point and Grinding Wheel

drag angle of 15 deg across the 1-in. face of the wheel at a rate of 0.0015 in. per revolution for six to eight runs of 50 passes each. The amount of wear was measured after each 50 passes, and the tool was rotated to a new position for each run.

The results of the tests on 60 diamonds are listed in Table 2 on an "adjusted" basis and on an "over-all" basis. The "adjusted" value of wear rate is derived by excluding values of runs in which chipping occurred and in which "soft" directions happened to be struck to give abrupt increases in wear. This latter effect was an indication that the variation in hardness of diamond influences the performance of dresser tools; for, when the orientation of the stone during a run happened to coincide roughly with the so-called soft direction, almost invariably the wear rate for the run was high and the flat usually had a polished or shiny appearance. The soft directions are crystallographically the same directions that the gem cutter uses in lapping on the facets of a cut stone. Analysis of a large number of runs on a large number of stones indicated that the rate of wear on the soft directions was on the order of 3 times as high as on the other or "hard" directions.

Incidentally, when a slight drag angle is used in the dressing operation, setting of the diamond with a crystallographic axis parallel with the axis of the tool would tend to avoid the possibility of striking soft directions as the tool is rotated to new positions; and thus the best results would be obtained.

Reference to Table 2 will indicate that the results on the "adjusted" basis show definitely that many of the lower-quality diamonds are as resistant to abrasion by grinding wheels as are the higher-quality stones. Taking each class as a whole, there were no distinct differences among the classes. The wear rates

TABLE 2 WEAR RATE OF DIFFERENT TYPES OF INDUSTRIAL DIAMONDS

GROUP	CRYSTAL CLASS NO.	OPACITY NO.	D.T.C. CATEGORY	STONE NO.	WEAR RATE ADJ.[1]	WEAR RATE OVERALL[2]	CHIPPING
A. Dodecahedron	1	1	1st Brown Round	102	20	49	None
	1	2	1st Yellow Shape	111	36	38	None
	1	2	Common Grey	141	31	37	None
	2	2	1st Grey Round	93	14	12	None
	2	2	1st Colored Round	1	13	11	None
	2	2	1st Colored Round	9	10	10	None
	2	2	Common Coated	271	11	17	None
	2	2	2nd Grey Brown	63	11	16	None
	2	2	2nd River Round	70	16	20	Chip
	2	4	Darkest Brown Round	43	15	14	None
B. Octahedron	3	1	2nd Yellow Round	126	24	41	Small Chip
	3	1	2nd Grey Shape	78	11	46	None
	3	1	1st Grey Round	97	24		None
	3	2	2nd Yellow Round	84	12	32	None
	3	2	1st Cleavage	139	16	50	None
	3	2	Dark Brown Round	37	21	19	None
	3	3	Black Rejection	273	10	5	Chip
	4	1	1st Brown Shape	129	18	23	Chip
	4	1	Colored Cleavage	136	14	108	Many chips
	4	1	Cut Gem Stone	158	12	18	Chip
	4	2	1st Grey Shape	120	32	34	Crumbled
	4	2	1st Grey Brown	52	16	20	Chips
	4	2	2nd Grey Brown	61	12	21	None
	4	5	Black Rejection	283	11	8	None
	4	6	Black Rejection	284	12	30	Chip
	5	5	Common Grey Colored	28	15	31	Large Chip
	5	5	Black Bort Stone	156	36	52	Large Chip
C. Combination Octa-Dodec-Cube	6	2	Common Coated	272	--	--	Large Chip
	6	3	Common Coated	275	12	18	None
	6	4	Colored Bort Stone	281	18	42	None
	6	4	Common Coated	154	18	10	None
	6	4	Colored Bort	250	20	--	None
	6	6	Colored Bort Stone	164	13	24	None
	6	7	Black Bort Stone	286	9	9	None
	7	2	2nd Colored Round	16	10	9	None
	7	4	Common Coated	160	10	37	Crumble
	7	4	Common Coated	276	13	15	Chip
	7	4	Common Coated	152	30	53	Chipping
	7	5	Common Coated	169	13	38	Crumble
	7	5	Colored Bort Stone	144	9	12	Small Chip
	7	5	Black Rejection	279	26	26	None
	7	5	Common Coated	282	29	356	Chipping
	7	5	Common Coated	174	11	--	None
	7	7	Black Rejection	148	22	160	Large Chip
	8	4	Black Bort Stone	277	31	78	Chip
	8	7	Black Bort Stone	150	11	290	Large Chip
	8	7	Black Bort Stone	287	47	353	None
	9	5	Colored Bort Stone	278	22	22	None
D. Cube	11	2	1st Colored Round	7	36	42	Large Chip
	11	2	Common Coated	270	13	15	None
	11	2	Common Coated	269	14	29	None
	11	2	Common Coated	163	18	--	None
	11	3	Common Coated	167	23	41	Many Chips
	11	3	Common Coated	274	21	59	Chips
	11	4	Colored Bort	162	22	--	None
	11	6	Black Rejection	285	24	24	Chip
	11	6	Colored Bort	280	25	37	None
	11	7	Black Rejection	289	18	38	Chips
E.	12	3	Common Coated	143	14	15	None
	12	6	Black Rejection	290	11	54	Crumble
	13	7	Black Rejection	288	24	69	None

[1] Adjusted wear rate in carats loss per cubic inch of wheel removed $\times 10^{-5}$. Values are adjusted to exclude high individual values due to wear on soft directions, chipping, crumbling, etc.

[2] Over-all wear rates in carats loss per cubic inch of wheel removed $\times 10^{-5}$. Values are actual over-all wear based on weighing stones before and after testing.

adjusted basis, in each group varied from about 10 to 25 and averaged 18×10^{-5} ct./cu in., with a few scattered values above 30×10^{-5} ct./cu in. in each group.

The "over-all" wear rate differs from the adjusted wear rate in that it was based on the total amount of diamond lost and included loss due to wear in all positions, chipping, and crumbling. The difference in rate between over-all and adjusted wear rates might be thought of as a measure of the structural failure which takes place. Excessive over-all losses, values over 40×10^{-5} ct./cu in. in Table 2, shown by a number of stones in all classes, were caused in most cases by chipping and crumbling of localized areas. This excessive over-all rate was more prevalent among the lower qualities, classes 4 to 11, than among other qualities. On the other hand, many of the lower qualities did not exhibit chipping or localized increases in wear, and the over-all wear rates were essentially equal to the adjusted wear rates.

In the progress of this research it became more and more apparent that the chief factor involved in the use of diamonds for wheel-dressing purposes is the ability of the stone to withstand fracture. Structural weaknesses of diamonds which may be potential sources of failure are the same as those for other crystalline materials, such as cleavage planes, twinning planes, internal fractures, incipient cracks, inclusions which act as loci of stress concentrations. To this list should be added the interface between the interior crystal and the exterior, or later growth, which is often of a dissimilar color, characteristic of coated stones. Relatively easy parting in the octahedron plane known as cleavage follows from the diamond structure. All that is needed is a sufficient force applied in the proper direction to cause cleavage. Incipient cracks in the cleavage directions increase the tendency to cleave and are potential sources of failure. Large inclusions of dissimilar material may be causes of failure, in particular, under thermal stresses. Flaws and internal fractures are potential starting points of failure.

What has been said of cleavage planes is also true of twinning planes. Diamond twins are common with the twinning plane parallel to the octahedron face. These are known as contact or spinel twins. In the trade the stones are called macles. Judging from the structure of the so-called coated stones, the interface between the interior crystal and the coating, or secondary growth, may be a plane of weakness. Pieces of the coating are likely to be pulled out when the stone is worn to expose the interior crystal. It would be expected that the position of the plane of weakness in the stone would be important. The further from the working point that the flaw, or plane of weakness, is removed, the less should be its influence. The setting metal and method is important in that a stone well supported at all points is less apt to fail through a plane of weakness.

To test for strength, in particular, the effect of weaknesses in structure, a large number of runs must be made to wear the stone down and expose the planes of weakness; and also, long use may develop cracks from continuous shocking. While the laboratory test was quite severe in that no coolant was used, the amount of abrasive wheel removed was small, and very little of the diamond was consumed in a test. In the life of a tool in the shop the number of passes is far greater by 50 to 100 times. Hence the chances of striking a plane of weakness in a stone are increased proportionately. In order to approach the requirement of a large number of dressings, tests were made with ten tools representing the most important classes of stones on a Cincinnati centerless grinder. The conditions of test were essentially the same as those of the standard laboratory test except that a coolant was used and the wheel was much larger. Each tool was given at least 850 passes over the wheel, removing between 250 to 270 cu in. of the wheel in a test. The amount of diamond consumed in each case was between 0.05 and 0.1 carat which amounted to 5 to 20 per cent of the stone, depending on the initial size. The results are listed in Table 3.

TABLE 3 WEAR RATE ON VARIOUS CLASSES OF STONES WHEN TESTED ON CINCINNATI CENTERLESS GRINDER USING 20-IN. × 6-IN. WHEEL, WET DRESSING

	Wear rate—carat loss × 10^{-5} per cu in. wheel removed—			
	Standard laboratory test	Cincinnati centerless grinder test, 20-in. × 6-in. wheel		
Class no.	12-in. × 1-in., wheel	Computed from volume loss	Weight-loss check	Remarks
2.2	12.5	11.1	8.4	
4.2	10.3	17.5	16.1	
4.3A	9.8	25.5	19.7	Some chipping
4.5	10.5	23.4	17.6	Some chipping
6.7	9.4	23.8	22.3	Slight chip at interface
7.4	12.9	15.8	94.2[a]	Large chip — 0.14 carat
7.5A	25.8	14.0	30.4[b]	Small chip at interface
10.5	21.8	15.5	15.7	
10.6T	24.5	14.7	12.2	Fissure opened
11.6	24.1	32.4	26.9	Some chipping
Average	16.2	19.4	18.8	

[a] Large chips caused by high infeed on last run accounts for high wear rate on weight check. If chip of 0.14 carat is allowed for, wear rate is about 25.

[b] Difference between computed and weight check can be accounted for with 0.03-carat chip.

Here again, there was very little difference in wear rate, chipping excluded, between the types of stones tested. Two out of the eight lower-quality stones chipped quite badly. The chipping occurred when the stones were worn sufficiently to expose the core under the coating. Fig. 6 shows the chipping progressively. Other coated stones were worn down to the point of exposing the plane between the primary and secondary growth but did not chip. Aside from failure by chipping it was observed that the wear rate did not change as the stones were penetrated from their exterior natural skins inward to depths equal to 50 per cent of the radius. This observation is contrary to the opinion of the trade, which has maintained that the natural skin of the diamond is harder than its interior.

Thus it appears that the performance of coated bort stones may be influenced by the thickness of the coating. When the coating is very thick in relation to the diameter of the stone, a large number of dressings at normal wear may be made before the interface is penetrated at which point chipping may or may not occur. Such chipping as may occur would then reduce the life of a stone by only a small amount. When the coating is relatively thin, flaking may occur after only a few dressings, but the life is not materially shortened since the chipping consumes only a small portion of the stone.

The practicability of bort for dressing purposes was further demonstrated by the results of tests which were made by Norton Company. These results were especially helpful in providing practical confirmation of the laboratory tests, which confirmation would have entailed considerable time and effort to obtain. Forty-eight tools made with selected bort, similar to classes 6 to 9, were used under regular shop conditions on most types of grinders in general use for over a year. The tools were used to the limit of the setting, no attempt being made to obtain maximum use by resetting. Thus the tools were worn down until the stone dropped out of the setting. In one half of the tools, the residual stone was lost. The results of these tests are compiled in Table 4 and are analyzed in Table 5.

The average size of stone used in the tools was 1.28 carats. An average of 0.6 carat was consumed which produced an average of 2000 dressings. In all, upward of 100,000 dressings were made with the forty-eight tools and six are still in use, with about 20 to be reset. Fifty per cent of the tools performed as well as first-quality stones to give over-all wear rates of less than 40×10^{-5} ct./cu in., and an average of 26×10^{-5} ct./cu in. Chipping proba-

TABLE 4 RESULTS OF SHOP TESTS ON DIAMOND DRESSERS USING SELECTED BORT BY NORTON CO.

Tool No.	Weights in Carats			No. Dressings	Weight Loss Carats x 10^{-5} per Dressing	Wear[2] Rate	Remarks
	Initial	Final	Loss				
1	1.52	.53*	.99	3000	33	44	Pulled out
2	1.46			6608	Still in use		
3	1.00	.22	.88	996	88	118	Fragment
4	1.67	.53	1.14	3587	31.8	42.5	Pulled out
5	1.21	.74	.47	3787	12.4	16.6	Normal wear
6	1.04	.44	.60	1382	43.5	58.0	High wear
7	1.08	.21*	.87	1692	51.3	68.5	Pulled out
8	1.66	1.12	.54	1120	48.4	64.5	High wear
9	1.44			5841	Still in use		
10	1.34	.98	.36	1056	34.2	45.6	High wear
11	1.47	.68*	.79	1699	46.5	62	Pulled out
12	1.16	.70*	.46	354	131	175	Fragment
13	1.25	.46*	.79	967	82	110	
14	1.30	.77*	.53	3049	17.3	23	Normal wear
15	1.18	.63	.55	504	109	146	Fragment
16	1.62	.94	.68	1942	35	46.8	High wear
17	1.46			1116	Still in use		
18	1.01	.22*	.79	3460	23	31	Pulled out
19	1.10	.84*	.26	1060	24.5	32.8	Normal wear
20		.95		560	Failed Setting		
21	1.42	.70	.72	3270	22	29.4	Normal wear
22	1.14	.64*	.50	2616	19.3	25.8	Normal wear
23	1.31	.60*	.71	2927	23.9	32	Normal wear
24	1.14	.21*	.93	3231	29.0	39	Pulled out
25	1.22	.60*	.62	2945	20.0	27	Normal wear
26	1.54	.42*	1.12	1451	77.4	103	Pulled out
27	1.50	.53	.97	2730	35.6	47.5	Pulled out
28	1.25	1.15	.10	1467	6.8	9.1	Normal wear
29	1.19	.51*	.68	1371	50	67	Pulled out
30	1.06			4458	Still in use		
31	1.02	.47*	.55	1452	37.8	50.5	High wear
32		.64		333	Failed Setting		
33	1.28	.96	.32	2062	15.5	20.8	Normal wear
34	1.68	1.23	.45	1250	36.4	48.6	High wear
36	1.16	.09	1.07	1240	86.7	116	Fragment
37	1.21	1.11	.10	1691	6.2	8.3	Normal wear
38	1.14	.37*	.77	2747	28.1	37.4	Pulled out
39	1.00	.39*	.61	1070	57.5	76.6	Pulled out
40	1.20	.54*	.66	1237	53.0	71	Pulled out
41		1.36		791	Failed Setting		
42	1.34	.48*	.86	2335	36.8	49	Pulled out
43	1.02	.53*	.49	2335	21.0	28	Normal wear
44	1.05	.34*	.71	1599	44.5	59.5	Pulled out
45	1.59			5552	Still in use		
46	1.27	.25	1.02	670	153	205	Fragment
47	1.27	.35*	.92	1886	49.0	65.5	Pulled out
48	1.53			2430	Still in use		

* Final weight estimated from cavity in tool nib since tool was used to the limit of the setting and the residual stone was pulled out and lost. All other values are weights of residual stone.

[2] Wear rate in carats lost $\times 10^{-5}$ per cubic inch of wheel removed. Wear per dressing divided by 0.75 cu. in., the average amount of wheel removed per dressing as estimated by Norton Company.

bly accounted for most of the high losses obtained with 30 per cent of the tools. Ten per cent of the tools exhibited the exceptionally high average loss of 152×10^{-5} ct./cu in. because the stones broke up into fragments. In all cases a fair number of dressings was obtained before failure occurred. All things considered, the coated Congo stones which were tested in the Norton shops performed exceptionally well. Costwise, the comparison is in favor of bort many times over.

TABLE 5 ANALYSIS OF NORTON CO. SHOP TESTS ON SELECTED BORT

	No. of tools	Per cent	Average wear rate $\times 10^{-5}$ ct./in.[3]	Average number of dressings
Setting failed	4	8	...	420
Fractured to fragments	5	10	152	750
Wear rate above 40, indicating chipping and fracturing	14	30	53	1450
Wear rate below 40, indicating normal wear	25	52	26	3000

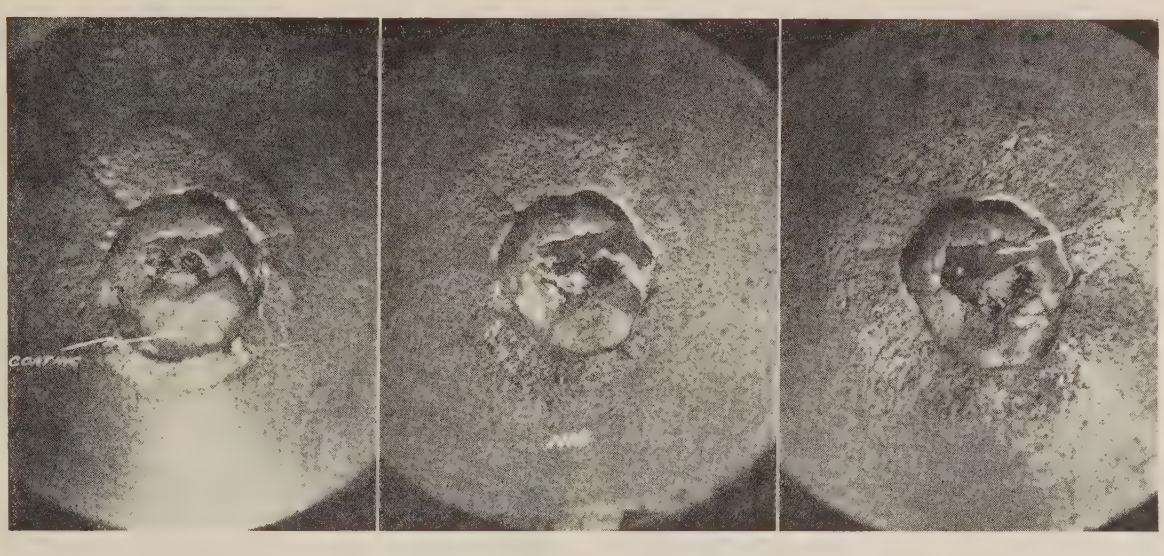

After 637 passes After 756 passes After 900 pastes

FIG. 6 TOOL WITH COATED STONE, SHOWING PROGRESSIVE FRACTURING OF COATING IN USE; ABOUT ×6
(Test conditions: Cincinnati centerless grinder, wet dressing, 20-in. × 6-in., 60M30 Carborundum Company wheel, 0.001 in. feed, 15-deg drag angle.)

CONCLUSIONS

The order of magnitude of the rate at which diamond wears when used to dress grinding wheels was established over the range of conditions encountered in dressing operations. A dressing of the average size and type of grinding wheel in the shop consumes about 0.0002 carat of diamond. A tremendous quantity of grinding wheel can be removed with a very small consumption of diamond; the ratio is on the order of 1 part diamond to 1,000,000 parts grinding wheel by weight. The consumption of diamond may vary between less than 0.00001 to 0.0004 carat per cu in. of wheel removed, depending on the combination of conditions. Fine-grained wheels and resin-bonded wheels abrade diamond at a much lower rate than coarse-grained wheels and vitreous-bonded wheels. To obtain the best and most economical performance with diamond dressers, particular attention should be given to the selection of the most efficient feed consistent with requirements and the adjustment of the coolant in wet dressings, since these two factors have the greatest effect on wear.

Grinding wheels can be dressed satisfactorily with lower-quality industrial diamonds. Results of laboratory and practical shop tests indicated that many of the so-called lower-quality types of stones, of which large quantities are available in better-bort and crushing-bort assortments, may perform as well as the higher-quality stones of the industrial-serie variety in a majority of standard dressing operations. The different varieties and types of diamond have essentially the same resistance to wear by abrasion of grinding wheels, when all factors are considered.

Factors other than the resistance to wear are of greater importance in determining the suitability of individual stones for dressing purposes. Soundness and structural strength and the ability of individual stones to withstand chipping and crumbling appear to be the limiting factors in their utilization.

The selection of sound stones from bort is difficult, because of the wide variation and the opacity of bort. The uncertainty in performance usually associated with bort arises from this difficulty in selection, and this difficulty probably accounts for the preference in the trade for the so-called higher qualities which can be more readily inspected because they are transparent. Even so, it should be possible to select sufficient quantities of single-coated stones from bort categories to make up shortages which may occur in the thirty-two categories of the industrial serie.

Care is necessary in the selection of suitable stones from better bort and crushing bort. Solid appearing more or less symmetrical whole stones, free from surface flaws, fissures, and granulated areas, octahedron to cubic in shape, may be expected to produce consistent results. Aggregated crystal masses, fractured stones, fragments and cleavages, can be used to dress grinding wheels, but their performance may not be entirely satisfactory because of a tendency to chip.

ACKNOWLEDGMENTS

The author wishes to express his appreciation for the assistance and co-operation in this investigation given by the following organizations: Buick Motor Division, Aviation Engine Plant, Chicago, Ill.; Carboloy Company, Detroit, Mich.; Arthur A. Crafts Company, Boston, Mass.; Ex-Cell-O Corporation, Detroit, Mich.; General Motors Corporation, Electromotive Division; LaGrange, Ill.; F. F. Gilmore and Company, Boston, Mass., Koebel Diamond Tool Company, Detroit, Mich.; J. Montezines, New York, N. Y.; Norton Company, Worcester, Mass.; Rough Diamond Company, New York, N. Y.; J. K. Smit and Sons, Inc., New York, N. Y.; H. R. Spandel, Inc., New York, N. Y.; Studebaker Aviation Engine Plant, Chicago, Ill.; United States Industrial Diamond Corporation, New York, N. Y.; Wheel Trueing Tool Company, Detroit, Mich.

Thanks are also due many others in the industrial-diamond and metalworking industries.

(Owing to travel emergency conditions existing when this paper was presented, discussion will be accepted until February 10, 1946)

Measurements of Temperatures in Metal Cutting

By A. O. SCHMIDT,[1] O. W. BOSTON,[2] and W. W. GILBERT[3]

Measurements of the heat developed in a metal-cutting operation, as well as investigation of cutting and chip temperatures by the authors have brought out that the chip temperature is uniform at the higher cutting speeds when all other conditions are kept constant. The temperature of the tool increases with the cutting speed, and the amount of metal removed before tool failure will generally be inversely proportional to the cutting speed.

Review and Discussion of Previous Investigations

IN a previous paper (1)[4] by the present authors, it was shown that the work done by a metal-cutting tool is transformed into heat which is carried away by the tool, workpiece, and chips. When the time of cutting is very short, the losses due to radiation, convection, and conduction are so small that they can be disregarded in most metal-cutting tests in which the calorimetric principle is applied. A comparison of the horsepower values in drilling, as computed from torque and thrust with those computed from the heat generated during cutting, showed that the calorimetric method gives results comparable to those of a well-calibrated dynamometer.

When the quantity of heat in the chips only is measured with a calorimeter (2), the average temperature increase of the chip resulting from a cutting operation can be computed by the thermal-balance method:

(ΔT_e) (chip weight) (specific heat) = (ΔT) (water equivalent of calorimeter, chips, and water)

where . ΔT_e = average temperature rise of chips, deg F; and
ΔT = temperature rise in calorimeter, deg F.

The foregoing formula does not take into account the change of specific heat with increasing temperatures. With the specific-heat values of gamma iron, a corrected maximum average chip-temperature value was computed for cutting tests in which the test-bar material was S.A.E. 1055.

Boston and Kraus (3) evaluated cutting temperatures when machining an annealed low-carbon steel in a lathe at cutting speeds between 20 and 320 fpm. A constant depth of cut of 0.150 in. and a constant feed of 0.030 in. were used. The cutting temperatures were measured with a thermocouple arrangement in which one element was the tool and the other the workpiece. These were calibrated in a furnace and the temperatures evaluated in millivolts. The temperatures obtained during cutting operations at different speeds are plotted in their paper and indicate an increase in temperature from 650 to 900 F between 56 and 115 fpm cutting speed.[5] For the cutting speeds between 115 and 320 fpm, the cutting temperatures are reported as varying between 900 and 1000 F, the maximum temperature of 1000 F being obtained at a cutting speed of 210 fpm.

Plotted on the same co-ordinates are chip temperatures determined from temper colors. Very little variation could be detected for the cutting speeds between 100 and 320 fpm, and the authors state in their conclusions: "The temperature of the chip as determined by temper colors was changed less than 5 per cent in the range of cutting speed from 90 to 320 fpm."

This finding is supported by the measurements of chip temperatures with the calorimeter. The temperatures were determined as almost constant for the higher cutting speeds. This is not the case at the lower cutting speeds. Even though the work to remove the chip is the same, at a low cutting speed the workpiece and tool will conduct a higher percentage of the heat generated in the chip because of the slow separation of the chip from the workpiece.

Even though work, which is transformed into heat, must be done in metal cutting, it is possible to remove metal at extremely low speeds with a relatively low temperature increase in the chip. This is because the chip is separated slowly, and the heat in the chip is given a chance to flow into the tool and workpiece. It is recognized that at the low cutting speeds less heat per unit time is generated, although a larger proportion of this smaller amount of heat generated at low speeds goes by conduction into the tool and workpiece. At higher speeds the work done is nearly proportional to the increased cutting speed, and most of the heat developed is carried away with the chip because of the short time the chip is in contact with the workpiece and tool. Assuming that the energy or work required to remove a given amount of metal is the same regardless of the time involved in removing it, it follows that for a longer period of time, that is, at low cutting speeds, the heat per unit time is less. At higher cutting speeds the time to remove the chip is reduced, and the amount of heat developed at any one instant is higher. It is therefore held that the temperature of the tool is much higher at higher speeds than at low speeds because the work done per unit time is much greater. For this reason a tool will generally remove a greater amount of metal at low cutting speeds before failure than at high cutting speeds.

The average chip temperature measured at higher cutting speeds is more uniform because there is less chance for the heat to travel into the tool and workpiece. On the other hand, as soon as the temperature at the cutting edge is equal to that in the chip, there will be no heat flow from the chip into the tool. The higher amount of work which is done per unit time at higher cutting speeds and the resulting greater amount of heat is also carried by a correspondingly larger weight of chips.

When the cutting speed is increased, the tool will have to do a proportionately greater amount of work. This results in a temperature increase in the tool material. The heat will not be uniform in the tool, but most intense near the point at which the cutting takes place. The zone which is near the cutting edge

[1] Research Engineer in Charge of Metal Cutting Research, Kearney & Trecker Corporation, Milwaukee, Wis. Mem. A.S.M.E.

[2] Professor of Metal Processing, Chairman of Department, University of Michigan, Ann Arbor, Mich. Mem. A.S.M.E.

[3] Associate Professor, Metal Processing, University of Michigan, Ann Arbor, Mich. Mem. A.S.M.E.

[4] Numbers in parentheses refer to the Bibliography at the end of the paper.

Contributed by the A.S.M.E. Research Committees on Cutting Fluids, and on Metal Cutting Data and Bibliography and presented at the meeting of the Chicago Section, Chicago, Ill., June 16–19, 1945, of The American Society of Mechanical Engineers.

[5] Bibliography (3), Fig. 12.

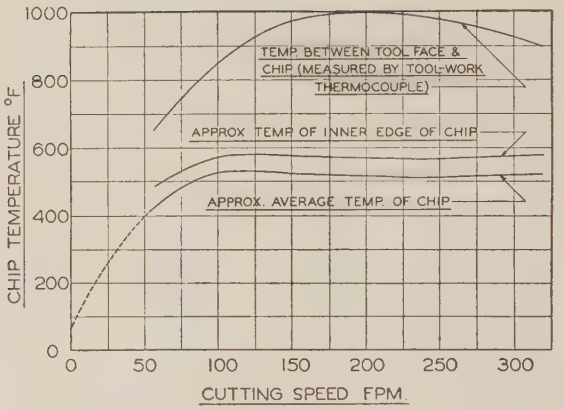

FIG. 1 CURVES OF CHIP TEMPERATURE VS. CUTTING SPEED

(From diagram by Boston and Kraus, reference 3, Fig. 12. The upper temperature line was determined by the tool-work thermocouple while the lower ones were estimated from the temper colors of the chips. Annealed 0.21C steel, depth of cut 0.150 in., feed 0.030 in. per revolution. The dotted line indicates average temperature values at the low speeds.)

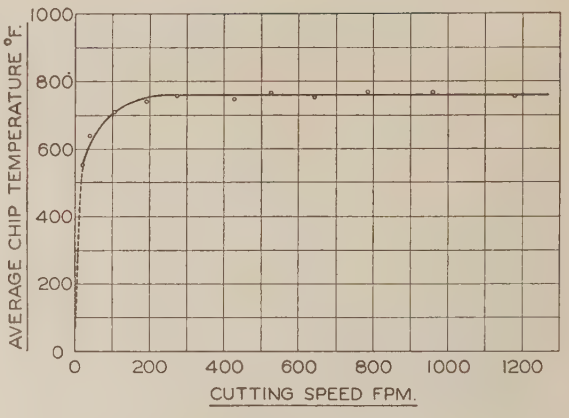

FIG. 2 AVERAGE CHIP TEMPERATURE IN RELATION TO CUTTING SPEED

(These chip temperatures were measured with a calorimeter when machining 1-in-diam test bars of S.A.E. 1055, normalized, with a face mill which had two tungsten-carbide tips of 6-deg negative radial rake. Depth of cut 0.125 in., feed per tooth 0.008 in. The dotted line indicates estimated temperature values at lower cutting speeds.)

will reach the highest temperature and will break down first.

When using the tool-work thermocouple, Boston and Gilbert (4) came to the conclusion that the temperatures measured may be affected by changed electrical properties of the metal in the test log which is compressed and deformed by the tool point. However, this change of electrical properties is brought about not only by the changes in the test log but also by those in the tool. Because the thermocouple was calibrated with the tool and workpiece at the same temperature, the calibration was not made under the condition which generally exists in a metal-cutting operation. During cutting, tool and workpiece temperatures will vary, and at the higher cutting speeds the temperature of the tool will be higher than that of the chip. This is a condition which can hardly be obtained during the calibration of the tool-work thermocouple, and its readings in an actual test will not reveal true cutting temperatures.

MEASUREMENTS OF CHIP TEMPERATURES

From the investigation carried out on the calorimetric principle, it was found that the cutting force for a particular radial rake angle and chip cross section has substantially the same value at any cutting speed (5). In the foregoing tests the cutting speed was varied between 100 and 800 fpm.

At a cutting speed of 300 fpm, the tool forces were the same as those at 600 fpm. Since the maximum volume of metal removed with any test cutter was 0.6 cu in., the cutters could be considered sharp. Therefore, any error introduced by a change in the cutting edge could be disregarded entirely. However, when cutting at 600 fpm, twice as much metal is removed per unit time as at 300 fpm and, consequently, the power required for cutting is doubled. In computing the chip temperature with the formula given, the same value was obtained for both cutting speeds. Although twice as much work was done per unit time when cutting at a speed of 600 fpm as compared with 300 fpm, the temperature of the chips remained the same because the work was done in removing twice the amount of metal. This means there is twice as much chip material to carry away twice as much heat. (The amount of heat per unit weight of chips remains constant.)

Most of the work expended in a metal-cutting operation is carried away as heat in the chips. The remainder of the heat is absorbed by the tool and workpiece.

The heat in the tool is of greatest importance because it is the

FIG. 3 CEMENTED CARBIDE CUTTING TOOL AFTER MACHINING 10.8 CU IN. OF STEEL AT 580 FPM CUTTING SPEED. DEPTH OF CUT 0.150 IN., FEED 0.010 IN. PER TOOTH

(Two passes were taken over the workpiece and the chips are arranged in columns in the order in which they were removed. Chip formation is uniform throughout the cut. Abrasive action of chips on blade face has formed a shallow crater 0.006 in. deep.)

accumulation and concentration of intense heat at the cutting edge of the tool which hastens failure. Comparing tool life with cutting speed, as brought out in numerous investigations (6), it is evident that the amount of metal removed before tool failure will generally be inversely proportional to the cutting speed when the chip cross section is kept constant. This happens despite the fact that the chip temperature will remain substantially the same. Assuming an ideal case in which the tool does not wear and thus change the cutting forces, the same volume of

FIG. 4 CEMENTED CARBIDE CUTTING TOOL AFTER MACHINING 10.8 CU IN. OF STEEL UNDER CONDITIONS IDENTICAL WITH THOSE IN FIG. 3 EXCEPT THAT THE CUTTING SPEED WAS 2650 FPM

(Note that at the start the chip formation is similar to Fig. 3 but, due to the rapid increase in heat at the cutting edge, wear of the tip has made a crater 0.050 in. deep through which the chip formation is affected.)

tool metal has to dissipate twice the amount of heat per unit time when the cutting speed is doubled. For this reason, a tool will break down faster at higher cutting speeds, and remove a smaller volume of metal than at a lower cutting speed. There is only a small zone including the cutting edge of the tool which will have a high heat increase with an increase in cutting speed. It is in this zone also that most of the friction between the chip and the tool occurs (7).

The temperature of the workpiece is affected mainly by its size, its heat conductivity, and specific heat. Other factors which also influence the workpiece temperature include cutting speed, cross section of chip, tool design, and wear at the cutting edge. All these must be taken into consideration.

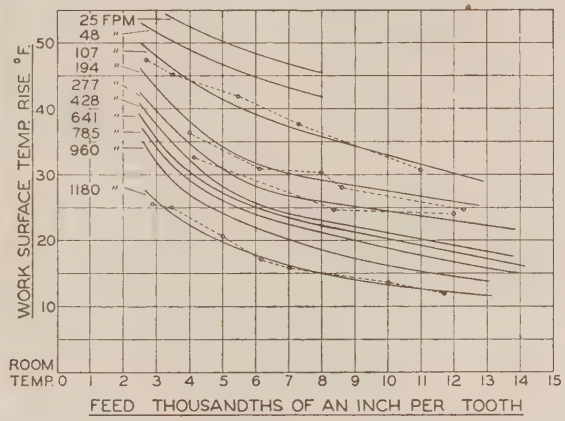

FIG. 5 SURFACE TEMPERATURE RISE OF WORKPIECE

(This graph is based on the evaluation of 500 readings taken with an Alnor low-range thermocouple when machining workpieces of S.A.E. 1055 of identical properties and dimensions at speeds and feeds as indicated and a constant depth of cut of 0.125 in. The cutter was the same as the one used in tests plotted in Fig. 2.)

However, if all conditions except cutting speed are kept constant, the following can be stated with regard to the chips, tool, and workpiece.

1 The temperature of chips of uniform cross section remains approximately the same in the high range of cutting speeds.

2 The temperature at the cutting edge of a tool increases with the cutting speed.

3 The temperature of the workpiece is lower at the higher cutting speeds.

BIBLIOGRAPHY

1 "A Thermal-Balance Method and Mechanical Investigation for Evaluating Machinability," by A. O. Schmidt, W. W. Gilbert, and O. W. Boston, Trans. A.S.M.E., vol. 67, 1945, pp. 225–232.

2 "Determining Tool Forces in High-Speed Milling by Thermo-analysis," by A. O. Schmidt, *Mechanical Engineering*, vol. 66, 1944, pp. 439–442; *Mechanical World*, Sept. 15, 1944, pp. 301–303.

3 "A Study of the Turning of Steel Employing a New-Type Three-Component Dynamometer," by O. W. Boston and C. E. Kraus, Trans. A.S.M.E., vol. 58, 1936, pp. 47–53.

4 "Cutting Temperatures Developed by Single-Point Turning Tools," O. W. Boston and W. W. Gilbert, Trans. American Society for Metals, vol. 23, 1935, pp. 703–726.

5 "An Investigation of Radial Rake Angles in Face Milling," by J. B. Armitage and A. O. Schmidt, Trans. A.S.M.E., vol. 66, 1944, pp. 633–643; *Western Metals*, July and August, 1945.

6 "Influence of Applying Cutting Fluids at Different Temperatures When Turning Steel," by O. W. Boston, W. W. Gilbert, and R. E. McKee, Trans. A.S.M.E. vol. 67, 1945, pp. 217–224.

7 "Radial Rake Angles in Face Milling," by J. B. Armitage and A. O. Schmidt, *Mechanical Engineering*, vol. 67, 1945, pp. 453–456.

(Owing to travel emergency conditions existing when this paper was presented, discussion will be accepted until February 10, 1946)

Charts for Fuselage Torsion Versus Control-Surface Flutter

By W. T. THOMSON,[1] SAN DIEGO, CALIF.

Charts for evaluating the allowable unbalance in the control-surface product of inertia for tail flutter involving fuselage torsion are presented. The basic theory, assumptions, and limitations are fully discussed.

Nomenclature

The following nomenclature is used in the paper:

θ_s = torsional displacement of tail, radians
θ_w = torsional displacement of wings, radians
β = control-surface rotation with respect to fixed surface, radians
b = semi-chord of tail surface, in.
c = location of control-surface hinge axis measured from tail-surface mid-chord, as a fraction of tail-surface semi-chord
e = location of control-surface leading edge, measured from tail-surface mid-chord, as a fraction of tail surface semi-chord
x_β = distance from hinge line to center of gravity of the control surface (positive if CG is behind hinge), in.
y = span distance measured from torsional axis, in.
L = control-surface span, in
J_w = mass moment of inertia of wings with respect to torsional axis, lb-in. sec^2
J_T = mass moment of inertia of tail with respect to torsional axis, lb-in. sec^2
$J_\theta = J_T + \left(\frac{\theta_w}{\theta}\right)^2 J_w$ = effective torsional moment of inertia, lb-in. sec^2
J_β = mass moment of inertia of control surface with respect to hinge line (rudder or two elevators), lb-in. sec^2
m_β = mass of rudder or two elevators, lb-in.$^{-1}$ sec^2
ρ = mass density of air, lb-in.$^{-4}$ sec^2
v = flight velocity, in. sec^{-1}
ω = circular frequency of flutter, radians sec^{-1}
ω_θ = natural torsional frequency of fuselage, radian sec^{-1}
ω_β = natural circular frequency of control-surface system, radians sec^{-1}
g = structural damping coefficient $\left(\frac{1}{\pi}\right.$ times logarithmtic decrement$\left.\right)$

Introduction

Flutter of control surfaces may be avoided by balancing. The complete balancing of control surfaces, however, is costly in weight and often unnecessary in avoiding flutter.

The study of varying the amount of balance by flutter calculations is long and tedious. To avoid such calculations, charts enabling the determination of the allowable static unbalance of the control surfaces have been presented by the Army Air Force (1)[2] for flutter modes involving fuselage bending. The purpose of this paper is to present a similar type of labor-saving device for the flutter modes involving fuselage torsion.

Development of Equations

In the following analysis with two degrees of freedom, Lagrange's equation

$$\frac{d}{dt}\left(\frac{\partial T}{\partial \dot{q}_s}\right) + \frac{\partial U}{\partial q_s} = Q_s \quad \ldots\ldots [1]$$

will be used, where T and U are kinetic and potential energies, respectively, Q_s the generalized force associated with the work done in a virtual displacement δq_s, and q_s the generalized co-ordinate for the particular mode.

The kinetic energy of the airplane in the torsional oscillation then becomes

$$T = \frac{1}{2}J_\theta\dot{\theta}^2 + \frac{1}{2}\int_0^L [(y\dot{\theta} + x_\beta\dot{\beta})^2 - (y\dot{\theta})^2]dm_\beta + \frac{1}{2}\int_0^L \dot{\beta}^2(dJ_\beta - x_\beta^2 dm_\beta) \quad \ldots\ldots [2]$$

Differentiating with respect to the generalized co-ordinates and time, and assuming harmonic motion, the Lagrangian inertia forces become

$$\left.\begin{aligned}\frac{d}{dt}\left(\frac{\partial T}{\partial \dot{\theta}}\right) &= -\omega^2 (J_\theta\theta + \int x_\beta y dm_\beta \cdot \beta)\\ \frac{d}{dt}\left(\frac{\partial T}{\partial \dot{\beta}}\right) &= -\omega^2(\int x_\beta y dm_\beta \cdot \theta + J_\beta \cdot \beta)\end{aligned}\right\} \quad \ldots\ldots [3]$$

The potential energy represents the strain energy stored in the structure. Assuming Hooke's law, it may be written as

$$U = \frac{1}{2}K_{\theta\theta}\theta^2 + \frac{1}{2}K_{\beta\beta}\beta^2 \quad \ldots\ldots [4]$$

The Lagrangian elastic forces then become

$$\left.\begin{aligned}\frac{\partial U}{\partial \theta} &= K_{\theta\theta}\theta = \omega_\theta^2 J_\theta\theta\\ \frac{\partial U}{\partial \beta} &= K_{\beta\beta}\beta = \omega^2\beta \int x_\beta y dm_\beta \cdot \beta\end{aligned}\right\} \quad \ldots\ldots [5]$$

where the K coefficients have been replaced by the inertia coefficients by considering uncoupled motion in each co-ordinate.

For terms which remove energy from the system, structural damping which is nearly independent of frequency and proportional to the amplitude must be considered. This can be accomplished by multiplying the elastic coefficients K by $(1 + ig)$.

---

[1] Design Specialist in Charge of Vibration and Flutter Analysis, Ryan Aeronautical Company.

Presented at a meeting of the Aviation Division, Los Angeles, Calif., June 11–14, 1945, of The American Society of Mechanical Engineers.

[2] Numbers in parentheses refer to the Bibliography at the end of the paper.

The aerodynamic forces and moments supplying the energy for flutter are defined by Theodorsen (2) and Kussner and Schwarz (3), for the two-dimensional flow. These equations have been organized in a form convenient for flutter analysis by B. Smilg (4).

The expressions applicable to this analysis are ones for the lift per unit span and the torque about the control-surface hinge per unit span, and may be written as follows

$$\left.\begin{aligned} L' &= \pi\rho b^3\omega^2\left(A_{\theta\theta}\frac{y}{b}\theta + A_{\theta\beta}\cdot\beta\right) \\ T' &= \pi\rho b^4\omega^2\left(A_{\beta\theta}\frac{y}{b}\theta + A_{\beta\beta}\cdot\beta\right) \end{aligned}\right\} \quad \ldots\ldots [6]$$

where the aerodynamic coefficients A are complex functions of $\frac{v}{b\omega}$ and have been evaluated in terms of the following coefficients appearing in reference (4)

$$\left.\begin{aligned} A_{\theta\theta} &= L_h \\ A_{\theta\beta} &= L_\beta - L_z(c-e) \\ A_{\beta\theta} &= T_h - P_h(c-e) \\ A_{\beta\beta} &= T_\beta - P_\beta(c-e) - T_z(c-e) + P_z(c-e)^2 \end{aligned}\right\} \quad \ldots [7]$$

The generalized forces Q are determined from the work associated with the virtual displacements as follows

$$\left.\begin{aligned} \delta W &= \int_0^L L'\delta(y\theta)dy + \int_0^L T'\delta(\beta)dy \\ Q_\theta &= \frac{\delta W}{\delta\theta} = \int_0^L L'ydy = \pi\rho b^2\omega^2\left(A_{\theta\theta}\frac{L^3}{3}\theta + A_{\theta\beta}\frac{bL^2}{2}\beta\right) \\ Q_\beta &= \frac{\delta W}{\delta\beta} = \int_0^L T'dy = \pi\rho b^2\omega^2\left(A_{\beta\theta}\frac{bL^2}{2}\theta + A_{\beta\beta}b^2L\beta\right) \end{aligned}\right\} \quad \ldots [8]$$

The Stability Equation

Substituting the expressions of the previous section into Equation [1], the following two equations are obtained

$$\left.\begin{aligned} E\theta + F\beta &= 0 \\ G\theta + H\beta &= 0 \end{aligned}\right\} \quad \ldots\ldots [9]$$

where

$$E = -J_\theta[\omega^2 - \omega_\theta^2(1+ig_\theta)] - \pi\rho b^2\omega^2 A_{\theta\theta}\frac{L^3}{3}$$

$$F = -\omega^2\int_0^L x_\beta ydm_\beta - \pi\rho b^2\omega^2 A_{\theta\beta}\frac{bL^2}{2}$$

$$G = -\omega^2\int_0^L x_\beta ydm_\beta - \pi\rho b^2\omega^2 A_{\beta\theta}\frac{bL^2}{2}$$

$$H = -J_\beta[\omega^2 - \omega^2_\beta(1+ig_\beta)] - \pi\rho b^2\omega^2 A_{\beta\beta}b^2L$$

Dividing each term by $-\pi\rho b^3\omega^2L^2$ and equating the determinant to zero, the stability equation becomes

$$\left\{\frac{\left(\frac{J_\theta}{L}\right)}{(\pi\rho b^2)L^2}\left[1-\left(\frac{\omega_\theta}{\omega}\right)^2(1+ig_\theta)\right] + \frac{1}{3}A_{\theta\theta}\right\}\left\{\frac{\left(\frac{J_\beta}{L}\right)}{(\pi\rho b^2)b^2}\left[1-\left(\frac{\omega_\theta}{\omega}\right)^2(1+ig_\beta)\right] + A_{\beta\beta}\right\} - \left\{\frac{\int_0^L x_\beta ydm_\beta}{(\pi\rho b^2)bL} + \frac{1}{2}A_{\beta\theta}\right\}$$

$$\left\{\frac{\int_0^L x_\beta ydm_\beta}{(\pi\rho b^2)bL} + \frac{1}{2}A_{\beta\theta}\right\} = 0 \quad \ldots\ldots [10]$$

Equation [10] is a quadratic in ω^2, resulting in two roots corresponding to the two flutter modes. The equation is nondimensional, the three parameters being as follows

$$A = \frac{\left(\frac{J_\theta}{L}\right)}{(\pi\rho b^2)L^2}$$

which involves the moment of inertia of the airplane about the torsional axis.

$$B = \frac{\left(\frac{J_\theta}{L}\right)}{(\pi\rho b^2)b^2}$$

which involves the moment of inertia of the control surface about its hinge line.

$$P = \frac{\int_0^L x_\beta ydm_\beta}{(\pi\rho b^2)bL}$$

which involves the product of inertia of the control surface about the hinge and torsional axis.

Considerable simplification results from assuming the control-surface natural frequency to be zero, under which condition the solution of the foregoing equation results in a real and an imaginary part as follows

$$\left.\begin{aligned} \text{Real} &= \frac{\left(\frac{J_\theta}{L}\right)}{(\pi\rho b^2)L^2}\left[1-\left(\frac{\omega_\theta}{\omega}\right)^2\right] \\ \text{Imaginary} &= -\frac{\left(\frac{J_\theta}{L}\right)}{(\pi\rho b^2)L^2}\left(\frac{\omega_\theta}{\omega}\right)^2 g \end{aligned}\right\} \quad \ldots\ldots [11]$$

Since $\left(\frac{\omega_\theta}{\omega}\right)$ is near unity in the critical-flutter ranges, the value of the structural damping g, necessary to sustain steady-state oscillation, may be determined from the imaginary part.

Charts for Allowable Product of Inertia

The numerical evaluation of Equation [10] was carried out under the following assumptions:

1 The natural frequency of the control surface at zero air speed equals zero ($\omega_\beta = 0$).

2 The leading edge of the control surface is at mid-chord ($e = 0$). The effect of varying the leading-edge position is indicated by one set of calculations for 40 per cent control surface ($e = 0.2$).

3 The effective torsional axis of the airplane is along the center line of the fuselage.

4 The control-surface aerodynamic balance equals 20 per cent or 33 per cent (chosen arbitrarily).

5 Aerodynamic vectors for infinite aspect ratio are applicable.

The real and imaginary parts of Equation [10], as indicated by Equations [11], are tabulated as shown herewith. The charts, Figs. 1 to 9, represent the imaginary part of the solution as function of $\frac{v}{b\omega}$. Since the ordinate is proportional to the structural damping, while the abscissa is proportional to the true

FUSELAGE TORSION VERSUS CONTROL-SURFACE FLUTTER ($\omega\beta = 0$) COMPUTATION FORM

$$\frac{1}{3}\begin{bmatrix} (A_{\theta\theta})_R \\ (A_{\theta\theta})_I \end{bmatrix} \boxtimes \begin{bmatrix} B + (A_{\beta\beta})_R \\ (A_{\beta\beta})_I \end{bmatrix} = \begin{bmatrix} a \end{bmatrix}$$

$$\begin{bmatrix} P \end{bmatrix}^2 = \begin{bmatrix} b \end{bmatrix}$$

$$\frac{1}{2}\begin{bmatrix} P \end{bmatrix} \cdot \begin{bmatrix} (A_{\theta\beta})_R + (A_{\beta\theta})_R \\ (A_{\theta\beta})_I + (A_{\beta\theta})_I \end{bmatrix} = \begin{bmatrix} c \end{bmatrix}$$

$$\frac{1}{4}\begin{bmatrix} (A_{\theta\beta})_R \\ (A_{\theta\beta})_I \end{bmatrix} \boxtimes \begin{bmatrix} (A_{\beta\theta})_R \\ (A_{\beta\theta})_I \end{bmatrix} = \begin{bmatrix} d \end{bmatrix}$$

$$\begin{bmatrix} B + (A_{\beta\beta})_R \end{bmatrix}^2 + \begin{bmatrix} (A_{\beta\beta})_I \end{bmatrix}^2 = \begin{bmatrix} e \end{bmatrix}$$

$$\begin{bmatrix} B + (A_{\beta\beta})_R \\ -(A_{\beta\beta})_I \end{bmatrix} \boxtimes \begin{bmatrix} a - b - c - d \end{bmatrix} = \begin{bmatrix} f \end{bmatrix}$$

$$A\left[i - \left(\frac{\omega_\theta}{\omega}\right)^2\right] = \frac{(f)_R}{e} = \_\_\_\_\_$$

$$A\left(\frac{\omega_\beta}{\omega}\right)^2 g = \frac{(f)_I}{e} = \_\_\_\_\_$$

$\frac{\nu}{b\omega}$ = _____
c = _____
e = _____
B = _____
P = _____

B = .30 c = .20 e = 0

P / $\frac{\nu}{b\omega}$	.10 R	.10 I	.20 R	.20 I	.50 R	.50 I	1.0 R	1.0 I
.83	.31	-.12	.24	-.032	-.29	.07		
2.00	.47	.014	.22	.65	.51	1.74	.06	2.7
3.33	-.13	.25	-.67	1.20	-2.2	3.80	-4.4	7.5
4.17	-.52	-.04	-1.40	.78	-3.8	3.13	-7.4	6.7
6.25	-.91	-.90	-2.0	-.38	-5.1	1.18	-10.2	3.7

B = .40 c = .20 e = 0

P / $\frac{\nu}{b\omega}$	.10 R	.10 I	.20 R	.20 I	.50 R	.50 I	1.0 R	1.0 I
.83								
2.00	.59	-.18	.73	.25	.98	1.28	.79	2.2
3.33	.19	.37	-.22	1.50	-1.3	4.5	-3.0	8.84
4.17	-.37	.16	-1.20	1.10	-3.6	3.9	-7.3	8.20
6.25	-.89	-.79	-2.00	-.22	-5.3	1.5	-10.5	4.2

B = .50 c = .20 e = 0

P / $\frac{\nu}{b\omega}$	.10 R	.10 I	.20 R	.20 I	.50 R	.50 I	1.0 R	1.0 I
.83								
2.00	.61	-.35	.79	-.01	1.16	.82	1.1	1.6
3.33	.57	.37	.38	1.6	-.16	4.9	-.95	9.7
4.17	-.14	.36	-.94	1.5	-3.2	4.8	-6.7	9.9
6.25	-.86	-.66	-2.01	-.04	-5.4	1.8	-10.9	4.8

B = .60 c = .20 e = 0

P / $\frac{\nu}{b\omega}$	.10 R	.10 I	.20 R	.20 I	.50 R	.50 I	1.0 R	1.0 I
.83					.02	-.04	-1.05	.003
2.00	.59	-.47	.78	-.20	1.18	.46	1.25	1.1
3.33	.94	.20	1.0	1.4	1.17	4.8	1.37	9.7
4.17	.16	.54	-.54	1.9	-2.6	5.7	-5.6	11.6
6.25	-.82	-.52	-2.02	.16	-5.5	2.2	-11.2	5.4

B = .50 c = .33 e = 0

P / $\frac{\nu}{b\omega}$	.10 R	.10 I	.20 R	.20 I	.50 R	.50 I	1.0 R	1.0 I
.83					.05	-.03	-1.15	.08
2.00					1.43	-.04	1.76	.43
3.33			2.06	-.64	4.61	.62	8.25	2.42
4.17			3.18	-.56	7.33	1.71	13.70	5.12
6.25	3.94	-1.68	6.94	.67	15.81	7.60	30.14	18.71
10.00	10.32	.22	15.17	8.58				

B = .30 c = .33 e = 0

P / $\frac{\nu}{b\omega}$	.10 R	.10 I	.20 R	.20 I	.50 R	.50 I	1.0 R	1.0 I
.83					-.13	.09	-2.07	.11
2.00			1.27	-.13	1.86	.67	2.24	1.46
3.33			2.57	.33	5.66	2.88	10.08	6.49
4.17	1.699	-.53	3.75	.97	8.44	5.31	15.62	11.87
6.25	4.262	.06	7.03	3.85	5.01	22.51		
10.0	8.962	3.75	11.46	13.84				

B = .60 c = .33 e = 0

P / $\frac{\nu}{b\omega}$	.10 R	.10 I	.20 R	.20 I	.50 R	.50 I	1.0 R	1.0 I
.83					.09	-.07	-.92	.05
2.00					1.26	-.21	1.57	.18
3.33					4.09	.06	7.34	1.38
4.17			2.84	-.97	6.62	.72	12.41	3.25
6.25			6.49	-.40	15.01	5.01	28.79	13.66
10.00			15.75	5.82	32.14	27.45		

B = .40 c = .33 e = 0

P / $\frac{\nu}{b\omega}$	.10 R	.10 I	.20 R	.20 I	.50 R	.50 I	1.0 R	1.0 I
.83					.012	.025	-1.51	.11
2.00					1.63	.22	1.99	.82
3.33			2.33	-.26	5.17	1.50	9.84	4.40
4.17	1.96	-1.03	3.52	.055	8.02	3.17	14.93	7.87
6.25	4.20	-.92	7.20	2.09	16.06	10.96	30.40	25.21
10.00	11.33	1.62	15.18	10.98			45.61	84.81

B = .60 c = .36 e = .20

P / $\frac{\nu}{b\omega}$	.10 R	.10 I	.20 R	.20 I	.50 R	.50 I	1.0 R	1.0 I
2.00	.56	-.67	.82	-.52	1.39	-.15		
3.33	1.80	-.57	2.87	.49	5.98	3.54	10.32	7.72
4.17	1.91	1.54	2.28	4.57	3.36	13.25	5.12	26.37
5.00	-.54	1.80	-2.28	4.52	-7.31	12.29	-15.10	24.52
6.25	-1.66	.21	-3.79	1.57	-10.08	5.59	-20.15	12.10

	c = .20		e = 0	
$\frac{v}{b\omega}$	$A_{\theta\theta}$	$A_{\theta\beta}$	$A_{\beta\theta}$	$A_{\beta\beta}$
.83	.8538 -.8833 i	-.5493 -.6746 i	.1075 -.02824 i	-.000864 -.1402 i
2.0	.3972 -2.3916 i	-4.0459 -.9812 i	.09293 -.07646 i	-.1699 -.3161 i
3.33	-.1950 -4.433 i	-12.4643 -.2001 i	.0740 -.1417 i	-.5620 -.4809 i
4.17	-.5520 -5.8242 i	-20.3737 .8505 i	.06259 -.18621 i	-.9230 -.56592 i
6.25	-1.3450 -9.5350 i	-49.6014 5.0100 i	.03724 -.3049 i	-2.2330 -.7295 i
10.0	-2.4460 -16.6400 i	-137.4490 16.4656 i	.00203 -.5320 i	-6.0960 -.8970 i

	c = .33		e = 0	
$\frac{v}{b\omega}$	$A_{\theta\theta}$	$A_{\theta\beta}$	$A_{\beta\theta}$	$A_{\beta\beta}$
.83	.8538 -.8833 i	-.5988 -.5805 i	.045988 -.007378 i	.01601 -.0724 i
2.0	.3972 -2.3916 i	-4.0467 -.7268 i	.04217 -.01998 i	.01709 -.1682 i
3.33	-.1950 -4.433 i	-12.4022 .2715 i	.0372 -.03703 i	.0116 -.2679
4.17	-.5520 -5.8242 i	-20.2736 1.4701 i	.0342 -.0487 i	.00238 -.3255 i
6.25	-1.3450 -9.5350 i	-49.4170 6.0244 i	.0276 -.0796 i	-.0448 -.4564 i
10.0	-2.4460 -16.6400 i	-137.1474 18.2358 i	.0184 -.1390 i	-.2266 -.6584 i

	c = .36	e = .20		
$\frac{v}{b\omega}$	$A_{\theta\theta}$	$A_{\theta\beta}$	$A_{\beta\theta}$	$A_{\beta\beta}$
2.0	.3972 -2.3916 i	-3.6876 -.5434 i	.05426 -.04325 i	-.1157 -.1606 i
3.33	-.1950 -4.433 i	-11.334 .4407 i	.04352 -.08018 i	-.3628 -.2499 i
4.17	-.5520 -5.824 i	-18.534 1.578 i	.03706 -.1053 i	-.5887 -.2938 i
5.00	-.8860 -7.276 i	-27.689 3.0608 i	.03102 -.1316 i	-.8712 -.3315 i
6.25	-1.3450 -9.5350 i	-45.1814 5.8428 i	.02272 -.1724 i	-1.4027 -.3779 i

air speed, the charts represent a series of flutter-stability curves. The real part of the solution presented in the tabulation may be used to determine the flutter frequency if this information is desired. All computations were carried out in the tabular form shown.

Effect of Finite-Control-Surface Frequency

Examination of Equation [10] indicates that the effect of finite-control-surface frequency may be readily determined from the charts presented by assuming $g = 0$, and using

$$B' = B\left\{1 - \left(\frac{\omega_\beta}{\omega}\right)^2\right\} \cong B\left\{1 - \left(\frac{\omega_\beta}{\omega_\theta}\right)^2\right\}$$

Due to neglecting the friction in the control-surface system, the results will be on the conservative side.

Illustrative Example. Determine the allowable rudder product of inertia from the following data:

Average rudder chord = 22 in.

Average fin chord = 22 in. (i.e., $e = 0$)

Aerodynamic balance $\frac{c - e}{1 - e} = 0.20$

Moment of inertia of rudder $J_\beta = 3.0$ lb-in. sec^2

Rudder span = fin span = $L = 80$ in.

Moment of inertia of tail about torsional axis = 1500 lb-in. sec^2

Moment of inertia of wings about torsional axis = 50,000 lb-in. sec^2

Ratio of torsional deflections $\left(\frac{\theta_w}{\theta}\right) = 0.20$

Torsional natural frequency of airplane = 1000 cycles per min

Maximum flight speed of airplane = 500 mph

The calculation of the nondimensional parameters are as follows:

$$\pi\rho b^2 = \pi(8.45 \times 10^{-8})22^2 = 0.0001285 \text{ (10,000 ft altitude assumed)}$$

$$J_\theta = 1500 + (0.20)^2\,50{,}000 = 3500 \text{ lb-in. sec}^2$$

$$Ag = \frac{3500 \times 0.03}{0.0001285 \times 80^3} = 53.2 \times .03 = 1.60 \text{ (3 per cent damping assumed)}$$

$$B = \frac{3.0}{0.0001285 \times 80 \times 22^2} = 0.603$$

$$\frac{v}{b\omega} = \frac{500 \times \frac{88}{60} \times 12}{22 \times \frac{1000}{60} \times 2\pi} = 3.82$$

From the stability curve for $B = 0.6$ find $P = 0.18$ corresponding to $Ag = 1.60$. The allowable product of inertia is then

$$\int x_\beta y dm_\beta = 0.18 \times 0.0001285 \times 22 \times 80^2 = 32.6 \text{ lb-in. sec}^2$$

From the real part of the solution $R \cong 0.2$ corresponds to the foregoing values. The frequency ratio then becomes

$$\left(\frac{\omega_\theta}{\omega}\right) = \sqrt{1 - \frac{R}{A}} = \sqrt{1 - \frac{0.2}{53.2}} = 0.998$$

and the error in neglecting this correction is less than 1 per cent.

Summary and Conclusions

Control-surface flutter involving fuselage torsion has been investigated in terms of nondimensional parameters and presented in chart form. The results are applicable to conventional tail surfaces with 20 or 33 per cent aerodynamic balance. The effect of fin or stabilizer bending was not included in the investigation since this mode is generally covered in the three-dimensional analysis involving fuselage bending. The real part of the solution was included in the tabulation as an indication of the frequency ratio $\left(\frac{\omega_\theta}{\omega}\right)$ which was assumed to be unity.

Several conclusions may be drawn by examination of the charts, as follows:

1 The stability of the control surface for this form of flutter is mainly a function of its product of inertia and aerodynamic balance.

2 For a given product of inertia, the flutter speed will be higher for a control surface with larger aerodynamic balance.

3 Large aerodynamic balance increases the explosiveness of flutter, as indicated by higher peaks of the stability curves.

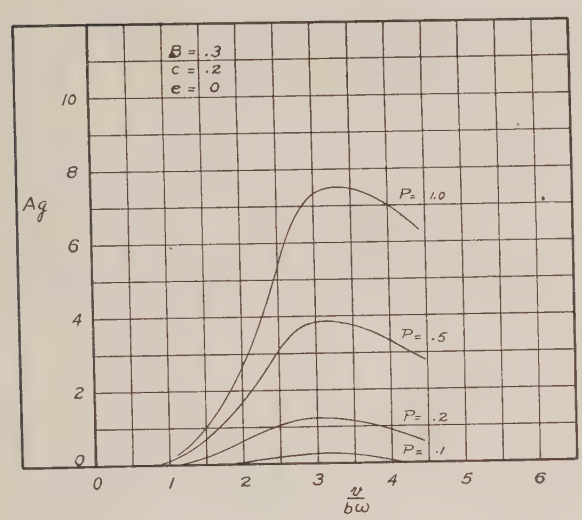

FIG. 1

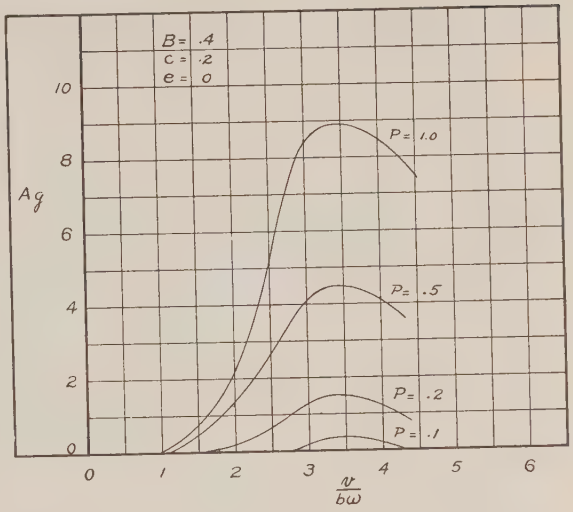

FIG. 2

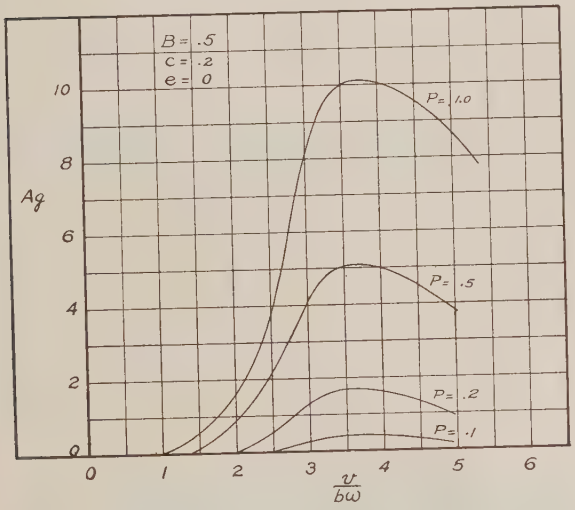

FIG. 3

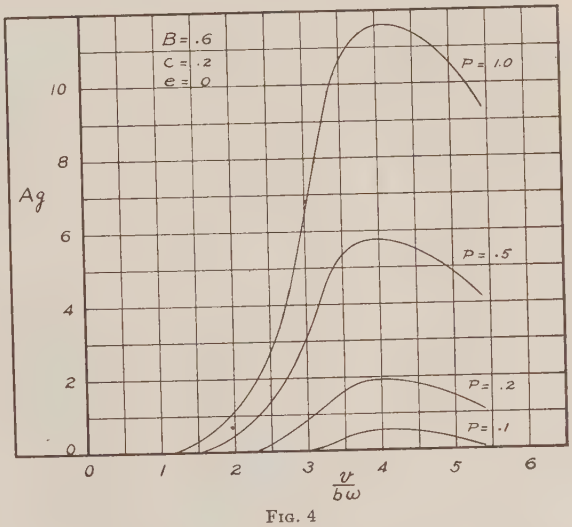

FIG. 4

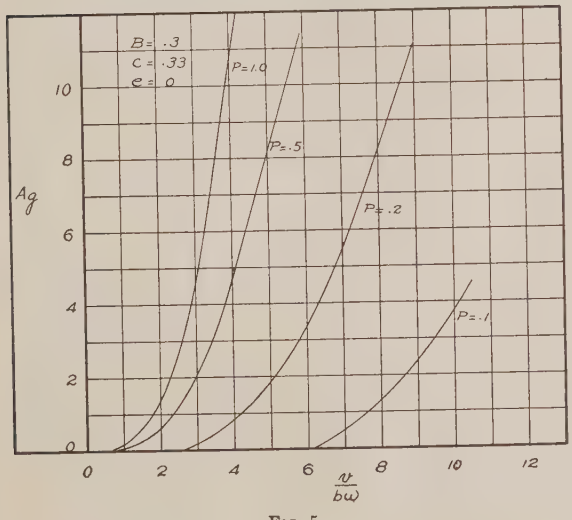

FIG. 5

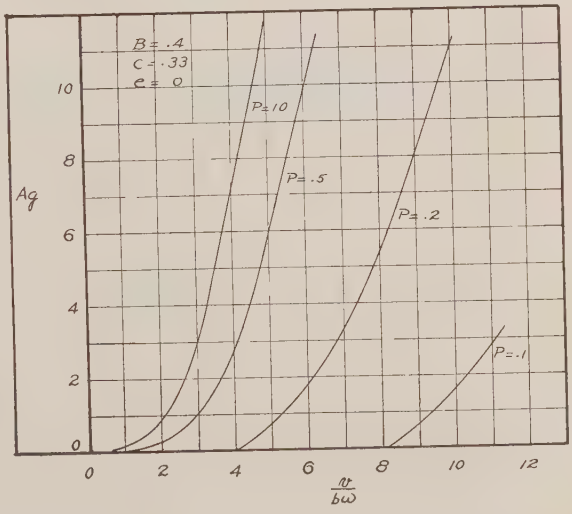

FIG. 6

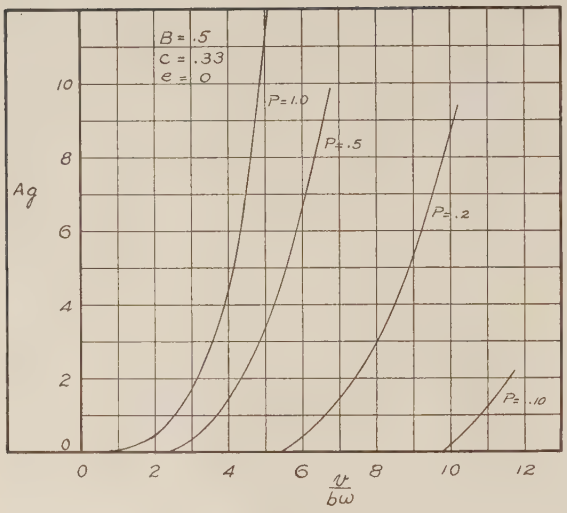

FIG. 7

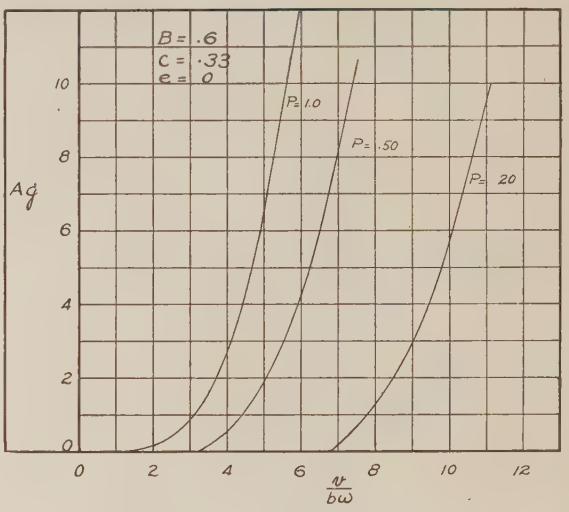

FIG. 8

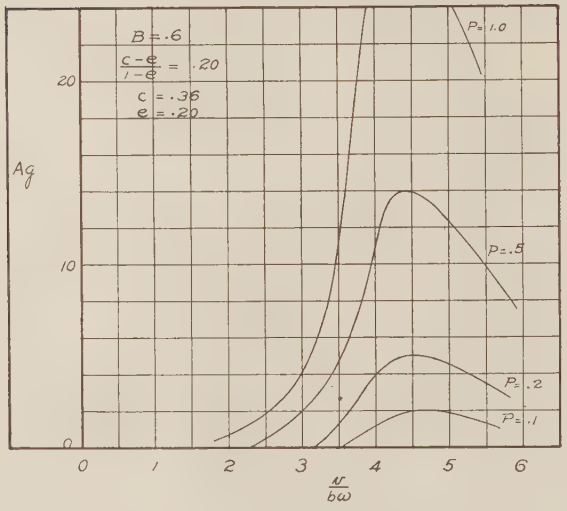

FIG. 9

4 Reducing the control-surface chord for the same aerodynamic balance increases the flutter speed and its explosiveness, as indicated by the shift of the stability peak to higher values of $\frac{v}{b\omega}$ and Ag.

5 The effect of the finite-control-surface frequency is to shift the stability curve to a lower value of B, the main effect of which is to decrease the stability peaks to lower values. The flutter speed is also lowered slightly.

The charts presented are intended to aid in the preliminary determination of the required product of inertia. They also enable a study to be made of the effect of varying the design parameters.

ACKNOWLEDGMENT

The author wishes to acknowledge his appreciation to Miss C. L. Dick who carried out the numerical work for the charts.

BIBLIOGRAPHY

1 "Charts for Fuselage Bending Vs. Control Surface Flutter," by L. S. Tolve, A.A.F. TR. 5107, April, 1944.

2 "General Theory of Aerodynamic Instability and Mechanism of Flutter," by T. Theodorsen, N.A.C.A. TR. 496, 1935.

3 "The Oscillating Wing With Aerodynamically Balanced Elevators," by H. G. Kussner and I. Schwarz, N.A.C.A. TM. 991, 1941.

4 "Application of Three Dimensional Flutter Analysis," by B. Smilg, A.A.F. TR. 4798, 1942.

(Owing to travel emergency conditions existing when this paper was presented, discussion will be accepted until February 10, 1946)

Thermal Accommodation Coefficients[1]

By M. L. WIEDMANN[2] AND P. R. TRUMPLER[3]

This investigation deals with the conduction of heat through a gas at low pressure. The theoretical work of M. Knudsen is extended to cover the case of conduction between two infinite concentric cylindrical surfaces of different properties. Experiments to determine the accommodation coefficients of air on flat black lacquer and nine metal surfaces indicate that the values lie between 0.87 and 0.97.

Nomenclature

The following nomenclature is used in the paper:

A = surface area, sq ft
a = radiant emissivity
E_1 = energy of a gas stream in equilibrium with surface 1
E_1' = energy of a gas stream after collision at surface 1
$F = \frac{r_1}{r_2}$
L = length of cylindrical test section, ft
M = molecular weight of the gas (O_2 is 32)
p = gas pressure, mm mercury
Q_c = net conduction heat transfer, Btu per hr
Q_R = net radiation heat transfer, Btu per hr
r = radius, ft
T = gas temperature, deg F abs
T_1 = temperature of surface 1, deg F abs
α = accommodation coefficient
$\gamma = \frac{c_p}{c_v}$ = ratio of specific heats of the gas
ρ = length of a path between inner and outer surfaces, ft
σ = Boltzmann constant = 0.172×10^{-8} Btu per hr per sq ft per (deg F)[4]
β, δ, θ = angles

Subscript 1 refers to inner surface, subscript 2 to outer surface.

Introduction

In a sense there are only two methods by which heat may be transferred between solids separated by a gas, i.e., radiation and molecular collision. Collisions may take place between the gas molecules themselves or between gas molecules and the surface of the containing vessel. The latter type of collision is the subject of this investigation.

At ordinary pressures the effect of surface collisions is lost in the large number of collisions involving only gas molecules. But if the pressure is reduced far enough there will be only a comparatively small number of gas molecules in the containing vessel, and most of the collisions will be made at the bounding surfaces. These collisions will then exert a controlling influence on the heat transfer.

Kinetic theory predicts that the conductivity of a perfect gas far from a solid surface is independent of the pressure. If certain dimensions of the containing vessel are of the order of magnitude of the mean free path,[4] the heat conduction is a function of the pressure and the surface characteristics. For the special case of gas pressure so low that collisions between gas molecules are infrequent compared with surface collisions, the heat conduction is proportional to the pressure (1, 2, 3).[5] The theoretical treatment to be presented applies to a perfect gas at this low pressure, hereafter called a "rarefied gas," and the experimental work was conducted with air in or near this pressure region.

Air at 32 F and 0.000001 atm pressure has a mean free path of 2.3 in. (4). It is apparent that the results here presented are applicable primarily to problems of heat conduction through a gas at very low pressure or in a very small space.

The characteristic properties of a surface which determine the radiation are the emissivity and the absorptivity. In heat transfer by surface collisions the characteristic property is the accommodation coefficient, which expresses the extent to which a particle stream impinging upon a solid surface comes to thermal equilibrium with the solid.

If a particle stream approaches a surface at energy E_2' and leaves at energy E_1', and if the energy of the stream at thermal equilibrium with the solid would be E_1, then the accommodation coefficient is defined as

$$\alpha = \operatorname*{Limit}_{E_2' \to E_1} \left[\frac{E_2' - E_1'}{E_2' - E_1} \right] \quad [1]$$

If only kinetic-energy changes are considered and the particle stream has a maxwellian velocity distribution before and after collision, the accommodation coefficient may be expressed in terms of temperatures

$$\alpha = \operatorname*{Limit}_{T_2' \to T_1} \left[\frac{T_2' - T_1'}{T_2' - T_1} \right] \quad [2]$$

Values of accommodation coefficient reported in the literature range from less than 0.1 to unity.

Results of Tests

The equation for heat conduction between two infinite concentric cylinders separated by a rarefied gas is

$$\frac{Q_c}{L} = 3600\, r_1 \frac{\gamma + 1}{\gamma - 1} \frac{p(T_1 - T_2)}{\sqrt{MT}} \frac{1}{\frac{r_1}{r_2}\left(\frac{1}{\alpha_2} - 1\right) + \frac{1}{\alpha_1}} \quad [3]$$

where

$\frac{Q_c}{L}$ = heat transfer by conduction, per unit cylinder length, Btu $hr^{-1}\,ft^{-1}$
$\gamma = \frac{c_p}{c_v}$ = ratio of specific heats of the gas
p = gas pressure, mm mercury

[1] This paper summarizes a dissertation submitted by one of the authors[3] to Yale University in partial fulfillment of requirements for the degree of Doctor of Philosophy.

[2] Associate Professor of Mechanical Engineering, Yale University, New Haven, Conn.

[3] Development Engineer, M. W. Kellogg Company, New York, N. Y. Jun. A.S.M.E.

Contributed by the Heat Transfer Division and presented at the Annual Meeting, New York, N. Y., Nov. 29–Dec. 3, 1943, of The American Society of Mechanical Engineers.

[4] The mean free path may be defined as the average distance a gas molecule travels between collisions with other gas molecules.

[5] Numbers in parentheses refer to the Bibliography at the end of the paper.

T = gas temperature at place where the pressure is p, deg FA
M = molecular weight of the gas (O_2 is 32)
T_1, T_2 = temperatures of inner and outer cylinders, respectively, deg FA
r = radius, ft
α = accommodation coefficient

Subscripts 1 and 2 refer to inner and outer cylindrical surfaces respectively.

Experiments were made to determine the accommodation coefficients and emissivities of aluminum, cast iron, and bronze. Polished, machined, and etched surfaces of each metal were tested. The values of $\frac{Q_c\sqrt{T}}{T_1 - T_2}$ are plotted against pressure for nine metallic surfaces and a reference surface of flat black lacquer in Figs. 1–3, inclusive. Maximum and minimum values of accommodation coefficients were taken from a plot of $\frac{Q_c\sqrt{T}}{p(T_1 - T_2)}$ as a function of pressure p, Fig. 4, and are tabulated with the emissivities in Table 1.

TABLE 1 SUMMARY OF RESULTS

Surface	Description	Emissivity	Accommodation coefficient — Minimum	Accommodation coefficient — Maximum
X	Flat black lacquer on bronze	0.932	0.881	0.894
A	Bronze, polished	0.103	0.91	0.94
F	Bronze, machined	0.110	0.89	0.93
D	Bronze, etched	0.192	0.93	0.95
B	Cast iron, polished	0.184	0.87	0.93
E	Cast iron, machined	0.391	0.87	0.88
G	Cast iron, etched	0.697	0.89	0.96
C	Aluminum, polished	0.221	0.87	0.95
J	Aluminum, machined	0.0909	0.95	0.97
H	Aluminum, etched	0.775	(0.89)	(0.97)

Two general conclusions may be drawn as follows:

1 The values of all measured accommodation coefficients lie between 0.87 and 0.97.

2 The effect of different technical surfaces on the accommodation coefficient, if such an effect exists, is small and is not shown by the present tests.

In evaluating the experimental results the abnormal behavior of two of the surfaces should be noted. The emissivities of the etched aluminum dropped from 0.833 to 0.753 during the tests, and the value of the accommodation coefficient is therefore unreliable. In testing the etched cast-iron surface *G* it was observed that the air pressure in the sealed system decreased appreciably in the course of each conduction test. The emissivity remained unchanged.

It is undoubtedly true that all the metallic surfaces were oxidized to some extent. The appearance of each surface was the same before and after the tests, and, except for the etched aluminum, the emissivity was constant. But even if the oxide coatings were stable their influence on the properties of the metallic surfaces must be considered in interpreting the data.

The values of accommodation coefficient found by the authors are of the same magnitude as those given by Knudsen (1) for oxygen in contact with polished platinum, platinum coated lightly and then heavily with platinum black. His values are 0.808, 0.910, and 0.934, respectively.

Theory

The apparatus employed by the authors for determining accommodation coefficient requires the heat-transfer equations for radiation and for rarefied-gas conduction between two infinite concentric cylinders having different surface properties. The radiation equation, assuming diffuse reflection, is well known (5) as

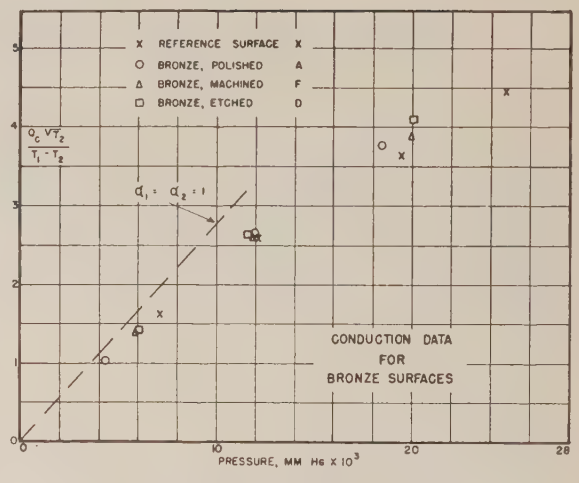

FIG. 1 CONDUCTION DATA FOR BRONZE SURFACES

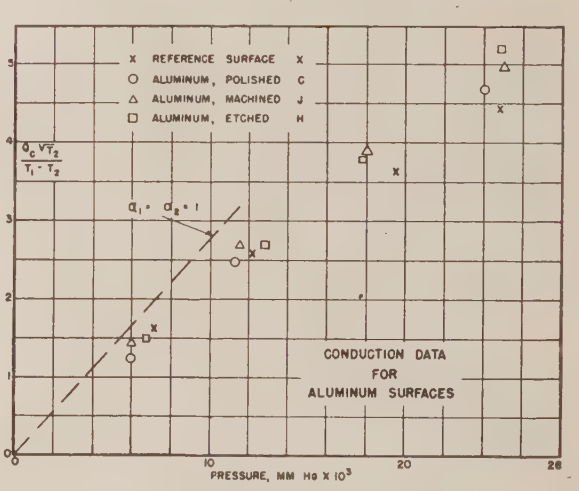

FIG. 2 CONDUCTION DATA FOR ALUMINUM SURFACES

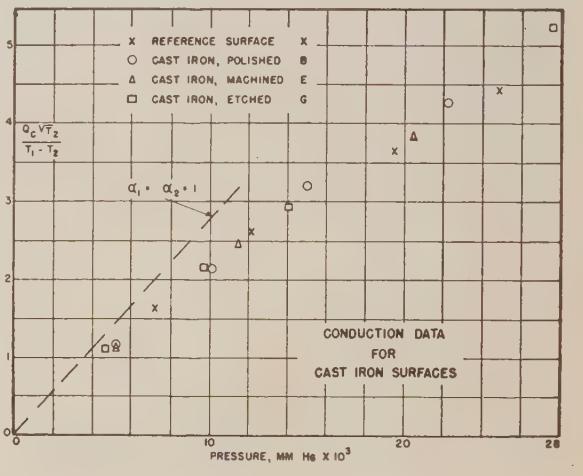

FIG. 3 CONDUCTION DATA FOR CAST IRON SURFACES

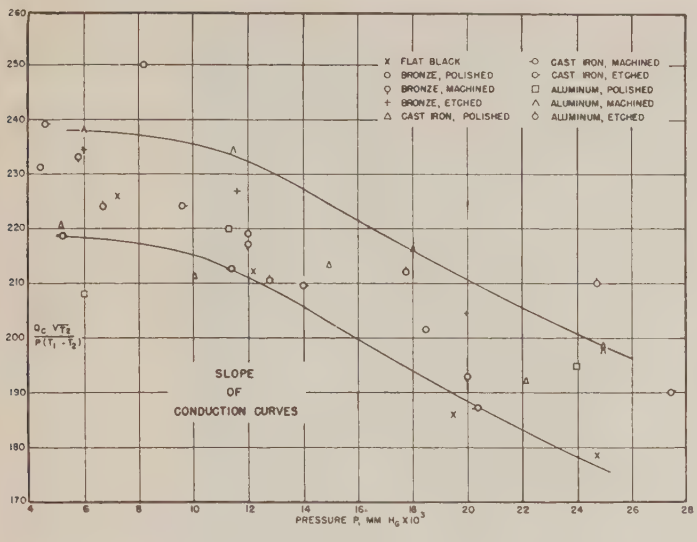

FIG. 4 SLOPE OF CONDUCTION CURVES

$$Q_R = \frac{\sigma A_1 (T_1^4 - T_2^4)}{\frac{A_1}{A_2}\left(\frac{1}{a_2} - 1\right) + \frac{1}{a_1}} \quad \ldots\ldots [4]$$

or

$$\frac{Q_R}{L} = \frac{2\pi r_1 \sigma (T_1^4 - T_2^4)}{\frac{r_1}{r_2}\left(\frac{1}{a_2} - 1\right) + \frac{1}{a_1}} \quad \ldots\ldots [5]$$

$\frac{Q_R}{L}$ = heat transfer by radiation, per unit cylinder length, Btu $hr^{-1} ft^{-1}$

A = area of cylindrical surface, sq ft

a = radiant emissivity

σ = Boltzmann constant = 0.172×10^{-8}

Although Equation [5] applies only to gray bodies, its use with metallic surfaces is justified as a means of separating radiation from conduction in the authors' experiments. Emissivities calculated from Equation [5] are not accurate if the surfaces differ appreciably from those of gray bodies.

The equation for the conduction through a rarefied gas (almost all particle collisions at the solid surfaces) may be derived by extending the work of M. Knudsen (1), the validity of which has been fairly well established (6, 7, 8, 9). His equation for maximum conduction between two concentric infinite cylinders (accommodation coefficients unity) is

$$\frac{Q_c}{L} = 3600\, r_1 \frac{\gamma + 1}{\gamma - 1} \frac{p(T_1 - T_2)}{\sqrt{MT}} \quad \ldots\ldots [6]$$

With reference to Fig. 5, consider a large number of gas molecules striking a unit area of surface 1 per unit time having a total energy E_2' before, and E_1' after collision. Then the energy transferred from surface 1 is $E_1' - E_2'$ per unit area per unit time and the accommodation coefficient is

$$\alpha_1 = \frac{E_2' - E_1'}{E_2' - E_1} \quad \ldots\ldots [7]$$

After collision with surface 2, a particle stream has energy E_2'. The same particle stream does not, however, approach the outer surface with energy E_1', for only a fraction F of the particles comes from the inner surface. The remainder $(1 - F)$ come from the outer surface at energy E_2'; therefore

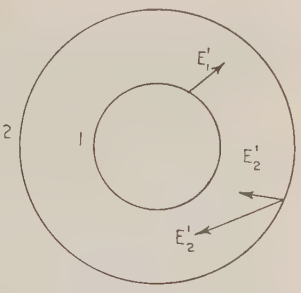

FIG. 5

$$\alpha_2 = \frac{FE_1' + (1 - F)E_2' - E_2'}{FE_1' + (1 - F)E_2' - E_2} \quad \ldots\ldots [8]$$

or

$$\alpha_2 = \frac{F(E_1' - E_2')}{FE_1' + (1 - F)E_2' - E_2} \quad \ldots\ldots [9]$$

From Equations [7] and [9]

$$E_1' - E_2' = \frac{E_1 - E_2}{F\left(\frac{1}{\alpha_2} - 1\right) + \frac{1}{\alpha_1}} \quad \ldots\ldots [10]$$

The symbol F is defined as the fraction of particles leaving the outer surface taking direct paths to the inner. Its value can be calculated on the basis of Knudsen's cosine law (7), which may be stated as follows: The probability that a gas molecule leaves a surface on a path making an angle θ with the normal to the surface is proportional to $\cos\theta$.[6]

For a given path between the surfaces if β and δ represent the angles made by the path with the normals to the surfaces at the points of contact, and if ρ is the path length, then

$$F = \frac{1}{\pi} \int_{A_1} \frac{\cos\beta \cos\delta}{\rho^2}\, dA_1 = \frac{r_1}{r_2} \quad \ldots\ldots [11]$$

Returning to Equation [10], since $E_1 - E_2$ represents maximum energy transfer as given by Equation [6], the general equation for heat conduction between two infinite concentric cylinders separated by a rarefied gas is

$$\frac{Q_c}{L} = 3600\, r_1 \frac{\gamma + 1}{\gamma - 1} \frac{p(T_1 - T_2)}{\sqrt{MT}} \frac{1}{\frac{r_1}{r_2}\left(\frac{1}{\alpha_2} - 1\right) + \frac{1}{\alpha_1}} \quad \ldots [12]$$

Using $M = 29.0$ and $\gamma = 1.404$ for air

$$\left(\frac{Q_c}{L}\right)_{air} = 3980\, r_1 \frac{p(T_1 - T_2)}{\sqrt{T}} \frac{1}{\frac{r_1}{r_2}\left(\frac{1}{\alpha_2} - 1\right) + \frac{1}{\alpha_1}} \quad \ldots [13]$$

In the experiments, r_1 varied from 0.1040 to 0.1042, $r_2 = 0.1094$, and $L = 0.667$. For this case

$$Q_c = 276 \frac{p(T_1 - T_2)}{\sqrt{T}} \frac{1}{0.952\left(\frac{1}{\alpha_2} - 1\right) + \frac{1}{\alpha_1}} \quad \ldots [14]$$

[6] This law is analogous to Lambert's cosine law for diffuse reflection of radiation.

Although Equation [14] should be used only with small values of $T_1 - T_2$, Knudsen's experiments show (1) that the maximum value of 60 F in the present experiments is well within the range of application.

Experimental Procedure

The apparatus generally used for the measurement of accommodation coefficients (1, 2, 10) is not well adapted to an investigation of various types of surfaces. This objection is overcome in the new design, shown in Fig. 6, which has the additional advantage of a center, or test cylinder of simple construction which can be easily changed without duplication of test equipment. With the exception of the disk washers at the ends of the test cylinder, which were designed for a press fit, all other parts were used interchangeably for all ten inner cylinders.

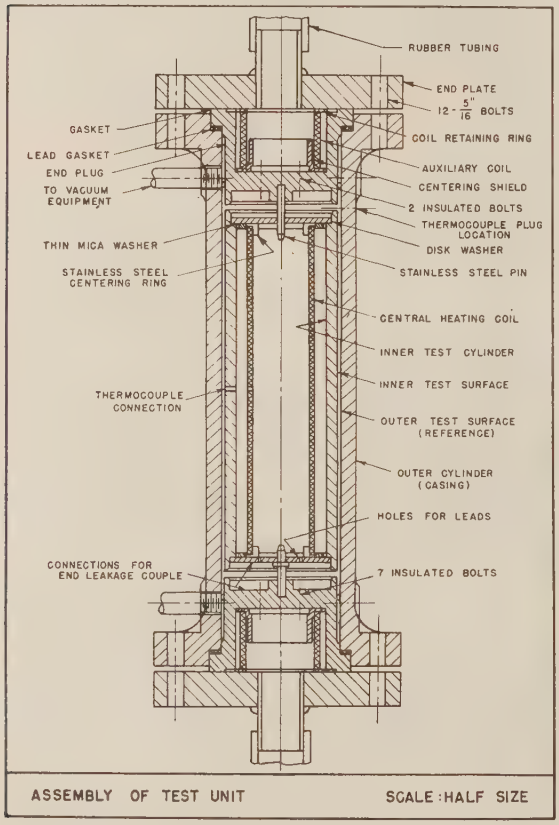

Fig. 6 Assembly of Test Unit

Heat supplied by the central heating coil flows outward between the two test surfaces approximately 2.50 and 2.62 in. diam. The test length is 8.00 in. Energy input to the auxiliary coil at each end is regulated to maintain a very small temperature differential between the disk washer and the inner face of the end plug. Therefore, substantially all the heat input to the central coil flows through the test surface.

The outer test surface was used as a reference and was given a double coat of flat black paint in order to make it nearly "gray" in response to radiation. Its properties were determined by testing a similarly prepared surface on an inner cylinder. The emissivity was 0.932 and the accommodation coefficient 0.89. The five radiation tests on this surface for temperature differences from 40 to 80 F checked the Stefan-Boltzmann law with an average deviation of 0.25 per cent. To prevent damage to the reference surface while changing test cylinders, a special fixture, not shown in the illustration, was designed.

Energy to the heating coils was supplied by a direct-current generator driven by a synchronous motor. Heat loss from the central coil leads was experimentally measured and a correction established.

The test section was evacuated by a Cenco Megavac pump, and the pressure was measured by a McLeod gage with a dry-ice trap. The system included a phosphorus pentoxide drier. The pressure was corrected for thermal diffusion between air at water temperature entering the test casing and air between the test cylinders. No correction was made for pressure drop in the piping from gage to casing because the correction is less than 4 per cent at the lowest conduction test pressures. The diffusion correction is actually applied by substituting T_2 for gas temperature T in Equation [3].

Temperatures inside the test unit were measured with calibrated copper-constantan thermocouples of 24 B&S gage wire, with arc-welded junctions. A Leeds and Northrup Type K potentiometer served to measure the temperature difference between the test cylinders, and a galvanometer sensitive to 0.05 deg F was used for the end-loss couples.

The thermocouple installations should be noted. Contact between the couple junction and the inner test cylinder was established mechanically by a set screw, Fig. 9(*c*). The junction on the reference cylinder, being electrically insulated from the casing, provides poor thermal contact and therefore conduction through the leads should be held to a minimum. The plug containing the element is shown in Fig. 7, its assembly in the cylindrical shell extending from the casing in Fig. 9(*a*), and the position of the shell on the casing in Fig. 10. Installation of the end-loss couples is shown in Fig. 9(*d*), and Fig. 8 shows them connected to the end plugs but detached from the disk washers.

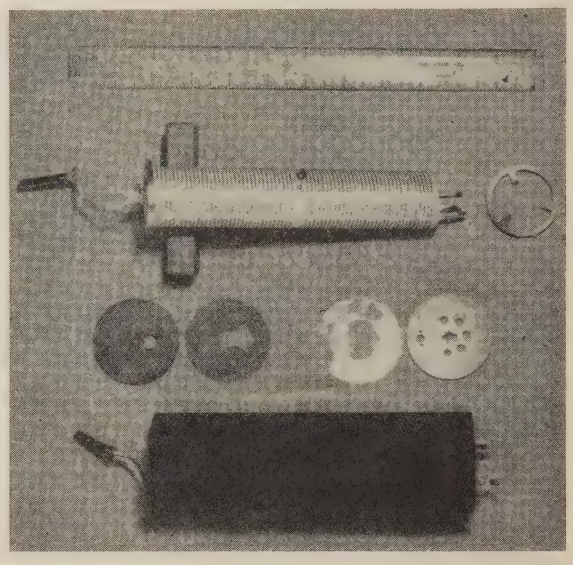

Fig. 7 Units Composing Inner Cylinder Assembly

To draw leads out of the test section, stainless-steel bolts, Figs. 8 and 9(*b*), were made part of each thermocouple circuit. An emf correction for the copper-to-steel junctions in each cir-

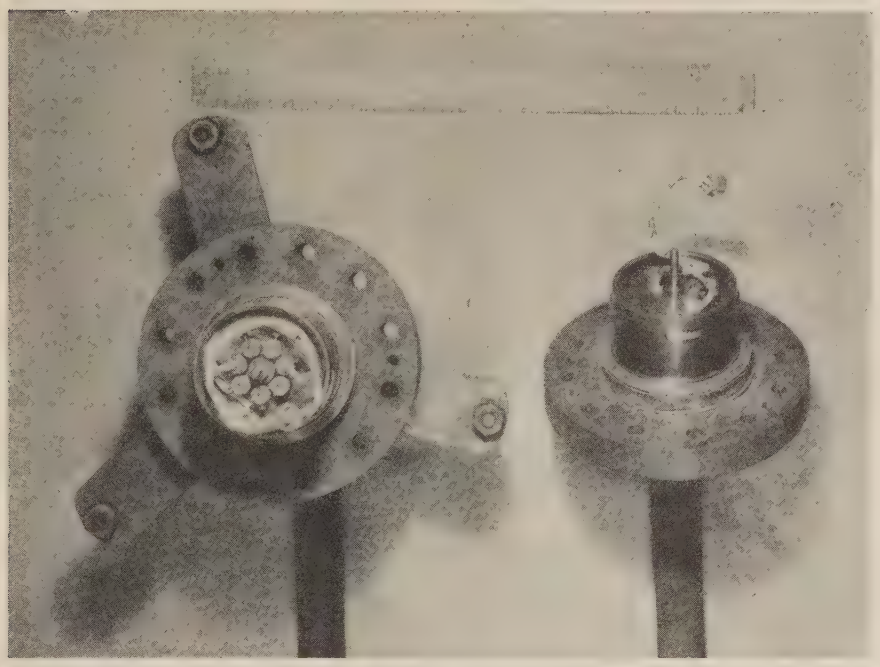

FIG. 8 END PLUGS AND END-LEAKAGE COUPLES

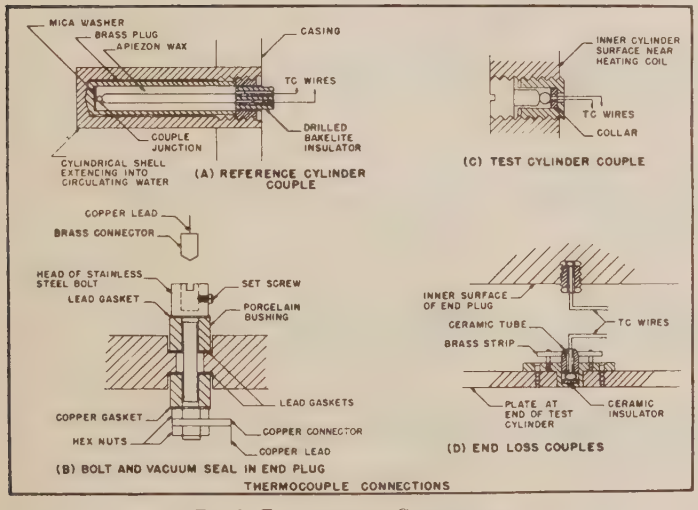

FIG. 9 THERMOCOUPLE CONNECTIONS

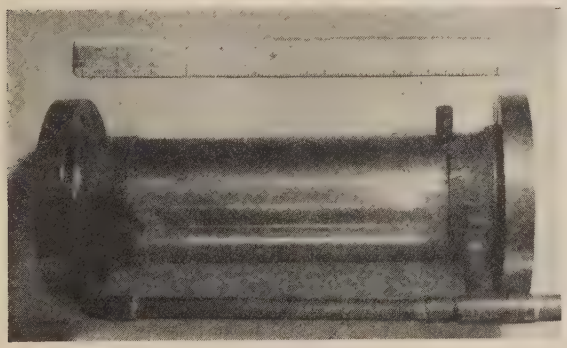

FIG. 10 CASING OF TEST UNIT

cuit was determined by joining the bolt heads with copper wire and operating the equipment under previously established conditions. The correction in no instance exceeded 2 deg.

Preparation of Test Surfaces. The test cylinders were machined from castings made by commercial foundries in Connecticut. The bronze was an alloy of 85 per cent copper, 5 per cent each of tin, lead, and zinc by weight; the cast iron was actually a semisteel, since steel scrap had been added; the aluminum was alloyed with traces of other elements to provide free machining and corrosion resistance. All castings of one metal came from the same lot. Only cylinders without flaws on the finished test surface were used.

Test cylinders were machined without lubrication. Before the final lathe cuts were made the cylinder and the plugs which supported it between centers were removed from the lathe and cleaned with soap solution, dioxane, and distilled water. After this cleaning the cylinder was not touched by hand. No further cleaning of any kind was given the machined or polished surface.

Polishing, except for cast iron, was done on a lathe with five grades of polishing paper ending with 4/0. Because of metal porosity cast iron was finished only to 1/0 paper. On aluminum the finer papers produced a dull finish on which the many fine surface pits were entirely covered up. Polishing at various speeds and pressures was tried without obtaining a brighter finish. The machined aluminum, on the other hand, was bright but clearly showed the porosity of the casting. The fact that the emissivity of the machined surface was found to be less than that of the polished was not entirely unexpected.

Etching was done with nitric acid, reducing the over-all diameter of a cylinder 0.004 to 0.005 in. Upon removal from the acid bath, the cylinders were washed and scrubbed in tap water, a dilute ammonium hydroxide solution, more tap water, and finally distilled water.

TABLE 2 TEST DATA

Run No.	r_1 inches	Pressure mm Hg x 10^3	T_2 °FA	T_1 °FA	Energy Input I amp.	Energy Input E volts	Energy Input Q watts	a_1	Q_r watts	Q_c Btu/hr	$\frac{Q_c\sqrt{T_2}}{T_1 - T_2}$	$\frac{Q_c\sqrt{T_2}}{p(T_1 - T_2)}$
X-1	1.2505	0.1	535.8	597.9	0.801	10.96	8.779	0.932	8.761	0.061		
X-1a		0.1	535.3	598.8	.808	11.06	8.936	.929	8.918	.061		
X-2		0.1	536.9	585.8	.704	9.63	6.780	.938	6.766	.048		
X-3		0.1	536.5	578.7	.644	8.79	5.661	.931	5.649	.041		
X-4		0.09	536.3	618.1	.936	13.05	12.215	.931	12.194	.072		
X-5		7.2	537.9	585.2	.734	10.15	7.450	.932	6.480	3.312	1.62	226
X-6		12.2	538.3	587.0	.774	10.73	8.305	.932	6.711	5.440	2.59	212
X-7		19.5	537.4	586.4	.804	11.16	8.973	.932	6.726	7.669	3.63	186
X-8		24.8	536.8	588.2	.847	11.76	9.961	.932	7.079	9.836	4.43	178
X-9		111.	536.0	582.8	.990	13.77	13.63	.932	6.338	24.88	12.31	111
X-10		25,500	537.4	569.4	.990	13.71	13.57	.932	4.191	32.01	23.19	0.91
A-1	1.2495	0.06	538.1	606.2	.296	3.97	1.175	.104	1.164	.038		
A-2		0.09	536.9	606.8	.296	4.00	1.184	.102	1.166	.061		
A-3		4.4	536.2	579.9	.304	4.11	1.249	.103	0.686	1.922	1.02	231
A-4		8.2	537.8	582.4	.371	5.01	1.859	.103	0.708	3.932	2.04	250
A-5		12.0	536.9	588.2	.434	5.83	2.530	.103	0.825	5.819	2.63	219
A-6		18.5	536.6	590.6	.505	6.82	3.444	.103	0.874	8.771	3.76	202
B-1	1.2490	0.1	538.1	604.9	.391	5.26	2.057	.187	2.040	.061		
B-2		5.2	537.8	592.6	.421	5.66	2.383	.184	1.588	2.713	1.15	220
B-3		10.1	537.5	587.5	.455	6.10	2.776	.184	1.428	4.601	2.13	211
B-4		15.0	538.6	588.1	.504	6.78	3.417	.184	1.420	6.816	3.20	213
B-5		22.2	539.0	591.4	.568	7.63	4.334	.184	1.518	9.611	4.26	192
B-6		0.1	537.6	594.0	.348	4.69	1.632	.181	1.616	.055		
C-1	1.2490	0.06	532.5	593.4	.400	5.28	2.112					
C-2		0.09	533.0	594.6	.404	5.34	2.157	.223	2.142	.051		
C-3		0.07	531.8	569.8	.303	4.01	1.215	.219	1.208	.024		
C-4		6.0	531.6	571.3	.380	5.02	1.908	.221	1.279	2.147	1.25	208
C-5		11.3	532.6	576.2	.460	6.09	2.801	.221	1.427	4.689	2.48	220
C-6		24.0	532.6	583.6	.599	7.91	4.738	.221	1.704	10.36	4.69	195
C-7		92.0	531.9	580.6	.816	10.89	8.89	.221	1.611	24.85	11.77	128
D-1	1.2480	0.06	535.8	614.8	.441	5.81	2.562	.194	2.549	.044		
D-2		0.05	536.2	580.1	.310	4.11	1.274	.191	1.268	.020		
D-3		6.0	536.8	586.0	.421	5.53	2.328	.192	1.455	2.980	1.40	234
D-4		11.6	537.4	589.7	.501	6.59	3.302	.192	1.565	5.928	2.63	226
D-5		20.0	536.4	592.6	.589	7.81	4.600	.192	1.691	9.928	4.09	204
D-6		91.	537.0	585.4	.808	10.74	8.68	.192	1.430	24.74	11.85	130
E-1	1.2500	0.1	537.6	592.9	.507	6.71	3.402	.394	3.387	.051		
E-2		0.09	536.1	575.2	.412	5.45	2.245	.387	2.235	.034		
E-3		5.2	536.6	578.6	.480	6.36	3.052	.391	2.448	2.061	1.14	218
E-4		11.4	536.5	582.4	.556	7.39	4.109	.391	2.703	4.799	2.42	212
E-5		20.4	535.6	584.1	.627	8.31	5.210	.391	2.863	8.010	3.82	187
E-6		90.5	536.7	581.4	.826	11.04	9.12	.391	2.626	22.15	11.48	127

TABLE 2 (*Continued*)

Run No.	r_1 inches	Pressure mm Hg x 10^3	T_2 °FA	T_1 °FA	Energy Input I amp.	E volts	Q watts	a_1	Q_r watts	Q_c Btu/hr	$\frac{Q_c\sqrt{T_2}}{T_1 - T_2}$	$\frac{Q_c\sqrt{T_2}}{p(T_1 - T_2)}$
F-1	1.2500	0.09	535.7	603.9	0.310	4.09	1.268	.113	1.251	.058		
F-2		0.1	534.3	583.3	.250	3.30	0.825	.108	0.811	.048		
F-3		5.8	535.8	584.5	.354	4.69	1.660	.110	0.826	2.846	1.35	233
F-4		12.0	534.6	585.0	.436	5.77	2.516	.110	0.853	5.676	2.60	217
F-5		20.0	536.0	587.9	.518	6.85	3.548	.110	0.839	9.075	3.86	193
F-6		38.0	535.2	596.4	.682	9.06	6.179	.110	1.070	17.44	6.59	173
G-1	1.2480	0.1	534.3	583.3	.619	8.19	5.070	.702	5.057	.044		
G-2		0.09	534.0	596.9	.705	9.44	6.655	.693	6.640	.051		
G-3		4.6	534.3	586.9	.679	9.09	6.172	.697	5.438	2.505	1.10	239
G-4		9.6	533.8	584.2	.700	9.34	6.538	.697	5.165	4.686	2.15	224
G-5		14.0	535.7	583.2	.705	9.42	6.641	.697	4.878	6.017	2.93	210
G-6		27.5	535.6	578.2	.729	9.78	7.130	.697	4.314	9.612	5.22	190
G-7		0.09	534.5	581.8	.604	8.01	4.838	.697	4.826	.041		
H-1	1.2495	0.11	536.7	575.4	.592	7.84	4.641	.833	4.629	.041		
H-2		0.11	537.2	595.8	.725	9.78	7.091	.792	7.073	.061		
H-3		6.7	534.9	589.0	.734	9.90	7.267	.775	6.239	3.509	1.50	224
H-4		12.8	534.4	584.1	.739	9.94	7.346	.775	5.647	5.799	2.70	210
H-5		17.8	535.3	585.9	.780	10.53	8.213	.775	5.792	8.263	3.78	212
H-6		24.8	535.8	584.0	.801	10.83	8.675	.775	5.495	10.85	5.21	210
H-7		0.1	534.4	586.0	.655	8.84	5.790	.758	5.776	.048		
H-7a		0.1	535.7	586.4	.649	8.75	5.679	.753	5.665	.048		
J-1	1.2495	0.1	537.8	608.7	.283	3.81	1.078	.0908	1.058	.068		
J-2		0.06	534.8	609.0	.289	3.89	1.124	.0911	1.112	.041		
J-3		6.0	537.9	575.4	.297	4.01	1.191	.0909	0.516	2.304	1.42	238
J-4		11.5	536.4	583.3	.409	5.50	2.250	.0909	0.657	5.437	2.68	234
J-5		18.0	537.8	586.8	.480	6.46	3.102	.0909	0.695	8.215	3.89	216
J-6		25.0	537.8	590.5	.550	7.37	4.053	.0909	0.755	11.26	4.95	198
J-6a		25.0	537.1	590.4	.553	7.43	4.108	.0909	0.762	11.42	4.96	198

Remarks: r_2 = 1.3125 inches; L = 8.00 inches.

C-1	Mica washers omitted
C-6	Fluctuation of 1% in I
E-6	Fluctuation of 1.5% in E
F-3,4,5	Pressure rise about 1% per hour
G-3,4,5,6	Pressure drop observed, about 5% per test
H-1 to 7	Fluctuation in E as much as 2%
J-6	Fluctuation of 3% in I

Method of Testing. All metallic surfaces subjected to low pressures were cleaned so as to be free of volatile impurities. Degassing was done at test-cylinder temperatures not exceeding 160 F. During radiation tests the vacuum pump was run continuously, but in conduction tests the system was closed at the desired pressure. The pressure rise for an 8- to 12-hr test was usually negligible. The one exception was cylinder *F*, machined bronze, for which the pressure increased as much as 1 per cent per hr.

For each surface at least two radiation tests (air pressure about 10^{-4} mm of mercury) and four conduction tests were made. The conduction tests were in or near the rarefied-gas region, the upper limit of which is about 0.01 mm of mercury for the apparatus. Each test was continued until the temperature change was within 0.1 deg F per hr. The temperature of the inner cylinder ranged from 109.5 to 158 F, and the water temperature, assumed to be the same as that of the reference surface, from 71.6 to 79 F.

ACKNOWLEDGMENT

The authors wish to express their appreciation to Prof. W. J. Wohlenberg of Yale University for general direction of the investigation and for his invaluable advice concerning many of the details.

BIBLIOGRAPHY

1 "Die Moleculare Wärmeleitung der Gase und der Akkommodationskoeffizient," by M. Knudsen, *Annalen der Physik*, vol. 34, 1911, p. 593.

2 "The Exchange of Energy Between a Platinum Surface and Gas Molecules," by W. B. Mann, Proceedings of the Royal Society of London, Eng., vol. A146, 1934, p. 776.

3 "Conduction of Heat Through Rarefied Gases," by F. Soddy and A. J. Berry, Proceedings of the Royal Society of London, Eng., vol. A83, 1910, p. 254; also vol. A84, 1911, p. 576.

4 "The Dynamical Theory of Gases," by J. H. Jeans, University Press, Cambridge, England, fourth edition, 1925.

5 "Heat Transmission," by W. H. McAdams, McGraw-Hill Book Company, Inc., New York, N. Y., second edition, 1942.

6 "Researches on Heat Conduction by Rarefied Gases," by W. H. Keesom and G. Schmidt, *Physica*, vol. 3, 1936, pp. 590 and 1085; also vol. 4, 1937, p. 828.

7 "Das Cosinusgesetz in der kinetischen Gastheorie," by M. Knudsen, *Annalen der Physik*, vol. 48, 1915, p. 1113.

8 "Radiometerdruck und Akkommodationskoeffizient," by M. Knudsen, *Annalen der Physik*, vol. 6, 1930, p. 129.

9 "Optische Untersuchung des Akkommodationskoeffizienten der Moleculartranslation und dessen Verteilungsfunktion in einem verdünnten Gase," by L. S. Ornstein and W. R. van Wyk, *Zeitschrift der Physik*, vol. 78, 1932, p. 734.

10 "Exchange of Energy Between Gas Atoms and Solid Surfaces," by J. K. Roberts, Proceedings of the Royal Society of London, Eng., vol. A129, 1930, p. 146; also vol. A135, 1932, p. 192, and vol. A142, 1933, p. 518.

11 "The Accommodation Coefficient of Helium on Nickel," by B. Raines, *Physical Review*, vol. 56, 1939, p. 691.

Certain Aspects of High-Pressure Centrifugal Pumping Cycles

By I. J. KARASSIK,[1] HARRISON, N. J.

The author discusses the hydraulic and mechanical limitations imposed upon centrifugal boiler feed pumps by certain features of the modern regenerative feedwater heating cycles, as well as the influence of the practical limitations of pump design on the cycles themselves.

REDUCED to its essential elements, a power plant is composed of a boiler feed pump, a boiler, and a heat engine such as a turbine. All other equipment represents refinements which supplement the functions of these three elements and which are directed at improving the over-all efficiency of the power plant.

As the size and number of steam-generating stations grew, the desire for improvements in operating economy dictated many refinements in the steam cycle. These refinements lay in two separate directions. The first of these refinements involved a steady increase in operating pressures and temperatures, in order to provide for a greater heat drop between boiler and condenser.

Operating pressures grew until at the present time 1250-psi boilers are quite common, and a few plants are operating at even higher pressures. Temperatures rose from a conservative 600 and 750 F, until today 900 to 950 F is not considered radical practice. Wartime experience with superchargers and gas turbines promises to lead to even higher steam temperatures. The direct effect of this rise in steam-plant operating conditions will be discussed later.

The second refinement was directed toward greater utilization of heat through increased feed heating. The problem presented by the introduction of multiple heaters centered in the choice between direct-contact heaters and closed heat exchangers. From the thermodynamic point of view, the former have certain definite advantages. It must be considered, however, that a separate boiler feed pump is required after each direct-contact heater, as shown in Fig. 1, while the use of a group of closed heaters permits the application of a single boiler feed pump discharging through these heaters and into the boiler, Fig. 2.

Multiple Direct-Contact Heaters

The first of the problems introduced by a feed cycle with multiple direct-contact heaters is the requirement of separate feed pumps for each of the heaters. This of course may be partially circumvented by the use of a multistage boiler feed pump with multiple inlets and discharge connections, each stage or group of stages serving an individual heater, and each such group operating at a successively elevated temperature.

The most difficult problem, however, resides in the control of the boiler feed pump or pumps. A centrifugal pump will always operate at those conditions of head and capacity which correspond to the intersection between its head-capacity characteristic at its operating speed and the system-head curve. Thus in order to alter the operating conditions, it becomes necessary to alter the shape either of the head characteristic by varying the operating speed, or of the system-head curve by varying one of its components. In a boiler-feed cycle this variation is provided by the feedwater-level regulator, as illustrated in Fig. 3, where curves (*a*) to (*d*), inclusive, correspond to various positions of the feedwater-regulator valve. Thus, depending on the boiler load and consequently on the position of the feedwater-regulator throttling valve, the pump-discharge capacity will correspond to the intersection of the H-Q curve with curves (*a*) to (*d*), or with any intermediate curve.

In the case of a feed cycle with multiple direct-contact heaters, as in Fig. 1, it becomes necessary to interpose a feedwater regulator in the discharge of each individual boiler feed pump. The controlling impulse would be the boiler-drum level in the case of the last discharge and the level in the storage space of the direct-contact heaters in the intermediate units. This multiplication

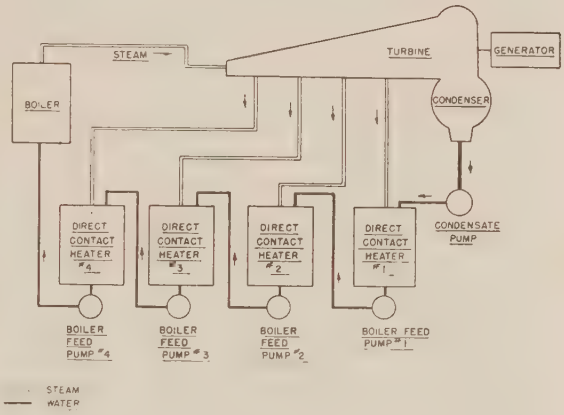

Fig. 1 Feed Cycle With Multiple Direct-Contact Heaters

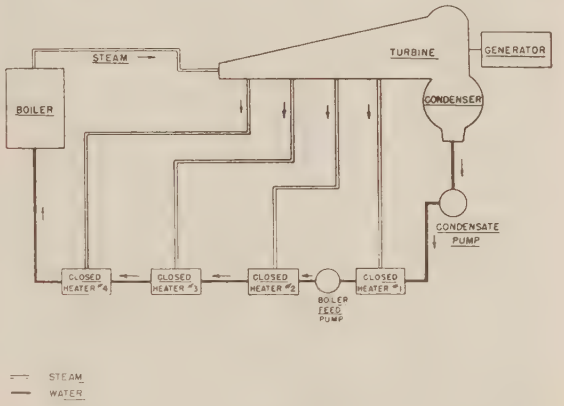

Fig. 2 Feed Cycle With Multiple Closed Heaters

[1] Application Engineer, Worthington Pump & Machinery Corporation. Mem. A.S.M.E.

Contributed by the Hydraulic Division and presented at the Spring Meeting, Birmingham, Ala., April 3–5, 1944, of The American Society of Mechanical Engineers.

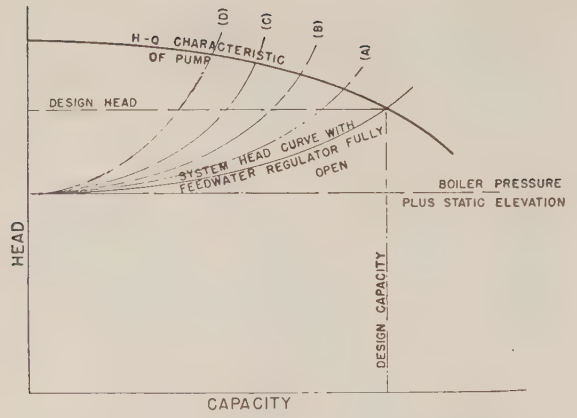

FIG. 3 OPERATION OF FEEDWATER REGULATOR

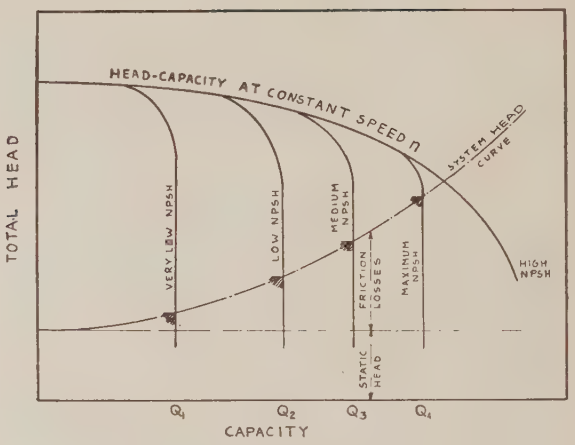

FIG. 4 OPERATION OF A CONDENSATE PUMP

of controls introduces additional expense as well as an increase in the source of potential maintenance troubles.

Of course, any centrifugal pump is, to a certain extent, self-regulating as regards delivery through the effect of suction conditions on the pump head-capacity curve. A typical example of a self-regulating installation is that of a hot well or condensate-removal pump. In this particular case, the delivery of the pump is generally controlled by the submergence over the pump center line, this submergence representing the net positive suction head available over and above the vapor pressure. If the inflow to the condenser hot well is reduced, the pump will withdraw more water than is returned to the condenser with a resultant change in the level of the hot well, a reduction in the available net positive suction head, and a consequent reduction in the delivery of the condensate pump. This operation is illustrated in Fig. 4.

In theory the same principle of operation could be applied to a feed cycle with multiple direct-contact heaters. The delivery of the last boiler feed pump would be controlled by a feedwater regulator while the intermediate units would be subjected solely to the control of the available net positive suction head, that is, of the submergence from the storage space of the direct-contact heater. As the boiler load would be reduced, each pump in turn would continue for a short period of time to handle more feedwater than was being returned into the direct-contact heater at the head of the system, with the result that levels in the storage space would fall and reduce the pump capacity through the reduction of the net positive suction head.

In practice, however, this would prove to be a difficult undertaking. It must be considered, in the first place, that in order to obtain satisfactory capacity variations through level control, the available net positive suction head itself must undergo variations of as much as 80 per cent or even more of its maximum value. This is entirely feasible in the case of a condenser hot well, where the available net positive suction head may vary between 4 ft and 1 ft. Condensate pumps are properly proportioned and designed to avoid excessive inlet and rotative speeds and are provided with special condensate-type impellers. The application of such designs to high-head boiler feed pumps would not be practical, as the latter operate at high speeds and require net positive suction heads of 15 to 20 ft or even more. Even if it were possible to provide suction-level control to the operation of boiler feed pumps, the storage space of the direct-contact heaters would have to extend to within 2 or 3 ft of the pump center line, increasing the cost of the heaters quite appreciably.

There is, finally, one more factor which presents difficulties in the application of a feed cycle with multiple direct-contact heaters. Operation of boiler feed pumps at extremely reduced capacities is conducive to a variety of undesirable effects due to the temperature rise experienced within the boiler feed pump at light flows. In the normal case, the boiler feed pump is provided with a by-pass in its discharge, leading to some region of lower pressure in the feed cycle where the excess heat in the by-passed feedwater may be dissipated without harmful effects. This by-pass is operated either manually or automatically whenever the flow through the pump falls to some predetermined minimum or whenever such a reduction in capacity is expected. A boiler-feed cycle such as illustrated in Fig. 1 would require the installation of an individual by-pass beyond each separate boiler feed pump, and each by-pass would require its own piping and its own individual control. An automatic-control system would be quite feasible but, again, would add to the initial investment and probable maintenance expense.

We have not touched upon the problem of heater construction because this analysis is concerned strictly with the effect of various feed cycles on the centrifugal pumping equipment involved. There is little doubt, however, that certain problems must arise in the design and operation of direct-contact heaters at the elevated pressures and temperatures imposed by the application of a feed cycle with multiple direct-contact heaters.

MULTIPLE CLOSED HEATERS

It cannot be said that the application of a feed cycle with multiple closed heaters is entirely devoid of problems. As a matter of fact, the average power-plant cycle is based on a modified system; one direct-contact heater fulfills the function of feedwater deaeration, while several additional heaters of the closed type are located upstream as well as downstream of the direct-contact heater and its boiler feed pump.

The condensate drains from the closed heaters must be returned to the cycle in order to avoid a waste of treated feedwater and of its heat and pressure energy. Two basic methods are available for the reintroduction of the heater drains into the feed cycle:

1 Pumping the drains into the feedwater cycle at some higher pressure point, as in Fig. 5.

2 Flashing the drains into the steam space of a lower-pressure portion of the feed cycle, as in Fig. 6. (When this is done successively with several closed heaters, the process is referred to as "cascading.")

Thermal-balance calculations indicate that the first method shows a gain in over-all plant economy over the straight cascading

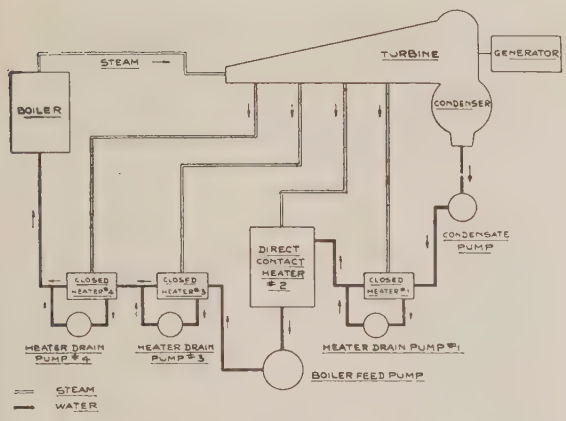

Fig. 5 Straight Pumping System

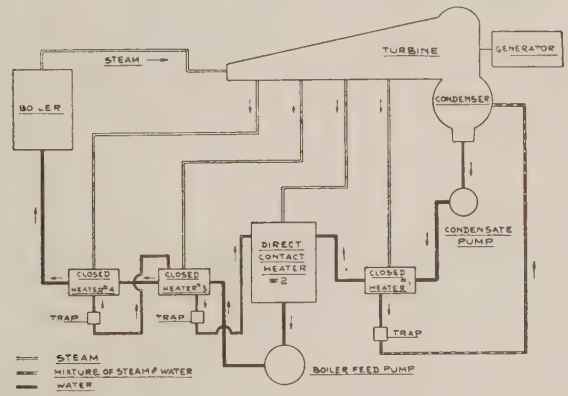

Fig. 6 Straight Cascading System

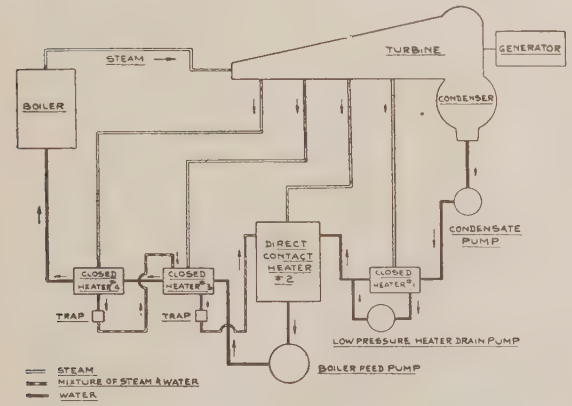

Fig. 7 Modified Cascading System

system. However, the economy to be gained by the inclusion of individual heater drain pumps at each closed heater is hardly justifiable in view of the added initial expense and greater maintenance required. As a matter of fact, pumping from the closed heaters on the discharge side of the boiler feed pump in a high-pressure installation is quite impractical. The capacity of the heater drain pumps is but a fraction of the design capacity of the feed pump itself, while the discharge pressures of the two are of an equivalent order or magnitude. As a result, it may become impossible to apply a centrifugal pump for the service strictly because of hydraulic-design considerations.

A compromise between these two basic methods is illustrated in Fig. 7. It consists of cascading the heater drains of all closed heaters located on the discharge side of the boiler feed pump back into the direct-contact heater and of pumping the drains of the low-pressure heater into the discharge from the condensate pump. The over-all losses in plant economy brought about by this modified cascading system, when compared to the straight pumping system, are negligible.

Effects of Rise in Operating Pressures

It has been mentioned that the rise in power-plant operating pressures had a very definite effect on centrifugal boiler-feed-pump construction and operation. The pump of some 20 or 30 years ago seldom operated at speeds in excess of 1800 rpm. While boiler pressures hovered around 200 to 250 psi, there was relatively little advantage to be gained from the introduction of higher operating speeds for any but the smallest-capacity boiler feed pumps. However, as soon as boiler pressures started on their upward climb, the lower operating speed of 1800 rpm became no longer practical and the modern practice of 3600 rpm for boiler feed pumps was launched.

It is interesting to note that high-pressure installations of the central stations have distinctly showed the way for the smaller units which started on a parallel growth toward 300, 600, and now even 1200 psi. What 3600 rpm did for the medium- and large-capacity boiler feed pump, it could no longer do for the smaller-capacity unit, until today there is a definite growing trend toward operating speeds in excess of 3600 rpm.

This might serve, incidentally, as a logical occasion to discuss the oft-quoted technical superiority of our European counterpart in the field of centrifugal-pump design. The more frequent use of high operating speeds in Europe stems not from the greater talent and ingenuity of their engineers but rather from a series of economic and geographical circumstances.

The first and probably least important of these circumstances is the fact that European electric-distribution practice is based on 50-cycle current, permitting a maximum synchronous speed of only 3000 rpm, compared to a possible 3600 rpm in the United States. This lower limit handicapped European designers sufficiently to make it desirable to exceed the 3000-rpm speed, either through greater use of turbine drive or through the application of stepup gears. Once the natural speed limit of motor-driven pumps was exceeded and abandoned, there was little reason to carry the increase to only 3600 rpm, and higher-speed pumps were widely introduced.

The more important reason, however, is the fact that, while raw-material costs are generally higher in Europe, labor costs were always abysmally low. The European designer has through necessity learned to spare materials even at the cost of increasing labor man-hours, both in production and in maintenance. Where an American engineer will use a safety factor of 5, European training dictates the choice of lighter structures, close figuring, and safety factors of 2 or even less.

Even after the advent of 3600 rpm as standard practice in this country, the rise in boiler pressures kept pace. Soon, discharge pressures in excess of 1200 psi became a common requirement and even the use of cast steel for the pump casings proved an insufficient barrier to internal leakage of the then common axially split casing boiler feed pump. The next step was the introduction of radially split casing designs, culminating in the well-known forged-steel-barrel double-casing construction of today for the higher-pressure range. It is interesting to note, incidentally, that the dividing line of approximately 1250 psi between axially

and radially split casings appears due for a slight upward revision, probably to 1350 or 1400 psi.

Damage to pump stationary parts was found to be the most troublesome item standing in the way of such upward increases in operating pressures, and it is being overcome now by the use of stainless-steel alloys of similar grade to those already in use for the rotating pump parts, such as impellers, impeller rings, and shaft sleeves. Thus the old dividing line will be greatly affected by a more general adaptation of erosion-resisting material in all the parts of the pump. Part of this revision may be said to derive from greater accumulated experience with axially split casings operating near the old dividing line; part may be ascribed to the availability of better materials than heretofore used.

Once the general principles of design for this higher pressure range had become more or less stabilized, there still remained the question of the limiting stage pressures. From a strictly hydraulic point of view, there was much to be gained from maintaining low- or medium-stage pressures, at the cost of multiplying the required number of stages. The lower heads per stage kept disk-horsepower losses to a minimum and avoided possible reduction of pump efficiencies. It also became necessary to reconsider the effects of the higher velocities brought by higher stage pressures on the erosion problems in the pump casings. The use of extremely low heads per stage, however, leads to a greatly increased number of stages, greater shaft spans and shaft deflections, and greater stresses on the pump casings. The increased number of running joints in a pump designed with too great a number of stages added seriously to its disadvantages. A satisfying compromise had to be reached, taking into account available materials, the optimum number of stages, and the required operating speed, the main consideration being to obtain a pump design which can be maintained in service with the least expenditure of cost, effort, and expert knowledge.

As a result of the availability of better materials, it has been the practice lately to increase stage pressures and keep the number of stages to an absolute minimum. Six stages are considered today the best possible combination for most pressures in excess of 1000 psi, although in the case of relatively low-capacity pumps it becomes necessary once in a while to provide seven or even eight stages. Assuming a net pressure of 1800 psi, a six-stage pump would develop 300 psi per stage (or about 725 ft). Once thought excessive and even impossible, 725 ft per stage can be considered as a very safe and reliable figure today.

High Suction Temperatures

Along with rising discharge pressures, boiler feed pump designers have had to contend with a trend toward higher suction temperatures and higher suction pressures. This trend can be traced to two separate power-plant developments. In certain cases, the desire to improve the station heat balance dictates the choice of a higher pressure stage in the main turbine for feed heating at the direct-contact heater. As a result, instead of 3 to 15 psig, direct-contact heaters are being more frequently designed for 65 psia, and even higher. In other cases, the pumping temperatures are increased through the application of two boiler feed pumps operating in series with one or more closed heaters being located between the primary and main feed pumps. This frequently occurs in topping installations, where the pumps which fed the low-pressure boilers are retained and serve as booster pumps to the higher-pressure addition.

When the direct-contact heater is fed with steam from a relatively high pressure stage of the main turbine, special attention must be given to the boiler feed pump suction conditions if the heater pressure is not held at a constant value regardless of bleed-pressure fluctuations, because there exists a danger of flashing in the pump suction whenever a severe and sudden drop is experienced in the station load.

As the generator dumps its electric load, the first tendency of the main turbine is to overspeed, because it is receiving an excess of steam over the requirements of the lighter load. However, since turbogenerators are so arranged in their controls as to prevent asynchronous operation, the turbine governor immediately acts to throttle the steam supply to the turbine and holds the turbine speed at its rated value.

The consequence of this reduction in pressure at the steam inlet is a proportionate reduction at all the successive stages of the turbine and of course at the bleed stage supplying the direct-contact heater. In the meantime, the water in the storage space of the heater, which was at a temperature corresponding to the pressure in the heater, is suddenly subjected to a severe decrease in pressure without a corresponding decrease in temperature. The net result of this situation is severe flashing which occurs in the heater as well as in the feedwater in the suction piping to the boiler feed pump.

The time element involved in again bringing the pressure and temperature within the heater to a correlated value will of course vary with each individual case. The variation in the time component is due to the great variation in the size and shape of the storage space, since these two elements are important factors in the rate of flashing at the free surface of the feedwater.

It must also be considered that the downward velocity of the feedwater in the suction piping is too high to permit the vapor bubbles generated by flashing, to rise up to the heater and thus to clear the boiler feed pump suction of the flashing steam. A safety factor must be provided to take care of the time lag which exists between a certain reduction of pressure in the heater and the ultimate reduction of temperature at the pump suction. It is therefore necessary either to provide an excessive factor of safety in the installation of the boiler feed pump through the addition of an empirical percentage to the calculated net positive suction head or else some means whereby any appreciable pressure reduction in the heater would be accompanied immediately by a temperature reduction at the pump suction.

The latter solution is obviously predicated upon the injection of colder water into the pump suction. While the design of a control for such injection is not an insurmountable problem, the practicability of this solution is governed by circumstances peculiar to each individual installation. The cooler injection water must be taken from the downstream side of the cycle, that is, either from the discharge of the condensate pump or from the drains of a low-pressure closed heater ahead of the direct-contact heater. To introduce nondeaerated condensate into the boiler feed pump suction is not recommended, especially in the case of high-pressure boilers where the possible effects of contamination are severe. It must be considered, however, that a high-pressure installation, including a direct-contact heater operating at high temperature, will probably also include a low-pressure closed heater between the condensate discharge and the direct-contact heater itself. It must be further considered that the drains from this heater, generally pumped by a separate pump into the direct-contact heater, are to all intents and purposes pure deaerated condensate, and that their injection into the feedwater suction stream will cause no harmful effects.

A logical precaution, therefore, might consist in the installation of a by-pass line from the low-pressure heater drain pump discharge into the boiler feed pump suction. This by-pass line would be properly valved and controlled by some means such as the difference between the suction pressure and the vapor pressure at the suction, any decrease of this difference below a predetermined minimum causing the by-pass valve to operate and inject colder water into the suction of the feed pump. Two charts

have been prepared to illustrate the effect of colder water injection on the available net positive suction head. Fig. 8 shows the temperature depression resulting from the injection, plotted against the difference in temperature between the feedwater and the injection stream and given for varying ratios of injection. Fig. 9 illustrates the effect of temperature depression on the available net positive suction head at various feedwater temperatures.

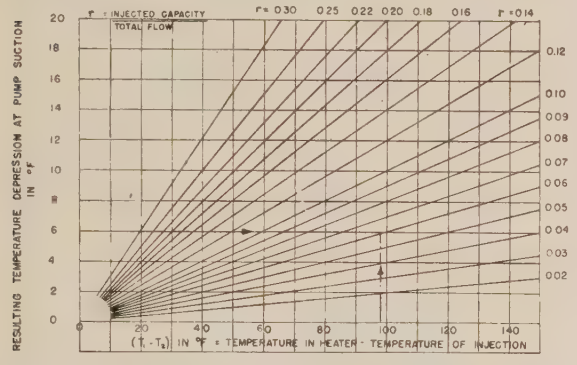

Fig. 8 Effect of Injection of Cooler Feedwater on Temperature of Mixture

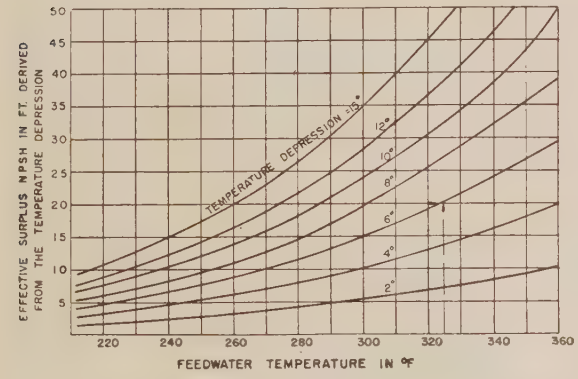

Fig. 9 Effect of Temperature Depression on Available Net Positive Suction Head

Thus, for instance, if it is desired to provide 20 ft surplus net positive suction head at the boiler feed pump suction and if the feedwater temperature is 325 F, the required temperature depression is 6 deg F. Assuming that the temperature of the heater drains is 227 F, allowing a 98-deg difference between feedwater and injection water, the by-pass line must be proportioned to pass 0.062 of the maximum boiler feed pump capacity, or 6.2 per cent.

Another serious problem introduced by high feedwater temperatures, especially when coupled to high suction pressures, resides in the operation of the stuffing boxes. The design of the pump interior parts can be accommodated to these conditions without undue difficulties, now that high-grade alloy stainless steels are readily available. The practice of shrinking impellers on the shaft in high-pressure applications has further helped solve some of the earlier problems. Finally, the design of the pump casing itself, through the application of materials such as forged steel and in some cases even stainless alloys, as well as through certain mechanical improvements, has likewise eliminated some of the earlier temperature limitations.

There remains, however, the problem of providing a reliable and economical stuffing-box design. Certain objectives may be said to have been attained even in this field. For instance, within the last few years a more thorough understanding of the interrelation of stuffing-box pressures, rubbing speeds, and leakage temperatures has led to an improved style of water-cooled stuffing-box design. Such stuffing boxes have been built suitable to withstand feedwater temperatures up to 400 F and stuffing-box pressures up to 500 psi, without recourse to pressure-reducing labyrinths. The construction of such a stuffing box is illustrated in Fig. 10. It will be noted that one of the outstanding features of this design is that the stuffing-box leakage is precooled before it reaches the packing proper. Operating records in excess of 6 months have been obtained with this construction without renewing the packing.

While this combination of pressures and temperatures does not necessarily represent the ultimate limit, further increases will probably be reached more slowly and after much careful laboratory and field experimentation. Furthermore, it may be noted that, at the present time and with very few exceptions, this range of pressures and temperatures represents the maximum conditions which might have to be imposed on boiler feed pump stuffing boxes.

Whenever boiler feed cycle requirements are such that these limits have to be exceeded, the only solution resides in the application of pressure-reducing devices ahead of the stuffing box proper. Since the design of such devices has now reached a high degree of proficiency, the only remaining drawback to their application is the necessity of bleeding a part of the effective capacity back to a lower pressure level and the attendant reduction in efficiency.

Pressure and Temperature Control in Closed Feed Cycles

There is a certain interesting although little known phase in the control problem of the so-called closed feed cycle, where

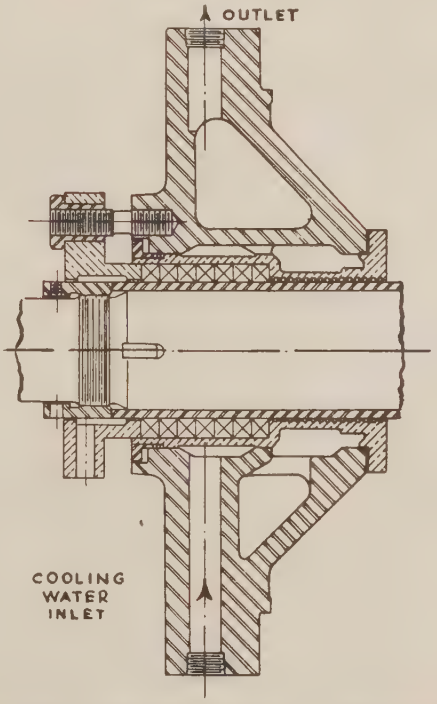

Fig. 10 Improved Style Stuffing Box for High Suction Pressures and Temperatures

several boiler feed pumps are operated in series with closed heaters interposed between successive pumps, and where one or more of these pumps is operated at variable speed, as illustrated in Fig. 11.

Normally, the variable-speed operation is restricted to the low-pressure unit of the combination, the controlling mechanism being either an excess-pressure or a constant-pressure regulator. This regulator is used to vary the speed of the centrifugal pump in question, which is driven by a steam turbine, a wound-rotor motor, or even through a variable-speed coupling.

This control is obviously unaffected by the relationship between the temperature and the pressure at the suction of any one of the pumps so that conditions might arise where the speed regulation on one pump lowers the suction pressure of the following pump dangerously close to or even below the vapor pressure of the feedwater at the suction.

While at full load the temperature of the feedwater leaving the individual pumps is for practical purposes equivalent to the temperature at the pump suction, this does not hold true at light loads, and for that reason the illustration indicates this by using different subscripts for the temperatures at the suction and discharge of each pump. It is obvious that the margin between the pressure at the suction of the secondary feed pump (P_4) and the vapor pressure corresponding to the temperature T_4 must never be allowed to fall below a certain predetermined value which depends on the pump design.

The selection of the individual pump-discharge pressures is a relatively complex problem which is affected by the amount of required pressure regulation, that is, by the system head curve of the boiler feed cycle, by the head-capacity characteristics of the individual pumps, the maximum temperatures of the feedwater at the outlet of the various heaters, the permissible speed variation of the variable-speed drivers, and finally by the desired maximum hydraulic pressure to be imposed on the intermediate closed heaters.

Fig. 12 illustrates qualitatively the characteristics of a typical closed system such as in Fig. 11. For purposes of simplification, frictional losses between the pumps have been neglected. It will be seen that the pressure at the discharge of the secondary pump considerably exceeds the required system head pressure at light loads if all the pumps are operated at constant speed, and that even if the primary feed pump is by-passed altogether, the secondary feed pump can develop sufficient pressure from shut-off to capacity "A." In other words, the speed variation required of the driver of the primary pump ranges all the way from 0 to 100 per cent. This, obviously, is impractical for a great many reasons, especially if the pump is driven by a wound-rotor motor where reduction of speed below 50 per cent of design speed is seldom practiced. As a result, the operation of such a cycle at variable speed generally takes place along the lines illustrated in Fig. 13. Whatever excess pressure remains is throttled by the feedwater regulator.

The important feature of a proper selection of primary feed pump conditions and of a suitable variable-speed control is that means must be made available to prevent the discharge pressure of the primary feed pump (P_3 in Fig. 11), from falling below a certain minimum determined by the relationship between P_4 (P_3 less losses through the closed heater), and the vapor pressure corresponding to the temperature T_4. Should certain operating conditions arise which might lead to a dangerous reduction of the difference between P_4 and the vapor pressure at T_4, some control must be instituted, actuated by this difference and arranged to set a definite limit to the speed reduction called for by the excess-pressure regulator.

Fig. 13 indicates the introduction of such a speed-reduction limiting control, whereby the discharge pressure of the primary

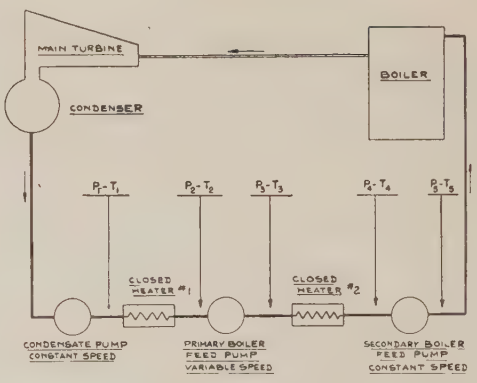

FIG. 11 CLOSED FEED CYCLE WITH VARIABLE-SPEED PRIMARY FEED PUMP

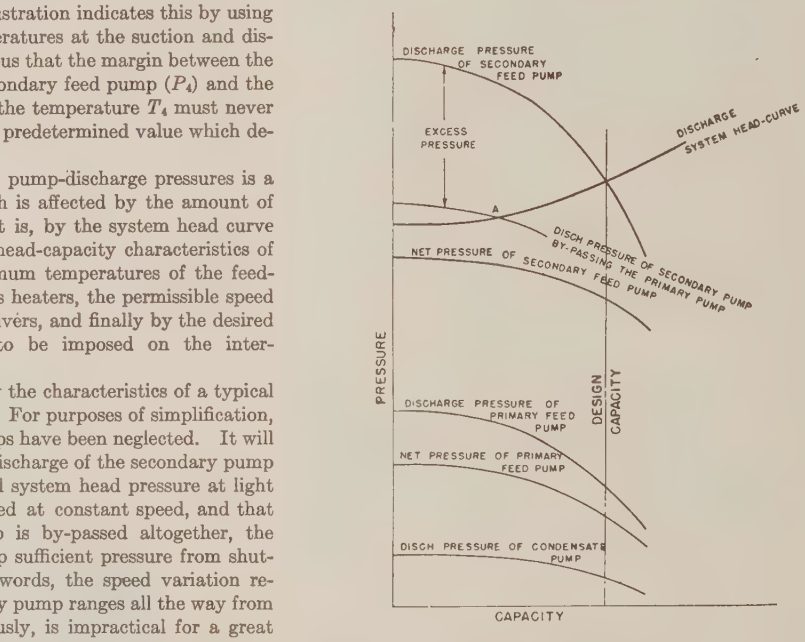

FIG. 12 CHARACTERISTICS OF A CLOSED FEED CYCLE AT CONSTANT SPEED

feed pump is not permitted to fall below a predetermined minimum. For the sake of simplification, it has been assumed that the value of T_4 is constant at all loads, and therefore that the minimum permissible value of P_3 is likewise constant. Actually, the closed heaters are fed with steam bled from some given stage of the main turbine and the pressure and temperature of this steam are reduced as the load is reduced. Thus in an actual installation, the process of checking the minimum permissible primary feed pump discharge pressures may be a little more tedious than indicated here.

CONCLUSIONS

The foregoing discussion of boiler feed cycles has been presented not as an attempt to catalogue in an exhaustive manner all the possible variations and ramifications which can be found in these cycles, but rather with the desire to illustrate the close relationship between cycle and pump design. There is no ques-

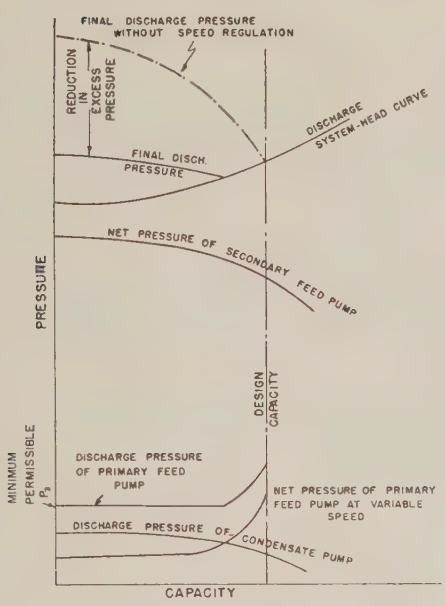

FIG. 13 CHARACTERISTICS OF A CLOSED FEED CYCLE WITH VARIABLE-SPEED REGULATION

tion that the degree of integration of the pump into the pumping cycle itself is a direct criterion of the ultimate success of the entire installation. It is toward such complete integration that the pump designer, the application engineer, and the technical operating personnel have had to apply their efforts, and it is through this integration that modern centrifugal-pump designs have achieved their relative success.

It is hoped that the present analysis will give rise to more studies of all the factors connected with high-pressure cycles, and thus the seed will be sown for further improvements based upon mutual understanding and co-operation between designer and operating personnel. The problems which high-pressure pumping cycles have presented have not grown easier with time. But it may be said, with a certain pardonable pride, that the centrifugal-pump designer has so far fully met the challenge.

Discussion

R. P. MOORE.[2] The author describes a clever means of preventing loss of the suction pressure on boiler feed pumps drawing water from direct-contact deaerating heaters when the load on the turbine is reduced. This scheme includes some automatic valving. Experience has proved, in certain cases at least, that it is possible to accomplish the same result without any automatic valves or other moving equipment. Proper design of the deaerating heater, as is described in an article by the writer,[3] accomplishes the desired result. The scheme consists of placing baffles in the heater so as to guide the freshly deaerated water directly to the boiler feed pump suction and to allow any flash steam which forms in the water in the heater to rise to the steam space without interference with this flow.

Fig. 14 of this discussion shows the baffles and vents added to the bleeder deaerating heater of standard design in use in Huntley Station No. 2 of the Buffalo Niagara Electric Corporation. The results accomplished by this addition are shown in curve form in

[2] Mechanical Engineering Department, Buffalo Niagara Electric Corp., Buffalo, N. Y. Mem. A.S.M.E.

[3] *Electrical World*, October 14, 1944.

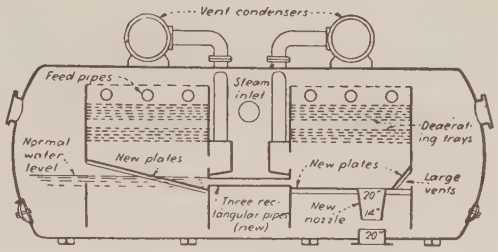

FIG. 14 LONGITUDINAL SECTION OF DEAERATOR, SHOWING NEW PARTS

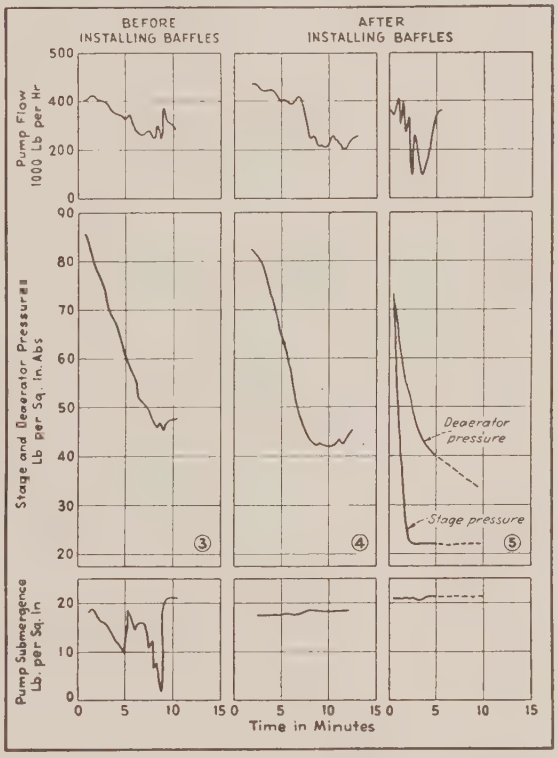

FIGS. 15, 16, AND 17 (*Left to Right*): AFTER INSTALLING BAFFLES, LOAD COULD BE REDUCED RAPIDLY, I.E., 10 PSI PER MIN IN FIG. 16, AND 20,000 KW PER MIN IN FIG. 17, WITHOUT OCCASIONING LOSS OF PUMP SUBMERGENCE THAT OCCURRED BEFORE THEY WERE INSTALLED, FIG. 15

Figs. 16 and 17, taken from the article referred to,[3] compared to the conditions prior to the change, Fig. 15. In Fig. 16, the rate of pressure drop was such that deaerator and stage pressures remained the same. In Fig. 17 the stage pressure dropped so rapidly that the bleeder nonreturn valve closed, and the deaerator pressure could not follow. Not only has loss of pump suction been eliminated when the turbine load drops, even if instantaneously, but the water continues to pass through the deaerator and is deaerated under all conditions.

R. M. SEAGO.[4] In connection with higher boiler feed pump

[4] Efficiency Engineer, New Orleans Public Service, Inc., New Orleans, La. Mem. A.S.M.E.

suction temperatures, the author states that in the event of a severe and sudden drop in station load, turbine-stage pressures will quickly drop resulting in severe flashing in the direct-contact heater serving as boiler feed storage tank and also in suction piping to the boiler feed pump. While drop in pressure of bleed steam to the boiler feed heater undoubtedly contributes to the condition of severe flashing, it is not, in the writer's opinion, the only factor involved.

To illustrate, let us follow the train of events resulting from a severe and sudden drop in station load:

1 Due to sudden decrease in load on the electric generator, the turbine tends to overspeed, resulting in a rapid throttling of control valves by the governor.

2 As a result of control valves throttling, stage pressures drop rapidly and throttle pressure rises rapidly.

3 Sudden rise in throttle pressure may result in one of two effects, in so far as the boiler is concerned, depending on the severity of the load drop, that is, depending on whether it is within or without the capability of combustion control.

If the drop is too severe for combustion control to handle, one or more safety valves will lift, causing an instantaneous rise in boiler-drum water level. The feedwater regulator might close completely, and if automatic recirculation is provided the boiler feed pump will be subjected to minimum flow as determined by its recirculating orifice capacity. If manual recirculation control is provided, under these conditions, the pump will probably be subjected to zero flow, resulting in severe flashing and probable damage to its internal parts.

On the other hand, if the load drop is within the capability of combustion control to prevent popping of safety valves, another train of events, detrimental to boiler feed pump operation, will be started. Rise in throttle steam pressure will result in an initial rise in boiler-drum pressure causing a drop in drum water level, followed by a more severe drop in water level as the firing rate is rapidly decreased. If the feedwater regulator is of the single-element type, it will open rapidly, placing a sudden demand on the boiler feed pump and also on the boiler-feed tank. If the regulator is of the multiple-element type, the water-level effect will probably override the effect of diminished steam flow to result in a similar though less pronounced increase in feeding rate. This will result in a rapid decrease in boiler feed pump npsh over and above the decrease imposed by drop in turbine stage pressure.

Further aggravation will also be imposed in some installations by quenching of vapor in the boiler feed tank by make-up water supplied from an auxiliary storage or surge tank.

If return of turbine loading is rapid, as in the case of a short-duration electrical interruption, similar hardships will be placed on the boiler feed pump. Rapid increase in boiler firing rate will result in almost instantaneous swelling of water within the boiler, often causing the feed regulator to close completely. Again the boiler feed pump will be subjected to minimum flow conditions followed by a gradual return to normal flow.

The foregoing is certainly not intended as a criticism of the author's analysis of causes of erratic boiler feed pump suction conditions, but rather is intended as an amplification of this analysis in line with a personal opinion that correction of such conditions should be, in the majority of cases, thrown back in the lap of engineers responsible for the heater, piping, and pump layout. Obviously, sufficient submergence of boiler feed pumps to provide ample static suction head in excess of any reductions imposed by normal surges would remedy the situation without recourse to injection of colder water into the boiler feed pump suction. For the majority of cases where space or operating pressure limitations will not allow provision of sufficient static suction head, the injection of colder water offers definite possibilities.

The use of low-pressure heater condensate as injection water presents another problem in connection with many existing systems. In a typical installation, for example, at full turbine load, low-pressure heater condensate represents 8 per cent of throttle steam flow (or boiler feed pump flow). However, at one half load, low-pressure heater condensate is only 5 per cent of throttle flow. This may or may not provide sufficient injection water to insure adequate temperature depression at the boiler feed pump suction.

In line with these possible restrictions, it might be well to re-examine the possibility of using condensate direct from main condensate pumps. It has been our experience, based on numerous tests on two modern condensers designed for de-aeration of hot-well water, that condensate leaving condensate pumps is oxygen-free within limits of detection, by the modified Winkler test, and consequently, from this standpoint, is suitable for injection directly into the boiler.

Papers of this type, together with the discussions which they evoke, are of tangible benefit to the engineer faced with similar problems. Encouragement should be given to preparation of more papers in which the equipment designer freely discusses the limitations as well as the capabilities of the apparatus.

A. J. Stepanoff.[5] The writer will call attention to a few problems in high-pressure boiler feed practice not mentioned in the paper, which are not caused directly by the high pressure, high temperatures, or pump high operating speed. One of them is the wear of internal parts resulting from corrosion and erosion commonly referred to as "cutting." The pH value of the pumped water does not indicate the corrosiveness of water when applied to pure water. A definite trend to purer feedwater in central-station application will demand wider use of stainless steels for pump parts than has been the case in the past.

Mechanical problems connected with high-pressure high-temperature boiler feed pumps were not different from those encountered with the hot-oil charging pumps. A number of these were in service some 10 to 15 years ago, pumping oils at 800 F, maximum pressures from 1000 to 1500 psi (2300 psi was used at one refinery) and 4000 rpm pump speed. Even with the most corrosive (sour) oils, pump-casing cutting was practically unknown with hot-oil pumps.

Pressure "surges," accompanied by the capacity, speed, and power fluctuations, presented another problem in boiler feed pump operation not previously encountered in hot-oil or any other pumping service. Such surges are of the same nature as those observed in hydroelectric power plants frankly and completely discussed in a paper by Rheingans.[6] Both systems have a mass of water suspended between the free surfaces at their ends. This is free to oscillate if some impulses appear at a frequency synchronous with that of the natural frequency of the system. As a result of such fluctuations, in the case of boiler feed pumps, the piping may require additional bracing, and some pumps cannot be operated at low capacities. R. Dziallas[7] has studied the surges and was able to reproduce those in a laboratory setup.

It should be noted that condensate-pump cycle presents another swinging system with two free water surfaces at the ends, but no surges are observed on this system as long as the condensate pumps operate beyond the breakdown point on the head-

[5] Engineer, Cameron Engineering Department, Ingersoll-Rand Company, Phillipsburg, N. J. Mem. A.S.M.E.

[6] "Power Swings in Hydroelectric Power Plants," by W. J. Rheingans, Trans. A.S.M.E., vol. 62, 1940, pp. 171–184.

[7] "Schwingungen bei Kreiselpumpen mit labiler Kennlinie," by R. Dziallas, *Archiv für Wärmewirtschaft und Dampfkesselwesen*, March, 1941, pp. 63–66.

capacity curve, Fig. 4 of the paper, because cavitation destroys the regularity of impulses in the system. Similarly, surges can be stopped on any boiler feed pump by throttling the pump discharge slightly (sometimes as little as 20 psi), thus destroying the regularity of the water mass oscillation.

The writer does not believe that the author's criticism of European engineering or training is justified. The high-pressure-boiler development is only one example of European engineering achievement.

In so far as pump speeds are concerned, the general trend toward higher speeds is very definite in this country too. While 3600 rpm was a top speed only recently, 6000 to 7000 rpm is quite common now. Cost is only secondary to weight and space saving, and hydraulic advantages in the advance in the operating speeds of boiler feed pumps.

G. H. Van Hengel.[8] The paper gives a good detailed description of the difficulties encountered when operating centrifugal pumps with net positive suction heads close to their guarantee. These pitfalls are generally not realized when the layout of a plant is made and are difficult to correct afterward because they are dependent on the elevations which have been fixed by the structure of the building.

In large power stations where bleeding is used, a change of load will change the pressures in all the turbine stages practically proportionally to the load. Thus in case 20 per cent of the turbine load is dropped, the stage pressures will also drop 20 per cent, and with them the heater pressures. All the pumps extracting from these bleeding heaters will therefore be suddenly robbed of 20 per cent of their suction pressure.

The stage temperatures, however, because of the heat storage in the condensate present in the heater, will not drop as rapidly. It is this phenomenon of the lag in temperature with respect to pressure that causes a difficult condition for the heater pumps. Because this lag depends on various conditions of the layout and the rate change of load, it differs for each individual case. The whole matter reduces to the question of how fast the load on the turbine drops in comparison to the ensuing rate of temperature changes in the heater.

This comment is intended to emphasize the severity of the condition of pump operation caused by the persistence of this lag, and to show a ready method of calculation to provide for any condition that may occur.

Let us now consider different cases of installation and required operation. For all cases, we assume: That no undercooling of the condensate leaving the heaters exists in regard to the steam entering the heaters or that the pump is running with a net positive suction head at the least value required for its operation.

The following cases are discussed:

1 Instantaneous load drop.
2 Very gradual load drop.
3 Decrease of load throughout a given period.
  (*a*) With no storage capacity.
  (*b*) With storage capacity.

Case 1. Instantaneous Load Drop. As a basis of calculation, let us assume that the load change on the turbine is instantaneous and that the temperature in the heater does not change, a case which corresponds to infinite storage capacity. For safe operation, an excess suction head has to be available to provide a corresponding pressure drop. To calculate this excess suction head, we can readily determine the head equivalent of the assumed sudden pressure drop by using the conservative formula, 1 psi pressure = 2.6 ft head. Thus a sudden drop of 10 psi on a heater would demand an excess net positive suction head of 26 ft on the pump to prevent unsafe operation.

Example: A condensing 80,000-kw turbine with 17 stages has a main steam pressure and temperature of 800 psia and 900 F. It has four direct-contact heaters supplied with steam bled from the 4th, 7th, 10th, and 13th stages at full-load stage pressures of 250, 100, 40, and 8 psia, respectively. If there is a sudden load drop of 20 per cent, the conditions which result are as listed in Table 1 of this discussion.

TABLE 1 CONDITIONS RESULTING FROM 20 PER CENT LOAD DROP

		Heater stages				Condenser
		4th	7th	10th	13th	
1	Full-load pressure, psia	250	100	40	8	0.50
2	80 per cent load pressure, 0.80 × (1), psia	200	80	32	6.4	0.47
3	Sat. temp corr. to (1), deg F	401	327	267	183	80
4	Sat. temp corr. to (2), deg F	382	312	254	173	28
5	Temp diff. due to load, (3–4), deg F	19	15	13	10	2
6	Head increment needed on heater pumps [2.6 (1–2)], ft water	130	52	21	4	0.08

Table 1 shows that with an instantaneous drop of load of 20 per cent and with the greatest possible temperature lag in the heaters, we would have to provide 130, 52, 21, 4 ft additional head on the pumps if this instantaneous drop in load is to be provided for.

For a hot-well pump on a condenser with automatic level control, however, the table shows that the sudden 20 per cent drop of turbine load demands only 0.08 ft excess suction head. Therefore, for the condenser hot-well pump, sudden drops of turbine load can never be a serious factor to be considered in design.

For the heaters this is somewhat different. It must be noted here that for the heaters the additional net positive suction head required is proportional to the absolute heater pressure. The higher the heater pressure, the more probability there is for losing the suction of the heater pump and the more margin in suction head we should have on the pump.

Case 2. Gradual Load Drop. At the other extreme is the case of dropping the load over a very long period which will cause the heater condensate temperature to follow the bled-steam temperature with no lag.

The suction head which must be provided on the pumps in excess of the manufacturer's guarantee would then be zero feet for this case.

The actual provision of suction head to be made must lie between the two extreme Cases 1 and 2.

Case 3(a). Decrease in Load Throughout a Given Period of Time—No Storage Capacity. Now assume that the load drops not instantaneously, but 20 per cent in 5 min; furthermore, that the condensate level is not in the heater but in the suction pipe; a case with practically no storage capacity. Then for the 4th-stage heater in the example, the condensate should increase its pressure by flowing downward at a rate of at least 130 ft in 5 min, or 0.43 fps if we want to prevent flashing. This 0.43 fps will thus determine the maximum size of our pump suction line.

If we have an existing installation, then our suction velocity should be greater than 0.43 fps for successful operation.

Case 3(b). Decrease in Load Throughout a Given Period of Time—With Storage Capacity. Assume again 20 per cent load drop in 5 min. The case can be considered first as Case 3(*a*), but the hot-well cross section replaces the suction-line area. In addition, the colder condensate flow will mix with the hot-well storage, reducing the required suction head. This problem has to be solved mathematically and is dependent on heater hot-well capacity and rate of steam going to the heater. Space limitations prevent treating this case.

All cases so far treated assumed no undercooling or no addi-

[8] The Detroit Edison Company, Detroit, Mich. Mem. A.S.M.E.

tional net positive suction head. In direct-contact heaters, the undercooling will be practically zero. In closed heaters some undercooling always exists. Assume a 5-deg F undercooling for a closed heater on the 4th stage of the example given. The net positive suction head needed would be reduced by

$$\frac{5}{19} \times 130 = 34 \text{ ft}$$

Also, if regulation of the pump discharge is taking place, it may be possible that additional suction head is available at the time the load is dropped.

For safe operation of the heater pump, with time for load drop as in Cases 3(*a*) and (*b*), the undercooling and the additional suction head available during operation reduce the maximum head required under Case 1.

Conclusion. Power stations should be designed not only to meet maximum load conditions, but also certain rate changes in load. For instance, the requirements for the net positive suction head on heater extraction pumps (boiler feed or heater drain pumps), due to sudden load drops, are not sufficiently recognized. Oversight of this fact often leads to dangerous operation which is difficult to correct because of the limitations of the building structure. The problem of variability in load during operation must therefore be thoroughly investigated during the preliminary layout of the station.

Author's Closure

The author wishes to acknowledge with appreciation the contributions of the discussers.

Mr. Moore's solution of the problems introduced by sudden load fluctuations is an extremely valuable contribution to satisfactory heater operation and, the author believes, should be well studied by feedwater heater designers. While the possibility remains that this solution may not meet all cases, it is gratifying to see that it attacks the problem exactly where it arises, that is in the feedwater heater. One of the features of this solution which remain to be investigated resides in the effect of the baffling arrangement described on installations embodying very large feedwater storage volumes, where such baffling may lead to excessive subcooling of that portion of the stored feedwater which is farthest removed from the heater outlet. The author is confident, however, that even this problem is not unsurmountable.

The additional effect of boiler controls on the phenomena which take place at a boiler feed-pump suction on a sudden drop of main turbine load are very well brought out by Mr. Seago. While a sudden increase in boiler feedwater demand may or may not impose additional difficulties, depending upon the margin available over the minimum npsh at maximum pump flow, the reverse case—that of complete closure of the feedwater regulator—introduces very serious possibilities.

If we were to assume that the sudden load drop occurs when operation was taking place between 50 and 100 per cent full load and that the by-pass is manually controlled, it is logical to expect that all by-passes are closed at the time of the load drop and the pumps may be severely damaged. This, incidentally, is quite independent of the suction pressure and temperature and could occur even if the pressure in the heater was pegged to a definite value. Much as it may be desired to avoid the introduction of additional controls, the sequence of events outlined by Mr. Seago shows the advantages and the added protection afforded by an automatically controlled by-pass.

If, as Mr. Seago states, the low pressure heater condensate at one-half load corresponds to but 5 per cent of the throttle flow, its injection into the feed pump suction may or may not be sufficient to afford the required protection against flashing. Assuming the conditions outlined in the paper, that is, 325 F feedwater, 227 F heater drains, and a required margin of 20 feet—the injected condensate must be 6.2 per cent of the boiler feed pump capacity and in accordance with Mr. Seago's statement, the available condensate is insufficient. On the other hand, assuming the same temperature conditions, a 5 per cent injection will provide about 17 ft surplus npsh (see Figs. 8 and 9) and may be sufficient in some cases. Obviously, where it is possible to use the discharge from the condensate pumps, the available flow is fully ample and because of the greater temperature differential, the percentage of injected feedwater appreciably reduced. It must be remembered that the injection is an emergency measure and that the slight danger of feedwater contamination is justifiable, especially since the emergency is not a frequent one.

The problems of corrosion and erosion of internal boiler feed-pump parts mentioned by Mr. Stepanoff have been purposely omitted from this paper as their importance merits a complete and separate study, while their inclusion would have lengthened the present paper unnecessarily without exhausting the subject matter. It may be of some interest to mention, however, that very serious studies have been carried out on these problems within the past twelve months. The preliminary results seem to justify the growing trend toward stainless steels mentioned in Mr. Stepanoff's discussion as well as in the author's paper. It is already becoming apparent that stainless steel casings in a range from a minimum of 4 per cent chromium content to the 25 per cent chromium-20 per cent nickel type, will be utilized to a much greater extent than heretofore. Coupled to the already prevalent use of stainless steel fittings, this trend gives definite indications of solving the twin problems of corrosion and erosion, even at the higher stage pressures predicted.

No criticism of European engineering or training was voiced or even implied by the author. The comparison of practices was brought out to illustrate the possible effect of economic and geographical circumstances on engineering designs and no issue can be taken with the fact that European labor is cheaper than in the U. S. A. and raw materials less available.

Mr. Van Hengel's calculations illustrate very forcefully the theoretical head increment needed on pumps taking suction from direct contract heaters operating at high pressures, both with instantaneous and gradual load drop. Fortunately for the power-plant designer, the usual case corresponds to Mr. Van Hengel's Case No. 3 and the entire theoretical increment in npsh need not be provided for. The determination of the minimum permissible safety margin in npsh is rather complex but can be carried out fairly accurately by the feedwater heater designer, once all the contributory factors and component data have been made available. It is highly important, however, that power stations be designed, as Mr. Van Hengel states, not only to meet maximum load conditions, but also the expected range of load changes.

The Behavior of a Hot-Wire Anemometer Subjected to a Periodic Velocity

By R. C. MARTINELLI[1] and R. D. RANDALL,[2] BERKELEY, CAL.

A method is presented which allows a rapid graphical prediction of the response of the constant-current hot-wire anemometer to a periodic velocity. From such a prediction the suitability of the hot-wire anemometer for any particular application can be readily determined. The method is demonstrated by several illustrative examples.

Nomenclature

The following nomenclature is used in the paper:

A = surface area of wire, sq ft
α = temperature coefficient of resistance, deg F^{-1}
c = constant of integration
C_p = heat capacity of wire, Btu/(lb)(deg F)
ϵ = base of Napierian logarithms
E = voltage across hot-wire anemometer at any temperature, t, volts
E_∞ = Voltage across hot-wire anemometer when wire is at room temperature, τ_∞, volts
$e = E - E_\infty$, voltage across hot wire referred to room-temperature voltage, volts
e_m = voltage across hot wire, referred to room-temperature voltage, corresponding to mean velocity, volts
e_0 = voltage across hot wire, referred to room-temperature voltage, corresponding to conditions of zero thermal lag, volts
f = unit thermal conductance between hot wire and air, Btu/(hr)(sq ft)(deg F) (actually f includes convection, radiation, and conduction to anemometer supports)
i = current through hot wire, amperes
$P(\theta)$ = function of time defined in text
$P(v)$ = function of velocity defined in text
Q = "characteristic" of hot wire, defined in text, volts per hr or volts per sec
R = resistance of wire at any temperature, t, ohms
R_∞ = resistance of wire at room temperature, ohms
$S = \frac{de}{d\theta}$ = rate of change of voltage with time, volts per hr or volts per sec
t = temperature of hot wire, deg F
τ_∞ = temperature of air around hot wire, deg F
W = weight of hot wire, lb
θ = time, hr
3.413 = number of Btu per hr in 1 watt

Introduction

The hot-wire anemometer, as normally operated, consists of a small wire (usually of platinum) suspended between supports in a fluid stream and heated by an electric current. Variations of the velocity of the fluid flowing past the hot wire produce corresponding variations in the heat lost from the wire and thus vary the wire temperature, which in turn alters its electrical resistance. By proper calibration, the wire resistance can be correlated with the velocity of the fluid flowing past the wire, and therefore the hot wire can be used for the measurement of fluid velocities.

The application of the hot wire to the measurement of steady velocities or to small velocity fluctuations about a large mean has been the subject of many studies (1 to 11).[3] Some work has also been done on the behavior of the hot wire when subjected to small velocity fluctuations about a zero mean, mainly in conjunction with the hot-wire "microphone" (12 to 15). The hot wire has also been utilized to measure fluctuating wind velocities, which are usually relatively large variations in velocity of rather low frequency (16, 17).

In all these applications the lag of the response of the hot wire to velocity variations, due to the heat capacity of the wire, has been given considerable attention. However, no complete analysis of the problem has been presented which would allow the prediction of the hot-wire behavior when subjected to large velocity variations of relatively high frequency. It is the purpose of this paper to present such an analysis.

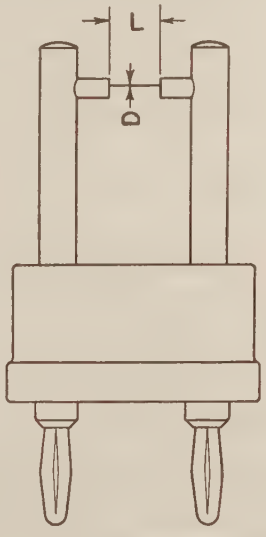

Fig. 1 Hot-Wire Anemometer

Description of Ideal System

In the following discussion a hot wire of length L and diameter D is considered suspended between two supports, Fig. 1. The actual system will be idealized as follows:

1 The temperature of the wire is considered uniform at all

[1] Assistant Professor of Mechanical Engineering, University of California. Jun. A.S.M.E.

[2] Research Engineer, Department of Engineering, University of California. Mem. A.S.M.E.

Contributed by the Heat Transfer Division and presented at the Aviation War Conference, Los Angeles, Cal., June 11–14, 1945, of The American Society of Mechanical Engineers.

[3] Numbers in parentheses refer to the Bibliography at the end of the paper.

times. This is not strictly true because of the cooling of the ends of the wire by the supports, and the radial temperature distribution existing in the wire during transient operation.

2 The wire operates at constant current. This requirement is easily met in the actual system.

3 All heat losses from the wire are proportional to the difference in temperature between the wire and the ambient air.

4 The heat loss from the wire at any fluid velocity during transient operation is exactly equal to the heat loss at the same velocity during steady-state operation.

Basic Equations

Since the operation of the hot wire depends upon its heat loss to the surrounding fluid, the basic equation describing the operation of the anemometer is a heat balance on the wire. During transient operation, the energy supplied to the wire by the electric current appears in two places; part of it is lost to the surroundings, and the remainder is used to heat the wire from one temperature to another. Thus the heat balance becomes

$$WC_p \frac{dt}{d\theta} + fA(t - \tau_\infty) = 3.413\, i^2 R \ldots\ldots [1]$$

The first term represents the heat required to change the temperature of the wire, by an amount dt in a time $d\theta$; the second term represents the heat lost to the surroundings; and the last term the heat supplied by the electric current. All term sare in Btu per hour. Equation [1] is the basic equation for the idealized hot-wire anemometer.

In practice it is more convenient to measure the voltage drop across the wire than to measure the wire temperature. The temperature and voltage are simply related, as shown below.

The resistance of the hot wire R, at any temperature t, may be written as

$$R = R_\infty [1 + \alpha(t - \tau_\infty)] \ldots\ldots [2]$$

where R_∞ is the resistance of the wire at the temperature of the ambient air τ_∞. The voltage across the wire at constant current is

$$E = iR = iR_\infty [1 + \alpha(t - \tau_\infty)] = E_\infty [1 + \alpha(t - \tau_\infty)] \ldots [3]$$

Thus

$$dt = \frac{dE}{i\alpha R_\infty} \ldots\ldots [4]$$

and

$$(t - \tau_\infty) = \frac{E - E_\infty}{i\alpha R_\infty} \ldots\ldots [5]$$

Substituting in Equation [1] yields

$$\frac{dE}{d\theta} + \frac{fA}{WC_p}(E - E_\infty) = \left(\frac{3.413\, i^2 R_\infty \alpha}{WC_p}\right) E \ldots\ldots [6]$$

For simplicity, a new variable $e = E - E_\infty$ may be defined. Then Equation [6] becomes

$$\frac{de}{d\theta} + \left(\frac{fA - 3.413\, i^2 R_\infty \alpha}{WC_p}\right) e = \left(\frac{3.413\, i^2 R_\infty \alpha E_\infty}{WC_p}\right) \ldots [7]$$

The problem of determining the behavior of the hot-wire anemometer subjected to a periodic (or fluctuating) velocity is then to solve Equation [7], obtaining e as a function of time, corresponding to a given variation of the velocity as a function of time. Although the velocity, per se, does not appear in Equation [7], variations in velocity cause definite variations of the unit thermal conductance f, and thus the coefficient of e in Equation [7] is a function of velocity, and finally of time, since the velocity depends upon time. An idea of the variation of f with time can be obtained as follows:

If the frequency of velocity variation is not too great, it may be postulated that, during a cycle of velocity variation, the value of f at any instantaneous velocity v is equal to the value of f which would have been obtained at an equal steady velocity. With a given current flowing through the wire, values of f versus v may be obtained at various steady velocities. A typical plot of f versus v is shown in Fig. 2. The variation of f with v is complex because at zero velocity, free convection, radiation, and conduction are important; while at high velocities forced convection controls. Now, assuming the data for Fig. 2 are applicable at each instant of a cycle of variable velocity, the construction of Fig. 3 would yield the corresponding variations of f with θ.

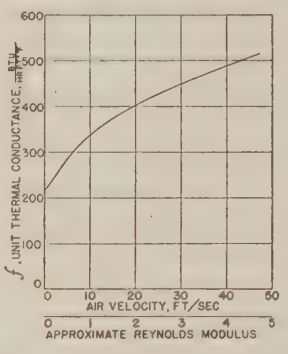

Fig. 2 Unit Thermal Conductance for 0.0005-In. Wire Suspended in Air

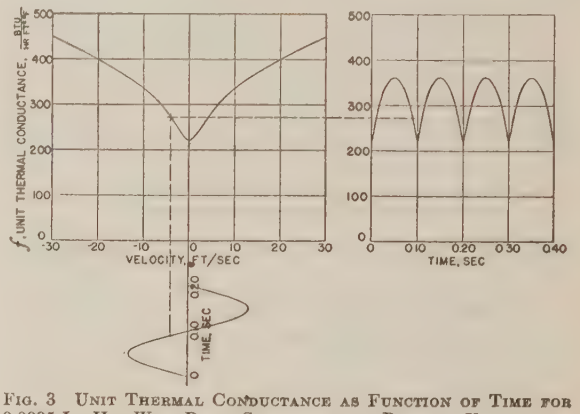

Fig. 3 Unit Thermal Conductance as Function of Time for 0.0005-In. Hot Wire Being Subjected to a Periodic Velocity of 13-Fps Amplitude About Zero Mean

It is noted that although the velocity v becomes negative, the value of f is, of course, always positive since heat is transferred regardless of the direction of air velocity. At the point $v = 0$ the curve of f versus v may not be exactly symmetrical due to free convection effects (2, 9, 12, 14).

Since f varies with time, the coefficient of e in Equation [7] is a function of time, and Equation [8] may be formally written as

$$\frac{de}{d\theta} + P(\theta)\, e = Q \ldots\ldots [8]$$

where

$$P(\theta) = \left(\frac{fA - 3.413\, i^2 R_\infty \alpha}{WC_p}\right)$$

and

$$Q = \left(\frac{3.413\, i^2 R_\infty \alpha E_\infty}{WC_p}\right)$$

The formal solution of Equation [9] is (18)

$$e = \epsilon^{-\int P d\theta}\left[\int Q \epsilon^{\int P d\theta}\, d\theta + c\right] \ldots\ldots\ldots\ldots [9]$$

Unfortunately, this formal solution is of little use, since the analytical expression for $P(\theta)$ is of such a nature that direct integration is impossible. Maxwell (15) has solved Equation [8] for small periodic-velocity variations about a zero mean by expanding the voltage e in a Fourier series. This method, however, is laborious and not practical for engineering purposes. Fortunately, another method of solution of Equation [8] is available, namely, the method of isoclines (19), which in this particular case leads quickly to an engineering answer.

In the isocline method, Equation [8] is plotted on the e-θ plane, using constant values of $(de/d\theta)$ as a parameter. Having established loci along which $de/d\theta$ is constant, short lines are drawn with a slope of $de/d\theta$ on these loci. The plane therefore becomes covered with these "direction" lines. Having the initial condition given locates a point in the plane, and the desired solution is found by drawing a curve from this initial point, always tangent to the direction lines. This curve will, of course, satisfy Equation [8] and also the initial condition and therefore is a solution of the equation.

A difficulty still remains, however, since the function $P(\theta)$ is not known. Inspection of Equation [8] reveals a method of obtaining this function by a simple graphical method.

When the steady-velocity calibration curve of the anemometer is obtained, since $\frac{de}{d\theta} = 0$, Equation [8] reduces to

$$P(v)e_0 = Q \ldots\ldots\ldots\ldots [10]$$

where P is now a function of v rather than θ, since f depends on v. The subscript 0 denotes a condition of zero thermal lag. A plot of e_0 versus v obtained experimentally then yields

$$e_0 = \frac{Q}{P(v)} \ldots\ldots\ldots\ldots [11]$$

A typical calibration curve, which can be readily obtained experimentally, is shown in Fig. 4. It is noted that Fig. 4 is closely akin to Fig. 2.

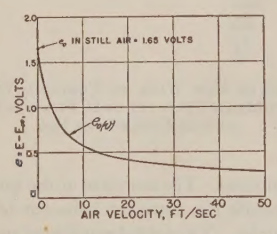

FIG. 4 STEADY-VELOCITY CALIBRATION OF A 0.0005-IN. HOT WIRE

Now if a periodic velocity of very low frequency, $\frac{de}{d\theta} \to 0$, is applied to the hot wire, the construction shown in Fig. 5 can be made. Projecting the instantaneous velocities on the steady-velocity calibration yields the voltage e_0, existing across the wire

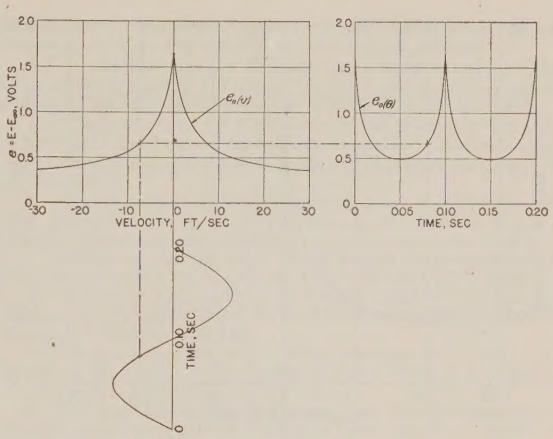

FIG. 5 VARIATION OF VOLTAGE ACROSS 0.0005-IN. HOT-WIRE ANEMOMETER SUBJECTED TO PERIODIC VELOCITY OF LOW FREQUENCY, $\frac{de}{d\theta} \to 0$, WITH NO THERMAL LAG

at each instant of time. Thus on the right of Fig. 5, the curve plotted represents the voltage-time variation across the anemometer if there is no thermal lag. The curve therefore represents

$$e_0(\theta) = \frac{Q}{P(\theta)} \ldots\ldots\ldots\ldots [12]$$

and is the locus of the isoclines $\frac{de}{d\theta} = 0$. Equation [12] allows the evaluation of the function $P(\theta)$. Returning to Equation [8] and substituting the foregoing relation

$$\frac{de}{d\theta} + \frac{Q}{e_0(\theta)} e = Q \ldots\ldots\ldots\ldots [13]$$

Thus curves of constant $\frac{de}{d\theta} = S$ become

$$e = \left(\frac{Q - S}{Q}\right) e_0(\theta) = e_0(\theta)\left(1 - \frac{S}{Q}\right) \ldots\ldots\ldots [14]$$

Equation [14] represents the locus of isoclines of value S and is immediately known once $e_0(\theta)$ and Q are known.

It should be remembered that this method is based on the postulate that the heat loss at any velocity v, during a cycle of periodic velocity variation, is exactly equal to the heat loss at the same velocity during steady-flow operation. This postulate may not be exactly true because of the difference in the hydrodynamic conditions about the wire in the two cases. Experimental work needs to be performed to check this point.

If the method is experimentally verified, it may be possible to correct an experimental response curve by means of Equation [14] to obtain $e_0(\theta)$, from which the true velocity existing at any instant may be determined.

NUMERICAL EXAMPLES

Two numerical examples, illustrating the application of the isocline method of solution, will be presented. The first example shows the prediction of the response of the hot-wire anemometer subjected to a periodic velocity of 13 fps about a zero mean, with a frequency of 5 cycles per sec. The second example shows the response of the hot wire to a periodic velocity with an amplitude of 8 fps about a mean of 20 fps, with a frequency of 5 cycles per sec, and also 50 cycles per sec.

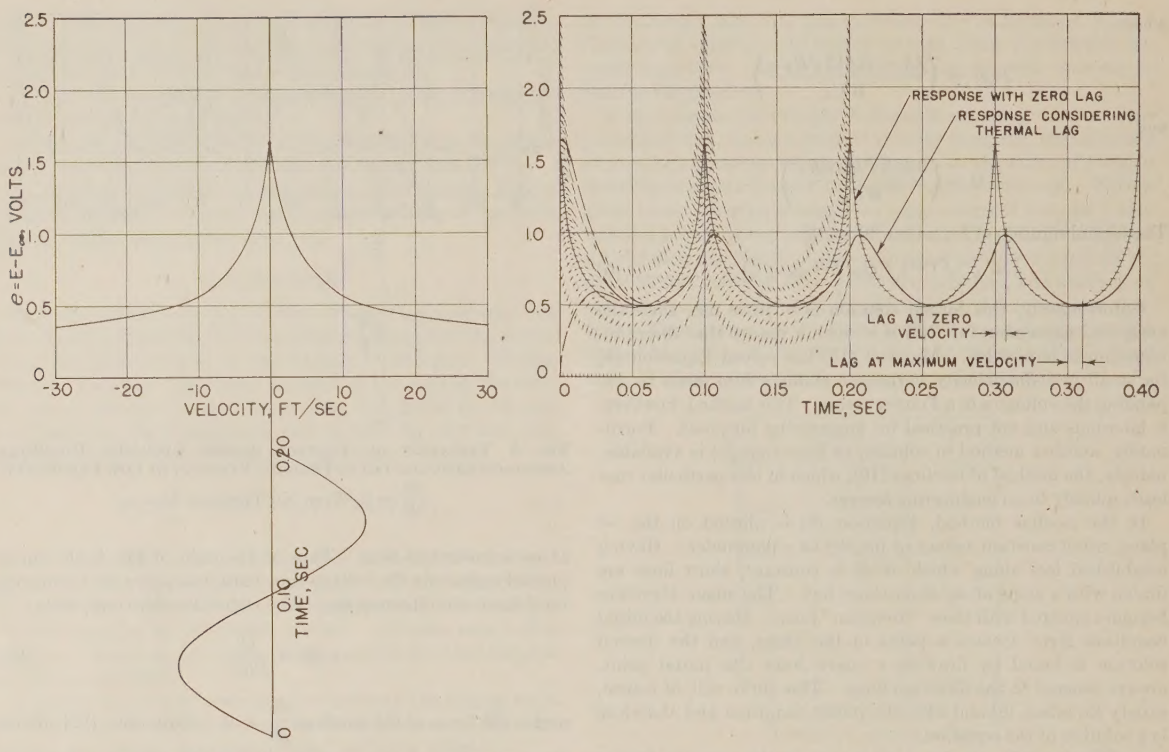

FIG. 6 ISOCLINE SOLUTION FOR RESPONSE OF HOT WIRE TO PERIODIC VELOCITY OF 13-FPS AMPLITUDE ABOUT ZERO MEAN

The following data are available for both examples:

1 Steady-velocity calibration curve of the wire operating with a constant current of 0.140 amp.

2 The properties of the hot wire as follows:

(*a*) Material = platinum

(*b*) Diameter = 0.000532 in. (may be calculated from resistance and resistivity of wire)

(*c*) Length of wire = 0.285 in.

(*d*) Resistance at room temperature = 4.60 ohms

The following properties of platinum are used in the calculations:

(*a*) Density = 1340 lb per cu ft

(*b*) Heat capacity = 0.032 Btu/(lb)(deg F)

From these data the quantity Q can be calculated

$$Q = 2.12 \times 10^5 \text{ volts per hr} = 59 \text{ volts per sec}$$

Example 1. The velocity cycle shown in Fig. 6, which has an amplitude of 13 fps and a frequency of 5 cycles per sec, is projected on the steady-state calibration curve, and the zero lag response determined. This curve is also the locus of the isocline $S = 0$. To determine the loci of other isoclines, the values of e_0 at each instant are multiplied by $\left(1 - \frac{S}{59}\right)$, where S is measured in volts per second. These loci, for several values of S, are shown in Fig. 6. Having established the isocline field, the response of the anemometer can be determined by starting at any point and following the isoclines until the resulting curve becomes periodic. The periodic curve represents the steady-state behavior of the hot wire. The initial point at which the curve is started is of no consequence, since the steady-state solution is independent

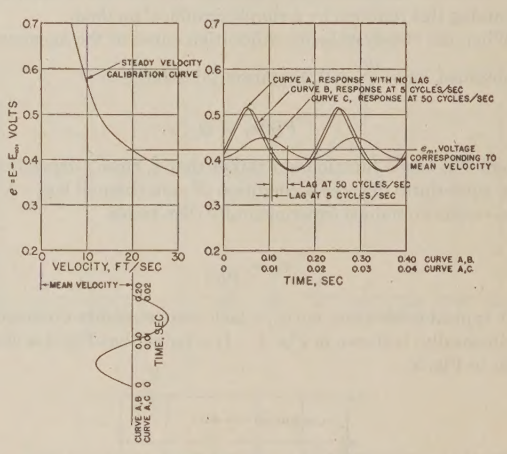

FIG. 7 RESPONSE OF HOT WIRE TO PERIODIC VELOCITY OF 8-FPS AMPLITUDE ABOUT MEAN VELOCITY OF 20 FPS, FOR FREQUENCIES OF 5 AND 50 CYCLES PER SEC

of the initial conditions. The response of the hot wire in the first cycle or so represents the transient behavior of the wire before reaching steady state. Two initial conditions are shown in Fig. 6, both, of course, leading to the same steady-state solution. Fig. 6 reveals clearly the effect of the heat capacity on the hot-wire response. It is interesting to note that due to the nonlinearity of the steady-state calibration curve, the lag differs at various parts of the cycle. Also the wire never heats up to its "still-air" temperature even when the velocity cycle passes through zero. Thus

the voltage across the wire never exceeds 1.0 volts, although the still-air voltage is 1.65 volts.

Example 2. In example 2, shown in Fig. 7, the wire is subjected to a periodic velocity of 8 fps. The isocline method is again used to predict the behavior of the hot wire for frequencies of 5 and 50 cycles per sec. For simplicity, the construction lines are not shown. The figure reveals that for a frequency of 5 cycles per sec, the lag and the reduction in amplitude are very small, but for 50 cycles per sec, they have become appreciable. It is also noted that at higher frequencies the higher harmonics in the response curve are damped out and the response curve approaches a pure sine wave. A comparison of the lags and reductions in amplitude obtained by the isocline method, with the approximate equation of Dryden and Keuthe (6), reveals a good check for the low-frequency response, and considerable divergence for the high-frequency curve.

Conclusions

A method has been presented which allows a rapid graphical prediction of the response of a hot-wire anemometer to periodic velocities. From such a prediction, the suitability of the hot wire for any particular application can be readily determined.

Acknowledgments

The authors wish to thank Prof. L. M. K. Boelter, F. A. Ryder, A. E. Harrison, and T. F. Reinhardt for providing them with a background for this paper.

BIBLIOGRAPHY

1 "On the Convection of Heat From Small Cylinders in a Stream of Fluid: Determination of the Convection Constants of Small Platinum Wires With Applications to Hot-Wire Anemometry," by L. V. King, Philosophical Transactions of the Royal Society of London, vol. A214, 1914, pp. 373–432.

2 "On the Precision Measurement of Air Velocity by Means of the Linear, Hot-Wire Anemometer," by L. V. King, *Philosophical Magazine*, series 6, vol. 29, 1915, pp. 556–577.

3 "The Hot-Wire Anemometer: Its Application to the Investigations of Velocity of Gases in Pipes," by J. S. G. Thomas, *Philosophical Magazine*, series 6, vol. 39, 1920, pp. 505–534.

4 "A Method for the Quantitative Measurement of Quick Changes in the Outflow of Liquids," by G. V. Anrep, A. C. Downing, *Journal of Scientific Instruments*, vol. 3, 1925–1926, pp. 221–224.

5 "Experiments on the Fluctuation of the Velocity in a Current of Air," by J. M. Burgers, Koninklijke Akademie v. Wetenschappen, Amsterdam, Proceedings of the Section of Sciences, vol. 29, 1926, pp. 547–558.

6 "The Measurement of Fluctuations of Air Speed by the Hot-Wire Anemometer," by H. L. Dryden, A. M. Keuthe, N.A.C.A. Technical Report no. 320, 1929.

7 "Effect of Turbulence on Wind Tunnel Measurements," by H. L. Dryden and A. M. Keuthe, N.A.C.A. Report no. 342, 1930.

8 "Improved Apparatus for the Measurement of Fluctuations of Air Speed in Turbulent Flow," by W. C. Mock, Jr., and H. L. Dryden, N.A.C.A. Report no. 448, 1932.

9 "Note on the Use of Hot Wire Anemometers," by D. LeB. Cooper, E. P. Linton, Nova Scotian Institute Science Proceedings, vol. 19, part 1, 1934–1935, pp. 119–120.

10 "Alternating-Current Equipment for the Measurement of Fluctuations of Air-Speed in Turbulent Flow," by W. C. Mock, Jr., N.A.C.A. Technical Report no. 598, 1937.

11 "A Note on a Hot Wire Speed and Direction Meter," by L. F. G. Simmons and A. Bailey, British Aeronautical Research Committee Reports and Memoranda No. 1019, 1926.

12 "A Selective Hot-Wire Microphone," by W. S. Tucker, E. T. Paris, Philosophical Trans. of the Royal Society of London, vol. A221, 1920–1921, pp. 389–430.

13 "The Resistance of a Hot Wire in an Alternating Air Current," by R. C. Richards, *Philosophical Magazine*, series 6, vol. 45, 1923, pp. 926–934.

14 "Die Theorie des Thermomikrophons," by Arthur Hippel, *Annalen der Physik*, vol. 75, 1924, pp. 521–548.

15 "The Escape of Heat From a Harmonically Oscillating Hot Wire," by R. S. Maxwell, *Philosophical Magazine*, series 7, vol. 6, 1928, pp. 945–964.

16 "A Method for the Instantaneous Determination of the Direction and Velocity of the Wind," by E. Huguenard, A. Magnan, A. Planiol, N.A.C.A. Technical Memo. No. 264, 1924.

17 "Method of Recording Rapid Wind Changes," by A. Magnan, N.A.C.A. Tech. Memo. No. 692, Nov., 1932.

18 "Mathematical Methods in Engineering," Th. von Kármán and M. A. Biot, McGraw-Hill Book Company, New York, N. Y., 1940, p. 11.

19 Ibid. ref. 17, p. 7.

(Owing to travel emergency conditions existing when this paper was presented, discussion will be accepted until February 10, 1946)